Waveform Design
via
Convex Optimization

Author
Dr. Silvio De Nicola

Tutor
Prof. Antonio De Maio

Thesis submitted for the degree of
Doctor Philosophiae
in Electronic and Telecommunication Engineering
University of Naples "*Federico II*"
Department of Biomedical, Electronic and Telecommunication Engineering

UNIVERSITÀ DEGLI STUDI DI NAPOLI "FEDERICO II"

Facoltà di Ingegneria

Dipartimento di Ingegneria Biomedica, Elettronica e delle Telecomunicazioni

Tesi di Dottorato
in Ingegneria Elettronica e delle Telecomunicazioni
Coordinatore: ch.mo prof. Niccolò Rinaldi
xxii Ciclo

Waveform Design via Convex Optimization

Tutor
Ch.mo Prof. Antonio De Maio

Candidato
Ing. Silvio De Nicola

A Pablo e Vladimir

πολυματίε νόον ἔχει οὐδιδάσκει
La conoscenza non insegna la saggezza
Eraclito, Fr.40

studio e affronto il problema,
traccio uno schema,
dimostro il teorema in forma di poema,
secondo il concetto assoluto e perfetto
che del mondo tu devi essere la causa, non l'effetto
Francesco Di Gesù, Faccio la mia cosa

Contents

Chapter 1

Introduction

Many spectacular advances in convex optimization have been achieved in the last two decades [1] [2]: the theoretical discovery of algorithms with a polynomial complexity (*interior point methods*[1]), and the practical implementation of reliable and fast solvers such as SeDuMi [4] and SDPT3 [5], have drawn the attention of the engineering community on convex optimization.

Recently, also the radar community has started to profit by the convex optimization framework, to solve the new challenging opportunities in this field, such as radar code design [6] [7], robust radar detection [8] [9] [10], and constrained estimation of typical radar parameters [11] [12].

In particular, radar waveform design has been promoted by the huge advances in high-speed signal processing hardware. Thus, the ability to adapt and diversify dynamically the waveform to the operating environment ensures a performance gain over nonadaptive systems. In this field, convex

[1]Interior point methods are iterative algorithms which terminate once a prespecified accuracy is reached. The number of iterations necessary to achieve convergence usually ranges between 10 and 100 [3].

optimization can be successfully applied, evaluating the best code for a given scenario.

In this thesis, we propose some original examples of **radar waveform design via convex optimization theory** [13] [14] [15]. After an initial section introducing some basic concepts about waveform design (chapter 2), we analyze in detail code design for a *stand-alone* radar in case of temporal (chapter 3) or spatial-temporal processing (chapter 4), and for a *networked* radar with constraints on the induced interference (chapter 5). Finally, some concluding remarks are presented (chapter 6).

1.1 Notation

We adopt the notation of using boldface for vectors $\boldsymbol{a}$ (lower case), and matrices $\boldsymbol{A}$ (upper case). $a(i)$ for $i = 0, \ldots, N-1$ is the i-th element of the $N-$dimensional vector $\boldsymbol{a}$, while $\boldsymbol{A}(n,m)$ for $(n,m) \in \{0,\ldots,N-1\} \times \{0,\ldots,M-1\}$ is the (n,m)-th entry of the $N \times M$ matrix $\boldsymbol{A}$. The conjugate operator, the transpose operator and the conjugate transpose operator are denoted by the symbols $(\cdot)^*$, $(\cdot)^T$ and $(\cdot)^\dagger$ respectively. $\mathrm{tr}(\cdot)$, $\mathrm{rank}(\cdot)$, $\lambda_{min}(\cdot)$, and $\lambda_{max}(\cdot)$ are respectively the trace, the rank, the minimum eigenvalue and the maximum eigenvalue of the square matrix argument. $\boldsymbol{I}$, $\boldsymbol{0}$ and $\boldsymbol{e}_h$ denote the identity matrix, the matrix with zero entries, and the vector containing all zeros except 1 in the h-th position (their size is determined from the context). The letter j represents the imaginary unit (i.e. $j = \sqrt{-1}$). $\mathbb{R}^N$ and $\mathbb{C}^N$ are the set of N-dimensional real and complex vectors, while $\mathbb{H}^N$ is the set of $N \times N$ hermitian matrices. For any complex number x, we use $\Re(x)$ and $\Im(x)$ to denote respectively the real and the imaginary parts of x, $|x|$ and $\arg(x)$ represent the modulus and the argument of x, and x^* stands for the conjugate of x. The Euclidean norm of the vector $\boldsymbol{x}$ is denoted by $\|\boldsymbol{x}\|$. $E[\cdot]$ denotes statistical expectation. The symbols $\odot$ and $\otimes$ represent the Hadamard element-wise and the Kronecker product, respectively. For any $\boldsymbol{A} \in \mathbb{H}^N$, the curled inequality symbol $\succeq$ (and its strict form $\succ$) is used to denote generalized inequality: $\boldsymbol{A} \succeq \boldsymbol{0}$ means that $\boldsymbol{A}$ is a positive semidefinite matrix ($\boldsymbol{A} \succ \boldsymbol{0}$ for positive definiteness).

Chapter 2

Design Principles

Accuracy, resolution, and ambiguity of the target range and radial velocity measurements, depend on the waveform exploited by the radar. While range is associated with the delay of the received signal, radial velocity depends on the Doppler frequency shift.

If a matched filter is used at the receiver, the ambiguity function represents a suitable tool to study the response of the filter in two dimensions: delay and Doppler. The constant volume underneath the squared ambiguity function involves some trade-offs in signal design. Precisely, a narrow response in one dimension is accompanied by a poor response in the other dimension or by additional ambiguous peaks. Moreover, if we prefer ambiguous peaks to be well spaced in delay, we have to accept them closely spaced in Doppler (and *viceversa*). If we want a good Doppler resolution, we need long coherent signal durations.

Several signals are used for different radar applications and systems. Modern pulsed radars generally use pulse compression waveforms characterized by high pulse energy (with no increase in peak power) and large pulse bandwidth. As a consequence, they provide high range resolution without sacrificing maximum range which depends on the pulse energy.

Unfortunately, there are not easily-handled mathematical techniques to calculate a signal with a prescribed ambiguity function. It follows that the design of a radar signal with desirable characteristics of the ambiguity function is mainly based on the designer's prior knowledge of radar signatures as well as on "*trial and check*" procedures.

In this chapter, we first present (Section 2.1) the mathematical definition of the ambiguity function and describe its relevant properties. Then, we explore, in Section 2.2, the ambiguity function of some basic radar signals: single-frequency rectangular pulse and coherent pulse train. Hence, in Section 2.3, radar coding is presented as a suitable mean to achieve ambiguity function shaping: the ultimate goal is to segregate the volume of the ambiguity function in regions of the delay-Doppler plane where it ceases to be a practical embarrassment [16].

2.1 Ambiguity Function: Definition and Properties

This function was introduced in signal analysis by Ville [17] and in the radar context by Woodward [16]. However, it was known in thermodynamic, since 1932, due to the Nobel prize winner Eugene Wigner, who studied quantum corrections to classical statistical mechanics [18].

The ambiguity function of a signal whose complex envelope is denoted by

$u(t)$ is defined as

$$|\chi(\tau,\nu)| = \left| \int_{-\infty}^{\infty} u(t)u^*(t+\tau)\exp(j2\pi\nu t)dt \right| ,$$

where τ and ν are the incremental delay and Doppler frequency shift respectively. Otherwise stated, it is the modulus of a matched filter output when the input is a Doppler shifted version of the original signal to which the filter is actually matched. It follows that $|\chi(0,0)|$ coincides with the output when the input signal is matched to the nominal delay and Doppler of the filter; nonzero values of τ and ν indicate a target from other range and/or velocity.

Assuming that $u(t)$ has unitary energy, $|\chi(\tau,\nu)|$ complies with the following four relevant properties.

1. **Maximum Value Property.**

$$|\chi(\tau,\nu)| \leq |\chi(0,0)| = 1 ,$$

   the maximum value of the ambiguity function is reached for $(\tau,\nu) = (0,0)$ and is equal to 1.

2. **Unitary Volume Property.**

$$\int_{-\infty}^{\infty}\int_{-\infty}^{\infty} |\chi(\tau,\nu)|^2 \, d\tau d\nu = 1 ,$$

   the volume underneath the squared ambiguity function is unitary.

3. **Symmetry.**

$$|\chi(\tau,\nu)| = |\chi(-\tau,-\nu)| ,$$

the ambiguity function shares a symmetry property about the origin.

4. **Linear Frequency Modulation Property.**

   Given the ambiguity function $|\chi(\tau, \nu)|$ of signal $u(t)$, the ambiguity function $|\chi(\tau, \nu - k\tau)|$ correspond to $u(t)\exp(j\pi kt^2)$.

A more concise way of representing the ambiguity function consists of examining the one-dimensional zero-delay and zero-Doppler *cuts*. The cut of $|\chi(\tau, \nu)|$ along the delay axis is

$$|\chi(\tau, 0)| = \left| \int_{-\infty}^{\infty} u(t)u^*(t+\tau)dt \right| = |R(\tau)|\,,$$

where $R(\tau)$ is the autocorrelation function of $u(t)$. The cut along the Doppler axis is

$$|\chi(0, \nu)| = \left| \int_{-\infty}^{\infty} |u(t)|^2 \exp(j2\pi\nu t)dt \right|\,,$$

which is independent of any phase or frequency modulation of the input signal. Further interesting properties of the ambiguity function can be found in Rihaczek's classic book *Principles of High Resolution Radar* [19].

2.2 Basic Radar Signals

In this section, we present the ambiguity function of some basic signals (single frequency rectangular pulse and coherent pulse train) [20, ch. 8] and discuss their suitability for radar applications.

2.2.1 Rectangular Pulse

The rectangular pulse of length t_p and unitary energy is given by[1]

$$u(t) = \frac{1}{\sqrt{t_p}}\text{rect}\left(\frac{t}{t_p}\right) ,$$

and the corresponding pulse ambiguity function is

$$|\chi(\tau,\nu)| = \begin{cases} \left|\left(1-\frac{|\tau|}{t_p}\right)\text{sinc}\left[t_p(1-|\tau|/t_p)\nu\right]\right|, & \text{if } |\tau| \leq t_p\,, \\ \\ 0 & \text{elsewhere,} \end{cases} \tag{2.1}$$

In Figures 2.1-2.2-2.3, (2.1) is plotted together with the contours and the cuts along the delay and Doppler axes. Notice that (2.1) is limited to an infinite strip whose size on the delay axis is $2t_p$. As to the cut at $\tau = 0$, it exhibits the first nulls at $\nu_{null} = \pm\frac{1}{t_p}$ and, since the sinc$(\cdot)$ function has a peak sidelobe at -13.5 dB, the practical extension of the ambiguity function along the Doppler axis can be considered $2/t_p$.

In general, the square pulse is not a desirable waveform from a pulse compression standpoint, because the autocorrelation function is too wide in time, making it difficult to discern multiple overlapping targets.

[1] The function rect(x) is equal to 1, if $|x| \leq 1/2$, and is equal to 0 elsewhere. The function sinc(x) is defined as sinc$(x) = \dfrac{\sin(\pi x)}{\pi x}$.

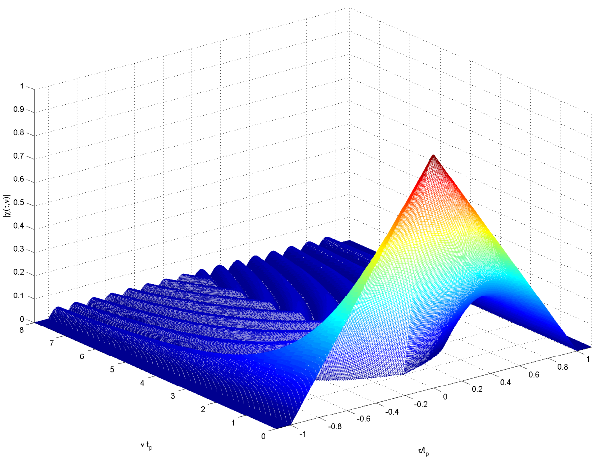

Figure 2.1: Ambiguity function of a constant frequency rectangular pulse of length t_p.

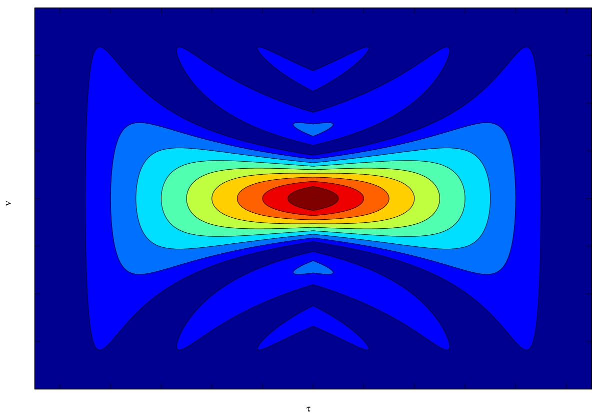

Figure 2.2: Ambiguity function contours of a constant frequency rectangular pulse of length t_p.

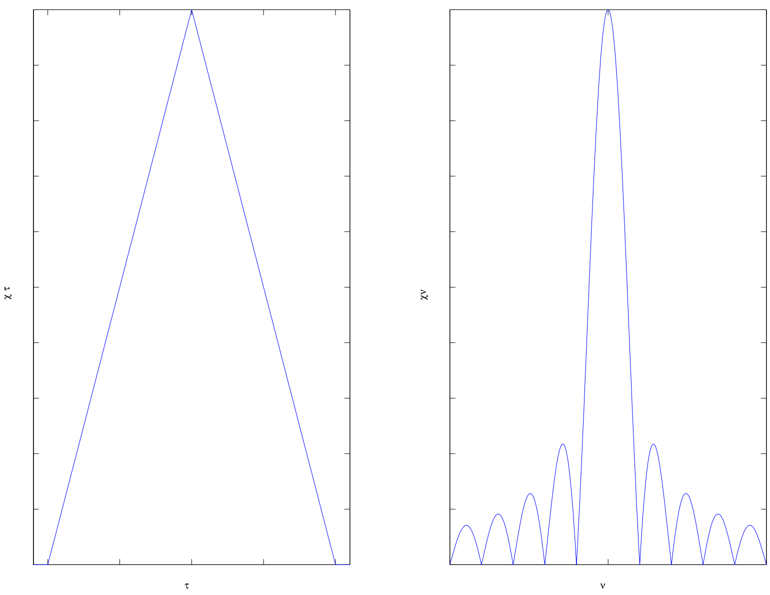

Figure 2.3: Ambiguity function of a constant frequency rectangular pulse of length t_p. a) Zero-Doppler cut. b) Zero-delay cut.

2.2.2 Pulse Train

The complex envelope of a coherent pulse train, composed by N equally spaced pulses, can be written as

$$u(t) = \frac{1}{\sqrt{N}} \sum_{n=1}^{N} p_n(t-(n-1)T_R)\,, \tag{2.2}$$

where T_R is the pulse repetition period and $p_n(t)$ is the complex envelope of the n-th unitary energy pulse. Assuming that the pulse train is uniform (i.e. $p_n(t) = p(t)$, $n = 1, \ldots, N$) and that $T_R/2$ is greater than the pulse duration t_p, the ambiguity function of (2.2) can be expressed as

$$|\chi(\tau,\nu)| = \frac{1}{N} \sum_{p=-(N-1)}^{N-1} |\chi_p(\tau - pT_R, \nu)| \left| \frac{\sin[\pi\nu(N-|p|)T_R]}{\sin(\pi\nu T_R)} \right| \,, \tag{2.3}$$

where $|\chi_p(\tau,\nu)|$ is the (pulse) ambiguity function of $p(t)$.

In Figure 2.4, we assume single-frequency rectangular pulses, $N = 6$, $T_R = 5t_p$ and plot (2.3) in the range-Doppler domain[2]. Due to its shape (2.3) is often referred to as *bed of nails*. The zero-Doppler cut shows that there are multiple triangular windows: the separation between two consecutive peaks is equal to the pulse repetition period T_R. Moreover, all the triangular windows have the same width $2t_p$, but their height decreases as the distance from the origin increases.

As to the cut for $\tau = 0$, there are multiple peaks spaced apart $1/T_R$ and $N-2$ smaller sidelobes between them. The first nulls occur at $\nu = \pm 1/NT_R$,

[2] In the following, the Matlab© toolbox of Levanon and Mozeson [21] is used to plot the ambiguity functions.

namely the width of the main peak (in Doppler) is ruled by the length of the coherent processing interval.

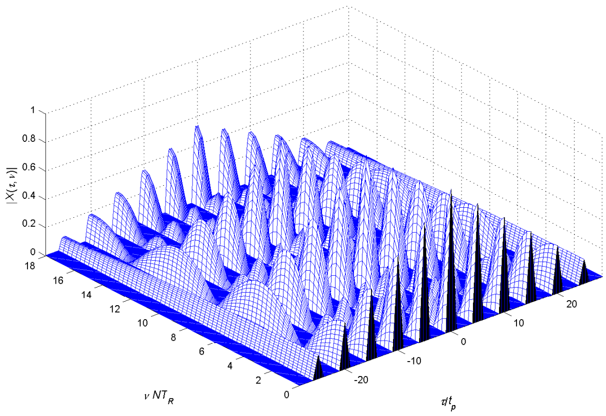

Figure 2.4: Ambiguity function of a coherent train of uniform pulses with $N = 6$, pulse length t_p, and pulse repetition period $T_R = 5t_p$.

2.3 Linearly Coded Pulse Train

The ambiguity function of a coherent pulse train allows a main peak narrow both in range and in Doppler, but exhibits some peaks with almost the same amplitude as the main peak. These might be deleterious and can lead to range/Doppler ambiguities very difficult to resolve.

If we wish to maintain a very narrow main peak but cannot accept the additional peaks typical of the bed of nails, we can spread the volume in a low but wide pedestal around the main peak. This kind of ambiguity function is referred to as *thumbtack* shape and can be obtained considering linearly coded pulse train, i.e.

$$u(t) = \sum_{i=0}^{N-1} c(i)p(t - iT_r)\,,$$

where $[c(0), c(1), \ldots, c(N-1)] = \boldsymbol{c} \in \mathbb{C}^N$ is the radar code, and, as usual, $u(t)$ is the signal's complex envelope and $p(t)$ is the signature of the transmitted pulse. In this case, the ambiguity function can be evaluated as

$$\chi(\lambda, f) = \int_{-\infty}^{\infty} u(\beta)u^*(\beta - \lambda)e^{j2\pi f\beta}d\beta =$$

$$\sum_{l=0}^{N-1}\sum_{m=0}^{N-1} c(l)c^*(m)\chi_p\left(\lambda - (l-m)T_r, f\right),$$

where $\chi_p(\lambda, f)$ is the (pulse) ambiguity function of $p(t)$. Each codeword $c(i)$ modulates both in amplitude and phase a different pulse (see Figure 2.5). Doing so, many advantages can be achieved, as for example better detection performance, reduction in range or Doppler, or rapid decay of the spectral tails [22].

Before proceeding, we remaind that waveform design algorithms usually anticipated their implementation by many years, due to complexity and hardware limitations [22]. For instance, the concept of pulse compression, developed during the Second World War, gained renewed interest only when high-power Klystrons became available [23]. In other words, what seems unpractical today, may not be definitely ruled out in the near future. The lack of signal coherence, which precluded the application of signal compression during the last World War, is today easy. Maybe, the linear power am-

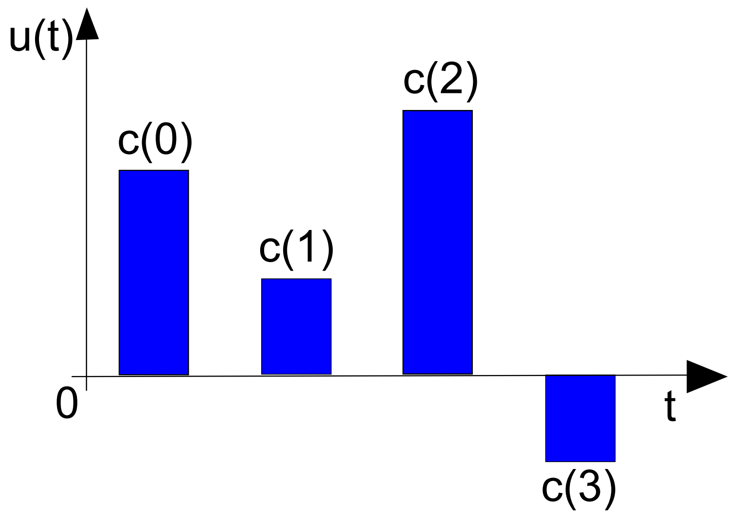

Figure 2.5: Coded pulse train, with length $N = 4$, rectangular pulse $p(t)$, and $T_r = 2t_p$.

plifiers, required to implement amplitude modulated radar signals, will not represent a technological limitation tomorrow.

In the following chapters, we present some original examples of linear pulse coding. First, we propose a coding technique for stand-alone radars, maximizing the detection performance under an accuracy constraint, in the case of temporal (chapter 3) or spatial-temporal processing (chapter 4). Then, we analyze the case of networked radar, evaluating a code which limit the interference induced on other networks elements (chapter 5).

Chapter 3

Coding for Temporal Processing

Radar coding for temporal processing is presented in this chapter. We determine the optimum radar code according to the following criterion: maximization of the detection performance under a control on the region of achievable Doppler estimation accuracies, and imposing a similarity constraint with a prefixed radar code. This last constraint is tantamount to requiring a similarity between the ambiguity functions of the devised waveform and of the pulse train encoded with the prefixed sequence. The resulting optimization problem is nonconvex. In order to solve it, we propose a technique (with polynomial computational complexity) based on the relaxation of the original problem into a Semidefinite Programming (SDP) problem. Thus, the best code is determined through a rank-one decomposition of an optimal solution of the relaxed problem. At the analysis stage, we assess the performance of the new encoding technique in terms of detection capabilities, region of achievable Doppler estimation accuracies, and ambiguity function.

The chapter is organized as follows. In Section 3.1, we present the model for both the transmitted and the received coded signal. In Section 3.2, we discuss some relevant guidelines to formulate the code design problem. In Section 3.3, we introduce the algorithm which solves the presented problem, exploiting SDP relaxation and decomposition. Finally, in Section 3.4, we assess the performance of the proposed encoding method also in comparison with a standard radar code.

3.1 System Model

We consider a radar system which transmits a coherent burst of pulses

$$s(t) = a_t u(t) \exp[j(2\pi f_0 t + \phi)] \, ,$$

where a_t is the transmit signal amplitude,

$$u(t) = \sum_{i=0}^{N-1} c(i) p(t - iT_r) \, ,$$

is the signal's complex envelope, $p(t)$ is the signature of the transmitted pulse, T_r is the pulse repetition time, $[c(0), c(1), \ldots, c(N-1)]^T = \boldsymbol{c} \in \mathbb{C}^N$ is the radar code (assumed without loss of generality with unit norm), f_0 is the carrier frequency, and ϕ is a random phase. Moreover, the pulse waveform $p(t)$ is of duration $T_p \leq T_r$ and has unit energy, i.e.

$$\int_0^{T_p} |p(t)|^2 dt = 1 \, .$$

The signal backscattered by a target with a two-way time delay τ and received by the radar is

$$r(t) = \alpha_r e^{j2\pi(f_0+f_d)(t-\tau)} u(t-\tau) + n(t)\,,$$

where α_r is the complex echo amplitude (accounting for the transmit amplitude, phase, target reflectivity, and channels propagation effects), f_d is the target Doppler frequency, and $n(t)$ is additive disturbance due to clutter and thermal noise.

This signal is down-converted to baseband and filtered through a linear system with impulse response $h(t) = p^*(-t)$. Let the filter output be

$$v(t) = \alpha_r e^{-j2\pi f_0 \tau} \sum_{i=0}^{N-1} c(i) e^{j2\pi i f_d T_r} \chi_p(t - iT_r - \tau, f_d) + w(t)\,,$$

where $\chi_p(\lambda, f)$ is the pulse waveform ambiguity function, and $w(t)$ is the down-converted and filtered disturbance component. The signal $v(t)$ is sampled at $t_k = \tau + kT_r$, $k = 0, \ldots, N-1$, providing the observables[1]

$$v(t_k) = \alpha c(k) e^{j2\pi k f_d T_r} \chi_p(0, f_d) + w(t_k), \qquad k = 0, \ldots, N-1\,,$$

where $\alpha = \alpha_r e^{-j2\pi f_0 \tau}$. Assuming that the pulse waveform time-bandwidth product and the expected range of target Doppler frequencies are such that the single pulse waveform is insensitive to target Doppler shift[2], namely

[1]We neglect range straddling losses and also assume that there are no target range ambiguities.

[2]Notice that this assumption might be restrictive for the cases of very fast moving targets such as fighters and ballistic missiles.

$\chi_p(0, f_d) \sim \chi_p(0,0) = 1$, we can rewrite the samples $v(t_k)$ as

$$v(t_k) = \alpha c(k) e^{j2\pi k f_d T_r} + w(t_k), \qquad k = 0, \ldots, N-1\,.$$

Moreover, denoting by $\boldsymbol{p} = [1, e^{j2\pi f_d T_r}, \ldots, e^{j2\pi(N-1) f_d T_r}]^T$ the temporal steering vector, by $\boldsymbol{v} = [v(t_0), v(t_1), \ldots, v(t_{N-1})]^T$ the collected received samples, and by $\boldsymbol{w} = [w(t_0), w(t_1), \ldots, w(t_{N-1})]^T$ the down-converted and filtered disturbance vector, we get the following vectorial model for the backscattered signal

$$\boldsymbol{v} = \alpha \boldsymbol{c} \odot \boldsymbol{p} + \boldsymbol{w}\,. \tag{3.1}$$

3.2 Problem Formulation

In this section, we introduce some key performance measures to be optimized or controlled during the selection of the radar code: they permit to formulate the design of the code as a nonconvex optimization problem. The metrics considered in this chapter are:

3.2.1 Detection Probability

This is one of the most important performance measures which radar engineers attempt to maximize. We just remind that the problem of detecting a target in the presence of observables described by the model (3.1) can be formulated in terms of the following binary hypotheses test

$$\begin{cases} H_0: & \boldsymbol{v} = \boldsymbol{w} \\ \\ H_1: & \boldsymbol{v} = \alpha \boldsymbol{c} \odot \boldsymbol{p} + \boldsymbol{w}\,. \end{cases} \tag{3.2}$$

Assuming that the disturbance vector $\boldsymbol{w}$ is a zero-mean complex circular Gaussian vector with known positive definite covariance matrix $E[\boldsymbol{w}\boldsymbol{w}^\dagger] = \boldsymbol{M}$, the Generalized Likelihood Ratio Test (GLRT) detector for (3.2), which coincides with the optimum test (according to the Neyman-Pearson criterion) if the phase of α is uniformly distributed in $[0, 2\pi[$ [24], is given by

$$|\boldsymbol{v}^\dagger \boldsymbol{M}^{-1}(\boldsymbol{c} \odot \boldsymbol{p})|^2 \underset{H_0}{\overset{H_1}{\gtrless}} G\,, \tag{3.3}$$

where G is the detection threshold set according to a desired value of the false alarm Probability (P_{fa}). An analytical expression of the detection Probability (P_d), for a given value of P_{fa}, is available both for the cases of nonfluctuating target (NFT) and Rayleigh fluctuating target (RFT). In the former case,

$$P_d = Q\left(\sqrt{2|\alpha|^2 (\boldsymbol{c} \odot \boldsymbol{p})^\dagger \boldsymbol{M}^{-1} (\boldsymbol{c} \odot \boldsymbol{p})}, \sqrt{-2 \ln P_{fa}}\right),$$

while, for the case of RFT with $E[|\alpha|^2] = \sigma_a^2$,

$$P_d = \exp\left(\frac{\ln P_{fa}}{1 + \sigma_a^2 (\boldsymbol{c} \odot \boldsymbol{p})^\dagger \boldsymbol{M}^{-1} (\boldsymbol{c} \odot \boldsymbol{p})}\right),$$

where $Q(\cdot,\cdot)$ denotes the Marcum Q function of order 1. These last expressions show that, given P_{fa}, P_d depends on the radar code, the disturbance covariance matrix and the temporal steering vector only through the SNR, defined as

$$\mathrm{SNR} = \begin{cases} |\alpha|^2(\boldsymbol{c}\odot\boldsymbol{p})^\dagger\boldsymbol{M}^{-1}(\boldsymbol{c}\odot\boldsymbol{p}) & \text{NFT} \\ \\ \sigma_a^2(\boldsymbol{c}\odot\boldsymbol{p})^\dagger\boldsymbol{M}^{-1}(\boldsymbol{c}\odot\boldsymbol{p}) & \text{RFT} \end{cases}$$

Moreover, P_d is an increasing function of SNR and, as a consequence, the maximization of P_d for a given α can be obtained maximizing the SNR over the radar code, i.e.

$$\underset{\boldsymbol{c}}{\mathsf{maximize}} \quad \boldsymbol{c}^\dagger\boldsymbol{R}\boldsymbol{c}\,, \tag{3.4}$$

with $\boldsymbol{R} = \boldsymbol{M}^{-1}\odot(\boldsymbol{p}\boldsymbol{p}^\dagger)^*$.

3.2.2 Doppler Frequency Estimation Accuracy

The Doppler accuracy is bounded below by Cramér-Rao bound (CRB), which provide a lower bound for the variance of unbiased estimate. Constraining the CRB is tantamount to controlling the region of achievable Doppler estimation accuracies, referred to in the following as $\mathcal{A}$. We just highlight that a reliable measurement of the Doppler frequency is very important in radar signal processing because it is directly related to the target radial velocity useful to speed the track initiation, to improve the track accuracy [25], and to classify the dangerousness of the target.

The CRB for known α is given by

$$\Delta_{CR}(f_d) = \frac{\Psi}{2\dfrac{\partial \boldsymbol{h}^\dagger}{\partial f_d}\boldsymbol{M}^{-1}\dfrac{\partial \boldsymbol{h}}{\partial f_d}}, \tag{3.5}$$

where $\boldsymbol{h} = \boldsymbol{c} \odot \boldsymbol{p}$, and $\Psi = \dfrac{1}{|\alpha|^2}$. Noticing that

$$\frac{\partial \boldsymbol{h}}{\partial f_d} = T_r\, \boldsymbol{c} \odot \boldsymbol{p} \odot \boldsymbol{u}\,,$$

with $\boldsymbol{u} = [0, j2\pi, \ldots, j2\pi(N-1)]^T$, (3.5) can be rewritten as

$$\Delta_{CR}(f_d) = \frac{\Psi}{2T_r^2(\boldsymbol{c} \odot \boldsymbol{p} \odot \boldsymbol{u})^\dagger \boldsymbol{M}^{-1}(\boldsymbol{c} \odot \boldsymbol{p} \odot \boldsymbol{u})}\,.$$

As already stated, forcing an upper bound to CRB, for a specified Ψ value, results in a lower bound on the size of $\mathcal{A}$. Hence, according to this guideline, we focus on the class of radar codes complying with the condition

$$\Delta_{CR}(f_d) \leq \frac{\Psi}{2T_r^2\delta_a}\,,$$

which can be equivalently written as

$$\boldsymbol{c}^\dagger \boldsymbol{R}_1 \boldsymbol{c} \geq \delta_a\,, \tag{3.6}$$

where $\boldsymbol{R}_1 = \boldsymbol{M}^{-1} \odot (\boldsymbol{p}\boldsymbol{p}^\dagger)^* \odot (\boldsymbol{u}\boldsymbol{u}^\dagger)^*$, and the parameter δ_a rules the lower bound on the size of $\mathcal{A}$. Otherwise stated, suitably increasing δ_a, we ensure that new points fall in the region $\mathcal{A}$, namely new smaller values for the estimation variance can be theoretically reached by estimators of the target Doppler frequency (see Figure 3.1 for a pictorial description).

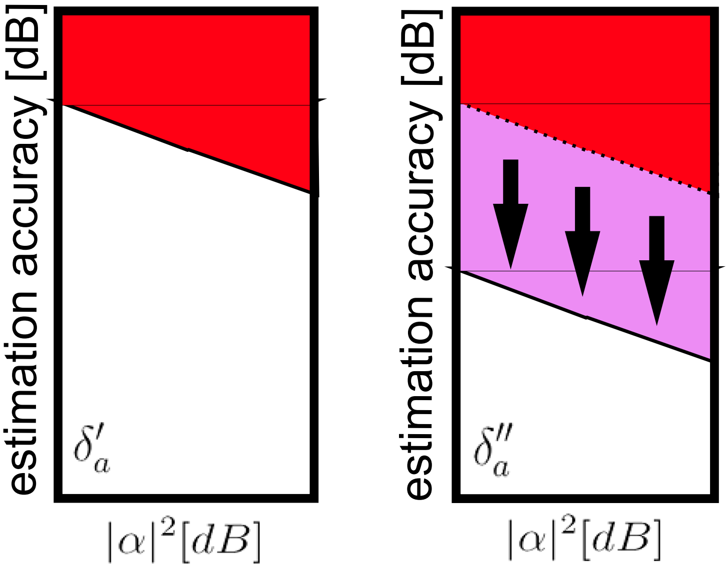

Figure 3.1: Lower bound to the size of the region $\mathcal{A}$ for two different values of δ_a ($\delta'_a < \delta''_a$).

3.2.3 Similarity Constraint

Designing a code which optimizes the detection performance does not provide any kind of control to the shape of the resulting coded waveform. Precisely, the unconstrained optimization of P_d can lead to signals with significant modulus variations, poor range resolution, high peak sidelobe levels, and more in general with an undesired ambiguity function behavior. These drawbacks can be partially circumvented imposing a further constraint to the sought radar code. Precisely, it is required the solution to be similar to a known unitary norm code $\boldsymbol{c}_0$ (i.e. $\|\boldsymbol{c}_0\|^2 = 1$), which shares constant modulus, reasonable range resolution and peak sidelobe level. This is tantamount to imposing that [6]

$$\|\boldsymbol{c} - \boldsymbol{c}_0\|^2 \leq \epsilon\,, \tag{3.7}$$

where the parameter $\epsilon \geq 0$ rules the size of the similarity region. In other words, (3.7) permits to indirectly control the ambiguity function of the considered coded pulse train: the smaller ϵ, the higher the degree of similarity between the ambiguity functions of the designed radar code and of $\boldsymbol{c}_0$.

Reminding the objective function (5.10) and the constraints (3.6) and (3.7), for an unitary norm code $\boldsymbol{c}$ (i.e. $\|\boldsymbol{c}\|^2 = 1$), the design problem can be formulated as follows

$$\mathrm{QP}_1 \begin{cases} \underset{\boldsymbol{c}}{\mathsf{maximize}} & \boldsymbol{c}^\dagger \boldsymbol{R} \boldsymbol{c} \\ \mathsf{subject\ to} & \boldsymbol{c}^\dagger \boldsymbol{c} = 1 \\ & \boldsymbol{c}^\dagger \boldsymbol{R}_1 \boldsymbol{c} \geq \delta_a \\ & \|\boldsymbol{c} - \boldsymbol{c}_0\|^2 \leq \epsilon \end{cases}$$

3.3 Problem Solution

In this section, we propose a technique for the selection of the radar code which attempts to maximize the detection performance but, at the same time, provides a control both on the target Doppler estimation accuracy and on the similarity with a given radar code.

Notice that the nonconvex optimization problem QP_1 can be equivalenty written as

$$\mathrm{QP}_1 \begin{cases} \underset{\boldsymbol{c}}{\text{maximize}} & \boldsymbol{c}^\dagger \boldsymbol{R} \boldsymbol{c} \\ \text{subject to} & \boldsymbol{c}^\dagger \boldsymbol{c} = 1 \\ & \boldsymbol{c}^\dagger \boldsymbol{R}_1 \boldsymbol{c} \geq \delta_a \\ & \Re\left(\boldsymbol{c}^\dagger \boldsymbol{c}_0\right) \geq 1 - \epsilon/2 \end{cases} \tag{3.8}$$

The feasibility of the problem[3] depends not only on the parameters δ_a and ϵ, but also on the prefixed code $\boldsymbol{c}_0$.

Now, we show that an optimal solution of (3.8) can be obtained from an optimal solution of the following Enlarged Quadratic Problem (EQP_1):

$$\mathrm{EQP}_1 \begin{cases} \underset{\boldsymbol{c}}{\text{maximize}} & \boldsymbol{c}^\dagger \boldsymbol{R} \boldsymbol{c} \\ \text{subject to} & \boldsymbol{c}^\dagger \boldsymbol{c} = 1 \\ & \boldsymbol{c}^\dagger \boldsymbol{R}_1 \boldsymbol{c} \geq \delta_a \\ & \Re^2\left(\boldsymbol{c}^\dagger \boldsymbol{c}_0\right) + \Im^2\left(\boldsymbol{c}^\dagger \boldsymbol{c}_0\right) = \boldsymbol{c}^\dagger \boldsymbol{c}_0 \boldsymbol{c}_0^\dagger \boldsymbol{c} \geq \delta_\epsilon \end{cases}$$

where $\delta_\epsilon = (1 - \epsilon/2)^2$. Since the feasibility region of EQP_1 is larger than that of QP_1, every optimal solution of EQP_1, which is feasible for QP_1, is also an optimal solution for QP_1 [3]. Thus, assume that $\bar{\boldsymbol{c}}$ is an optimal solution of EQP_1 and let $\phi = \arg(\bar{\boldsymbol{c}}^\dagger \boldsymbol{c}_0)$. It is easily seen that $\bar{\boldsymbol{c}} e^{j\phi}$ is still an optimal solution of EQP_1. Now, observing that $(\bar{\boldsymbol{c}} e^{j\phi})^\dagger \boldsymbol{c}_0 = |\bar{\boldsymbol{c}}^\dagger \boldsymbol{c}_0|$, $\bar{\boldsymbol{c}} e^{j\phi}$ is a feasible solution of QP_1. In other words, $\bar{\boldsymbol{c}} e^{j \arg(\bar{\boldsymbol{c}}^\dagger \boldsymbol{c}_0)}$ is optimal for both QP_1 and EQP_1.

Now, we have to find an optimal solution of EQP_1 and, to this end, we

[3] The interested reader can refer to a recent work of De Maio et al. [13] for a more detailed discussion on feasibility.

exploit the equivalent matrix formulation

$$\mathrm{EQP}_1 \begin{cases} \underset{\boldsymbol{C}}{\textsf{maximize}} & \mathrm{tr}(\boldsymbol{C}\boldsymbol{R}) \\ \textsf{subject to} & \mathrm{tr}(\boldsymbol{C}) = 1 \\ & \mathrm{tr}(\boldsymbol{C}\boldsymbol{R}_1) \geq \delta_a \\ & \mathrm{tr}(\boldsymbol{C}\boldsymbol{C}_0) \geq \delta_\epsilon \\ & \boldsymbol{C} = \boldsymbol{c}\boldsymbol{c}^\dagger \end{cases} \tag{3.9}$$

where $\boldsymbol{C}_0 = \boldsymbol{c}_0\boldsymbol{c}_0{}^\dagger$.

Problem (3.9) can be relaxed into a SDP, neglecting the rank-one constraint [26]. By doing so we obtain a Relaxed Enlarged Quadratic Problem (REQP_1)

$$\mathrm{REQP}_1 \begin{cases} \underset{\boldsymbol{C}}{\textsf{maximize}} & \mathrm{tr}(\boldsymbol{C}\boldsymbol{R}) \\ \textsf{subject to} & \mathrm{tr}(\boldsymbol{C}) = 1 \\ & \mathrm{tr}(\boldsymbol{C}\boldsymbol{R}_1) \geq \delta_a \\ & \mathrm{tr}(\boldsymbol{C}\boldsymbol{C}_0) \geq \delta_\epsilon \\ & \boldsymbol{C} \succeq \boldsymbol{0} \end{cases} \tag{3.10}$$

The dual problem of (3.10), REQP_1 Dual (REQPD_1), is

$$\mathrm{REQPD}_1 \begin{cases} \underset{y_1, y_2, y_3}{\textsf{minimize}} & y_1 - y_2\delta_a - y_3\delta_\epsilon \\ \textsf{subject to} & y_1\boldsymbol{I} - y_2\boldsymbol{R}_1 - y_3\boldsymbol{C}_0 \succeq \boldsymbol{0} \\ & y_2 \geq 0 \\ & y_3 \geq 0 \end{cases}$$

This problem is bounded below and is strictly feasible, so the optimal value is the same as the primal [27] and the complementary conditions are satisfied at the optimal point, due to the strict feasibility of the primal problem

In the following, we prove that a solution of EQP_1 can be obtained from a solution of REQP_1 $\bar{\boldsymbol{C}}$, and from a solution of REQPD_1 $(\bar{y}_1, \bar{y}_2, \bar{y}_3)$. Precisely, we show how to obtain a rank-one feasible solution of REQP_1 that satisfies optimality conditions (complementary conditions)

$$\operatorname{tr}\left[\left(\bar{y}_1\boldsymbol{I} - \bar{y}_2\boldsymbol{R}_1 - \bar{y}_3\boldsymbol{C}_0 - \boldsymbol{R}\right)\bar{\boldsymbol{C}}\right] = 0 \tag{3.11}$$

$$\left[\operatorname{tr}(\bar{\boldsymbol{C}}\boldsymbol{R}_1) - \delta_a\right]\bar{y}_2 = 0 \tag{3.12}$$

$$\left[\operatorname{tr}(\bar{\boldsymbol{C}}\boldsymbol{C}_0) - \delta_\epsilon\right]\bar{y}_3 = 0 \tag{3.13}$$

Such rank-one solution is also optimal for EQP_1. The proof we propose, is based on the following proposition.

Proposition I. Suppose that $\boldsymbol{X} \in \mathbb{H}^N$ is a positive semidefinite matrix of rank R, while $\boldsymbol{A}, \boldsymbol{B} \in \mathbb{H}^N$. There is a rank-one decomposition of $\boldsymbol{X}$ (synthetically denoted as $\mathcal{D}_1(\boldsymbol{X}, \boldsymbol{A}, \boldsymbol{B})$),

$$\boldsymbol{X} = \sum_{r=1}^{R} \boldsymbol{x}_r\boldsymbol{x}_r^\dagger$$

such that

$$\boldsymbol{x}_r^\dagger\boldsymbol{A}\boldsymbol{x}_r = \frac{\operatorname{tr}(\boldsymbol{X}\boldsymbol{A})}{R} \text{ and } \boldsymbol{x}_r^\dagger\boldsymbol{B}\boldsymbol{x}_r = \frac{\operatorname{tr}(\boldsymbol{X}\boldsymbol{B})}{R}$$

Proof. See Huang and Zhang decomposition theorem [28].

Moreover, we have to distinguish four possible cases:

1. $\operatorname{tr}\left(\bar{\boldsymbol{C}}\boldsymbol{R}_1\right) - \delta_a > 0$ and $\operatorname{tr}\left(\bar{\boldsymbol{C}}\boldsymbol{C}_0\right) - \delta_\epsilon > 0$
2. $\operatorname{tr}\left(\bar{\boldsymbol{C}}\boldsymbol{R}_1\right) - \delta_a = 0$ and $\operatorname{tr}\left(\bar{\boldsymbol{C}}\boldsymbol{C}_0\right) - \delta_\epsilon > 0$

3. $\mathrm{tr}\left(\bar{\boldsymbol{C}}\boldsymbol{R}_1\right) - \delta_a > 0$ and $\mathrm{tr}\left(\bar{\boldsymbol{C}}\boldsymbol{C}_0\right) - \delta_\epsilon = 0$

4. $\mathrm{tr}\left(\bar{\boldsymbol{C}}\boldsymbol{R}_1\right) - \delta_a = 0$ and $\mathrm{tr}\left(\bar{\boldsymbol{C}}\boldsymbol{C}_0\right) - \delta_\epsilon = 0$

Case 1: Using the decomposition $\mathcal{D}_1(\bar{\boldsymbol{C}}, \boldsymbol{I}, \boldsymbol{R}_1)$ of Proposition I, we can express $\bar{\boldsymbol{C}}$ as

$$\bar{\boldsymbol{C}} = \sum_{r=1}^{R} \boldsymbol{c}_r \boldsymbol{c}_r{}^\dagger$$

Now, we show that there exists a $k \in \{1, \dots, R\}$ such that $\sqrt{R}\boldsymbol{c}_k$ is an optimal solution of EQP_1. Specifically, we first prove that $(\sqrt{R}\boldsymbol{c}_k)(\sqrt{R}\boldsymbol{c}_k)^\dagger$ is a feasible solution of REQP_1, and then that $(\sqrt{R}\boldsymbol{c}_k)(\sqrt{R}\boldsymbol{c}_k)^\dagger$ and $(\bar{y}_1, \bar{y}_2, \bar{y}_3)$ comply with the optimality conditions, i.e. $(\sqrt{R}\boldsymbol{c}_k)(\sqrt{R}\boldsymbol{c}_k)^\dagger$ is a rank-one optimal solution of REQP_1 and, hence, $\sqrt{R}\boldsymbol{c}_k$ is an optimal solution of EQP_1.

The decomposition $\mathcal{D}_1(\bar{\boldsymbol{C}}, \boldsymbol{I}, \boldsymbol{R}_1)$ implies that every $(\sqrt{R}\boldsymbol{c}_r)(\sqrt{R}\boldsymbol{c}_r)^\dagger$, $r = 1, \dots, R$ satisfies the first and the second constraints in REQP_1. Moreover, there must be a $k \in \{1, \dots, R\}$ such that $(\sqrt{R}\boldsymbol{c}_k)^\dagger \boldsymbol{C}_0 (\sqrt{R}\boldsymbol{c}_k) \geq \delta_\epsilon$. In fact, if $(\sqrt{R}\boldsymbol{c}_r)^\dagger \boldsymbol{C}_0 (\sqrt{R}\boldsymbol{c}_r) < \delta_\epsilon$ for every r, then

$$\begin{aligned}
\sum_{r=1}^{R} (\sqrt{R}\boldsymbol{c}_r)^\dagger \boldsymbol{C}_0 (\sqrt{R}\boldsymbol{c}_r) &< R\delta_\epsilon \\
\mathrm{tr}\left[\left(\sum_{r=1}^{R} \sqrt{R}\boldsymbol{c}_r \boldsymbol{c}_r^\dagger \sqrt{R}\right) \boldsymbol{C}_0\right] &< R\delta_\epsilon \\
\mathrm{tr}(\bar{\boldsymbol{C}}\boldsymbol{C}_0) &< \delta_\epsilon
\end{aligned}$$

which is in contrast with the feasibility of $\bar{\boldsymbol{C}}$. This proves that there exists at least one $k \in \{1, \dots, R\}$ for which $(\sqrt{R}c_k)(\sqrt{R}c_k)^\dagger$ is feasible for REQP_1. As to fulfillment of the optimality conditions, $\mathrm{tr}\left(\bar{\boldsymbol{C}}\boldsymbol{R}_1\right) - \delta_a > 0$ and $\mathrm{tr}\left(\bar{\boldsymbol{C}}\boldsymbol{C}_0\right) - \delta_\epsilon > 0$ imply $\bar{y}_2 = 0$ and $\bar{y}_3 = 0$, namely (3.12) and (3.13) are verified for every $(\sqrt{R}\boldsymbol{c}_r)(\sqrt{R}\boldsymbol{c}_r)^\dagger$, with $r = 1, \ldots, R$. Therefore, (3.11) can be recast as

$$\operatorname{tr}\left[(\bar{y}_1\boldsymbol{I} - \boldsymbol{R})\bar{\boldsymbol{C}}\right] = \operatorname{tr}\left[(\bar{y}_1\boldsymbol{I} - \boldsymbol{R})\left(\sum_{r=0}^{R}\boldsymbol{c}_r\boldsymbol{c}_r^\dagger\right)\right] = 0$$

which, since $\boldsymbol{c}_r\boldsymbol{c}_r^\dagger \succeq \boldsymbol{0}$, $r = 1, \ldots, R$, and $\bar{y}_2\boldsymbol{I} - \boldsymbol{R} \succeq \boldsymbol{0}$ (from the first constraint of REQPD_1), implies

$$\operatorname{tr}\left[(\bar{y}_2\boldsymbol{I} - \boldsymbol{R})\left(\sqrt{R}\boldsymbol{c}_r{\boldsymbol{c}_r}^\dagger\sqrt{R}\right)\right] = 0$$

It follows that there exists one $k \in \{1, \ldots, R\}$ such that $(\sqrt{R}\boldsymbol{c}_k)(\sqrt{R}\boldsymbol{c}_k)^\dagger$ is an optimal solution of REQP_1, and thus, $\sqrt{R}\boldsymbol{c}_k$ is an optimal solution of EQP_1.

Cases 2 and 3: The proof is very similar to Case 1, hence we omit it.

Case 4: In this case, all the constraints of REQP_1 are active, namely $\operatorname{tr}(\bar{\boldsymbol{C}}) = 1$, $\operatorname{tr}(\bar{\boldsymbol{C}}\boldsymbol{R}_1) = \delta_a$, and $\operatorname{tr}(\bar{\boldsymbol{C}}\boldsymbol{C}_0) = \delta_\epsilon$. It follows that

$$\operatorname{tr}[\bar{\boldsymbol{C}}\,(\boldsymbol{R}_1/\delta_a - \boldsymbol{I})] \;=\; 0$$

and

$$\operatorname{tr}[\bar{\boldsymbol{C}}\,(\boldsymbol{C}_0/\delta_\epsilon - \boldsymbol{I})] \;=\; 0$$

According to $\mathcal{D}_1(\bar{\boldsymbol{C}}, \boldsymbol{R}_1/\delta_a - \boldsymbol{I}, \boldsymbol{C}_0/\delta_\epsilon - \boldsymbol{I})$, we decompose $\bar{\boldsymbol{C}}$ as

$$\bar{\boldsymbol{C}} = \sum_{r=1}^{R}\boldsymbol{c}_r{\boldsymbol{c}_r}^\dagger\,,$$

and observe that

$$\mathrm{tr}\left(\boldsymbol{c}_r\boldsymbol{c}_r{}^\dagger\right) = \frac{1}{\gamma_r}\,, \qquad r = 1, \ldots, R\,, \tag{3.14}$$

with $\gamma_r > 1$ such that $\sum_{r=1}^{R} 1/\gamma_r = 1$.

We now prove that each $(\sqrt{\gamma_r}\boldsymbol{c}_r)(\sqrt{\gamma_r}\boldsymbol{c}_r)^\dagger$ is an optimal solution of REQP_1. Precisely, we first show that $(\sqrt{\gamma_r}\boldsymbol{c}_r)(\sqrt{\gamma_r}\boldsymbol{c}_r)^\dagger$ is in the feasible region of REQP_1 and then we prove that $(\sqrt{\gamma_r}\boldsymbol{c}_r)(\sqrt{\gamma_r}\boldsymbol{c}_r)^\dagger$ satisfies the optimality conditions. Equation (3.14) implies that the first constraint in REQP_1 is satisfied. From the feasibility of $\bar{\boldsymbol{C}}$ and from the used decomposition, we can also claim that $(\sqrt{\gamma_r}\boldsymbol{c}_r)(\sqrt{\gamma_r}\boldsymbol{c}_r)^\dagger$ satisfies the second and the third constraints of REQP_1. In fact, with reference to the second constraint we have

$$\begin{aligned}
\mathrm{tr}[\bar{\boldsymbol{C}}\,(\boldsymbol{R}_1/\delta_a - \boldsymbol{I})] &= 0\\
\frac{\mathrm{tr}[\bar{\boldsymbol{C}}\,(\boldsymbol{R}_1/\delta_a - \boldsymbol{I})]}{R} &= 0\\
\boldsymbol{c}_r{}^\dagger\,(\boldsymbol{R}_1/\delta_a - \boldsymbol{I})\,\boldsymbol{c}_r &= 0\\
\boldsymbol{c}_r{}^\dagger(\boldsymbol{R}_1/\delta_a)\boldsymbol{c}_r &= \boldsymbol{c}_r{}^\dagger\boldsymbol{c}_r\\
\boldsymbol{c}_r{}^\dagger(\boldsymbol{R}_1/\delta_a)\boldsymbol{c}_r &= \mathrm{tr}\left(\boldsymbol{c}_r\boldsymbol{c}_r{}^\dagger\right)\\
\boldsymbol{c}_r{}^\dagger(\boldsymbol{R}_1/\delta_a)\boldsymbol{c}_r &= 1/\gamma_r\\
\sqrt{\gamma_r}\boldsymbol{c}_r{}^\dagger(\boldsymbol{R}_1/\delta_a)\sqrt{\gamma_r}\boldsymbol{c}_r &= 1\\
\sqrt{\gamma_r}\boldsymbol{c}_r{}^\dagger\boldsymbol{R}_1\sqrt{\gamma_r}\boldsymbol{c}_r &= \delta_a
\end{aligned}$$

As to the third constraint, we observe that

$$\begin{aligned}
\mathrm{tr}[\bar{\boldsymbol{C}}\,(\boldsymbol{C}_0/\delta_\epsilon - \boldsymbol{I})] &= 0\\
\frac{\mathrm{tr}[\bar{\boldsymbol{C}}\,(\boldsymbol{C}_0/\delta_\epsilon - \boldsymbol{I})]}{R} &= 0\\
{\boldsymbol{c}_r}^\dagger\,(\boldsymbol{C}_0/\delta_\epsilon - \boldsymbol{I})\,\boldsymbol{c}_r &= 0\\
{\boldsymbol{c}_r}^\dagger(\boldsymbol{C}_0/\delta_\epsilon)\boldsymbol{c}_r &= {\boldsymbol{c}_r}^\dagger\boldsymbol{c}_r\\
{\boldsymbol{c}_r}^\dagger(\boldsymbol{C}_0/\delta_\epsilon)\boldsymbol{c}_r &= \mathrm{tr}\left(\boldsymbol{c}_r{\boldsymbol{c}_r}^\dagger\right)\\
{\boldsymbol{c}_r}^\dagger(\boldsymbol{C}_0/\delta_\epsilon)\boldsymbol{c}_r &= 1/\gamma_r\\
\sqrt{\gamma_r}{\boldsymbol{c}_r}^\dagger(\boldsymbol{C}_0/\delta_\epsilon)\sqrt{\gamma_r}\boldsymbol{c}_r &= 1\\
\sqrt{\gamma_r}{\boldsymbol{c}_r}^\dagger\boldsymbol{C}_0\sqrt{\gamma_r}\boldsymbol{c}_r &= \delta_\epsilon
\end{aligned}$$

It remains to prove that $(\sqrt{\gamma_r}\boldsymbol{c}_r)(\sqrt{\gamma_r}\boldsymbol{c}_r)^\dagger$ complies with the three optimality conditions. As to the first, we note that

$$\begin{aligned}
\mathrm{tr}\left[(\bar{y}_1\boldsymbol{I} - \bar{y}_2\boldsymbol{R}_1 - \bar{y}_3\boldsymbol{C}_0 - \boldsymbol{R})\,\bar{\boldsymbol{C}}\right] &=\\
\mathrm{tr}\left[(\bar{y}_1\boldsymbol{I} - \bar{y}_2\boldsymbol{R}_1 - \bar{y}_3\boldsymbol{C}_0 - \boldsymbol{R})\textstyle\sum_{r=1}^{R}\boldsymbol{c}_r{\boldsymbol{c}_r}^\dagger\right] &= 0
\end{aligned}$$

which, since $\boldsymbol{c}_r{\boldsymbol{c}_r}^\dagger \succeq \boldsymbol{0}$ and $\bar{y}_1\boldsymbol{I} - \bar{y}_2\boldsymbol{R}_1 - \bar{y}_3\boldsymbol{C}_0 - \boldsymbol{R} \succeq \boldsymbol{0}$, implies that

$$\mathrm{tr}\left[(\bar{y}_1\boldsymbol{I} - \bar{y}_2\boldsymbol{R}_1 - \bar{y}_3\boldsymbol{C}_0 - \boldsymbol{R})\,(\sqrt{\gamma_r}\boldsymbol{c}_r\sqrt{\gamma_r}{\boldsymbol{c}_r}^\dagger)\right] = 0\,,$$

proving the first optimality condition. The compliance with the second optimality condition can be shown as follows

$$
\begin{aligned}
\boldsymbol{c}_r{}^{\dagger}\left(\boldsymbol{R}_1/\delta_a - \boldsymbol{I}\right)\boldsymbol{c}_r &= 0 \\
\left(\sqrt{\gamma_r}\boldsymbol{c}_r\right)^{\dagger}\left(\boldsymbol{R}_1/\delta_a - \boldsymbol{I}\right)\sqrt{\gamma_r}\boldsymbol{c}_r &= 0 \\
\left[\sqrt{\gamma_r}\boldsymbol{c}_r{}^{\dagger}\left(\boldsymbol{R}_1/\delta_a - \boldsymbol{I}\right)\sqrt{\gamma_r}\boldsymbol{c}_r\right]\bar{y}_2 &= 0 \\
\mathrm{tr}\left[\left(\boldsymbol{R}_1/\delta_a - \boldsymbol{I}\right)\left(\sqrt{\gamma_r}\boldsymbol{c}_r\boldsymbol{c}_r^{\dagger}\sqrt{\gamma_r}\right)\bar{y}_2\right] &= 0
\end{aligned}
$$

As to the third optimality condition, we have

$$
\begin{aligned}
\boldsymbol{c}_r{}^{\dagger}\left(\boldsymbol{C}_0/\delta_\epsilon - \boldsymbol{I}\right)\boldsymbol{c}_r &= 0 \\
\sqrt{\gamma_r}\boldsymbol{c}_r{}^{\dagger}\left(\boldsymbol{C}_0/\delta_\epsilon - \boldsymbol{I}\right)\sqrt{\gamma_r}\boldsymbol{c}_r &= 0 \\
\left[\sqrt{\gamma_r}\boldsymbol{c}_r{}^{\dagger}\left(\boldsymbol{C}_0/\delta_\epsilon - \boldsymbol{I}\right)\sqrt{\gamma_r}\boldsymbol{c}_r\right]\bar{y}_3 &= 0 \\
\mathrm{tr}\left[\left(\boldsymbol{C}_0/\delta_\epsilon - \boldsymbol{I}\right)\left(\sqrt{\gamma_r}\boldsymbol{c}_r\sqrt{\gamma_r}\boldsymbol{c}_r^{\dagger}\right)\bar{y}_3\right] &= 0
\end{aligned}
$$

and the proof is completed.

In conclusion, using the decomposition of Proposition I, we have shown how to construct a rank-one optimal solution of REQP_1, which is tantamount to finding an optimal solution of EQP_1. Summarizing, the optimum code can be constructed according to the procedure reported in Algorithm 1.

The computational complexity connected with the implementation of the algorithm is polynomial as both the SDP problem and the decomposition of Proposition I can be performed in polynomial time. In fact, the amount of operations, involved in solving the SDP problem, is $O\left(N^{3.5}\right)$ [27, p. 250] and the rank-one decomposition requires $O(N^3)$ operations.

Algorithm 1 Temporal Processing (TiP) Coding

```
Input: M, p, c_0, δ_a, δ_ε;
Output: c_TiP;
1: solve the SDP problem REQP_1 finding an optimal solution C̄;
2: if tr(C̄R_1) − δ_a = 0 and tr(C̄C_0) − δ_ε = 0 then
3:    decompose Σ_{r=1}^{R} c_r c_r^† = D_1(C̄, R_1/δ_a − I, C_0/δ_ε − I);
4:    compute c̄ = √γ_1 c_1, with γ_1 = 1/‖c_1‖^2
5: else
6:    decompose Σ_{r=1}^{R} c_r c_r^† = D_1(C̄, R_1, I);
7:    Find k such that c_k^† C_0 c_k ≥ δ_ε/R and compute c̄ = √R c_k;
8: end
9: c_TiP = c̄ e^{jφ}, with φ = arg(c̄^† c_0)
```

3.4 Performance Analysis

The present section is aimed at analyzing the performance of the proposed encoding scheme. To this end, we assume that the disturbance covariance matrix is exponentially shaped with one-lag correlation coefficient $\rho = 0.8$, i.e.

$$\boldsymbol{M}(i,j) = \rho^{|i-j|}\,,$$

and fix P_{fa} of the receiver (5.5) to 10^{-6}. The analysis is conducted in terms of P_d, region of achievable Doppler estimation accuracies, and ambiguity function of the coded pulse train which results exploiting the proposed algorithm, i.e.

$$\chi(\lambda, f) = \sum_{l=0}^{N-1}\sum_{m=0}^{N-1} c_{{}_{TiP}}(l)c^*_{{}_{TiP}}(m)\chi_p[\lambda - (l-m)T_r, f]\,,$$

where $[c_{{}_{TiP}}(0), \ldots, c_{{}_{TiP}}(N-1)]^T = \boldsymbol{c}_{{}_{TiP}}$ is an optimum code. As to the temporal steering vector $\boldsymbol{p}$, we set the normalized Doppler frequency[4] $f_{{}_d}T_r = 0$. The convex optimization Matlab© toolbox SeDuMi [4] is exploited for solv-

[4] We have also considered other values for the target normalized Doppler frequency. The results, not reported here, confirm the performance behavior showed in this section.

ing the SDP relaxation. The decomposition $\mathcal{D}_1(\cdot,\cdot,\cdot)$ of the SeDuMi solution is performed using the technique described by Huang and Zhang [28]. As similarity code, we set $\boldsymbol{c}_0$ as a generalized Barker Code: generalized Barker codes are polyphase sequences whose autocorrelation function has minimal peak-to-sidelobe ratio excluding the outermost sidelobe. Examples of such sequences were found for all $N \leq 45$ [29] [30] using numerical optimization techniques. In the simulations of this subsection, we assume $N = 7$ and set the similarity code equal to the generalized Barker sequence $\boldsymbol{c}_0 = [0.3780, 0.3780, -0.1072-0.3624j, -0.0202-0.3774j, 0.2752+0.2591j, 0.1855-0.3293j, 0.0057+0.3779j]^T$.

In Figure 3.2, we plot P_d of the optimum code (according to the proposed criterion) versus $|\alpha|^2$ for several values of δ_a, $\delta_\epsilon = 0.01$, and for nonfluctuating target. In the same figure, we also represent both the P_d of the similarity code as well as the benchmark performance, namely the maximum achievable detection rate (over the radar code), given by

$$P_d = Q\left(\sqrt{2|\alpha|^2\lambda_{max}\left(\boldsymbol{R}\right)}, \sqrt{-2\ln P_{fa}}\right).$$

The curves show that increasing δ_a we get lower and lower values of P_d for a given $|\alpha|^2$ value. This was expected since the higher δ_a the smaller the feasibility region of the optimization problem to be solved for finding the code. Nevertheless the proposed encoding algorithm usually ensures a better detection performance than the original generalized Barker code.

In Figure 3.3, the normalized CRB ($\mathrm{CRB}_n = T_r^2\mathrm{CRB}$) is plotted versus $|\alpha|^2$ for the same values of δ_a as in Figure 3.2. The best value of CRB_n is

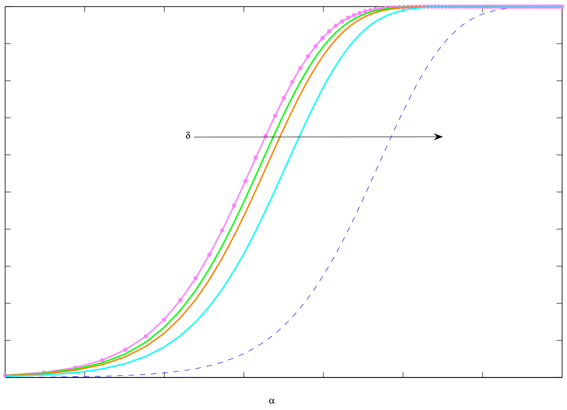

Figure 3.2: P_d versus $|\alpha|^2$ for $P_{fa} = 10^{-6}$, $N = 7$, $\delta_\epsilon = 0.01$, nonfluctuating target, and several values of $\delta_a \in \{10^{-6}, 6165.5, 6792.6, 7293.9\}$. Generalized Barker code (dashed curve). Code which maximizes the SNR for a given δ_a (solid curve). Benchmark code (dotted-marked curve). Notice that the curve for $\delta_a = 10^{-6}$ perfectly overlaps with the benchmark P_d.

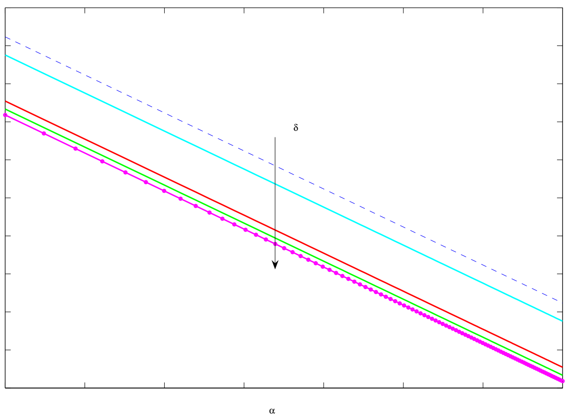

Figure 3.3: CRB_n versus $|\alpha|^2$ for $N = 7$, $\delta_\epsilon = 0.01$ and several values of $\delta_a \in \{10^{-6}, 6165.5, 6792.6, 7293.9\}$. Generalized Barker code (dashed curve). Code which maximizes the SNR for a given δ_a (solid curve). Benchmark code (dotted-marked curve). Notice that the curve for $\delta_a = 7293.9$ perfectly overlaps with the benchmark CRB_n.

plotted too, i.e.

$$\mathrm{CRB}_n = \frac{1}{2|\alpha|^2 \lambda_{max}\left(\boldsymbol{R}_1\right)} .$$

The curves highlight that increasing δ_a better and better CRB values can be achieved. This is in accordance with the considered criterion, because the higher δ_a the larger the size of the region $\mathcal{A}$. Summarizing, the joint analysis of Figures 3.2-3.3 shows that a trade-off can be realized between the detection performance and the estimation accuracy. Moreover, there exist codes capable of outperforming the generalized Barker code both in terms of P_d and size of $\mathcal{A}$.

The effects of the similarity constraint are analyzed in Figure 3.4. Therein, we set $\delta_a = 10^{-6}$ and consider several values of δ_ϵ. The plots show that increasing δ_ϵ worse and worse P_d values are obtained; this behavior can be explained observing that the smaller δ_ϵ the larger the size of the similarity region. However, this detection loss is compensated for an improvement of the coded pulse train ambiguity function. This is shown in Figures $3.6 - 3.7$, where the modulus of that function is plotted assuming rectangular pulses, $T_r = 5T_p$ and the same values of δ_a and δ_ϵ as in Figure 3.4. Moreover, for comparison purposes, the ambiguity function modulus of $\boldsymbol{c}_0$ is plotted too (Figure 3.5). The plots highlight that the closer δ_ϵ to 1 the higher the degree of similarity between the ambiguity functions of the devised and of the prefixed codes. This is due to the fact that increasing δ_ϵ is tantamount to reducing the size of the similarity region. In other words, we force the devised code to be similar and similar to the prefixed one and, as a consequence, we get similar and similar ambiguity functions.

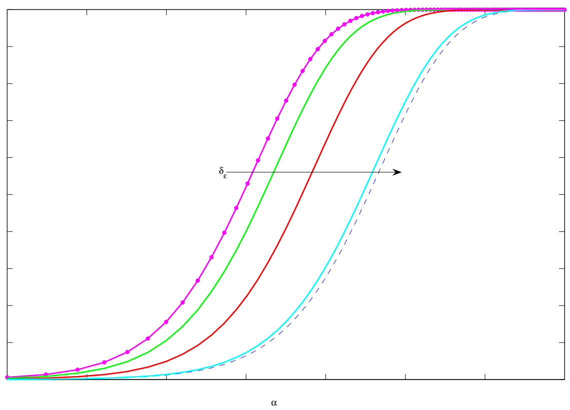

Figure 3.4: P_d versus $|\alpha|^2$ for $P_{fa} = 10^{-6}$, $N = 7$, $\delta_a = 10^{-6}$, nonfluctuating target, and several values of $\delta_\epsilon \in \{0.01, 0.6239, 0.8997, 0.9994\}$. Generalized Barker code (dashed curve). Code which maximizes the SNR for a given δ_ϵ (solid curve). Benchmark code (dotted-marked curve). Notice that the curve for $\delta_\epsilon = 0.01$ perfectly overlaps with the benchmark P_d.

Finally, Table 5.1 provides the average number of iterations N_{it} and CPU time (in seconds) which are required to solve the SDP problem (3.10). The computer used to get these results is equipped with a 3 GHz Intel XEON processor.

Table 3.1: Average N_{it} and CPU time in seconds required to solve problem (3.10). Generalized Barker code as similarity sequence.

δ_a	δ_ϵ	Average N_{it}	Average CPU time (sec)
10^{-6}	0.01	21	0.30
6165.5	0.01	11	0.15
6792.6	0.01	11	0.15
7293.9	0.01	16	0.19
10^{-6}	0.6239	22	0.28
10^{-6}	0.8997	19	0.24
10^{-6}	0.9994	17	0.23

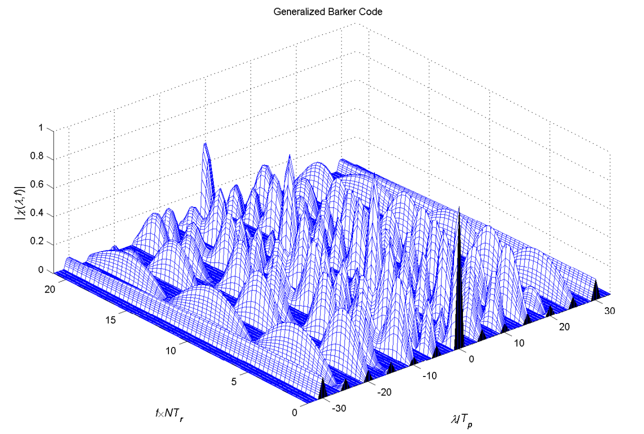

Figure 3.5: Ambiguity function modulus of the generalized Barker code $\boldsymbol{c}_0 = [0.3780, 0.3780, -0.1072 - 0.3624\jmath, -0.0202 - 0.3774\jmath, 0.2752 + 0.2591\jmath, 0.1855 - 0.3293\jmath, 0.0057 + 0.3779\jmath]^T$.

3.5 Conclusions

In this chapter, we have considered the design of coded waveforms in the presence of colored Gaussian disturbance. We have devised and assessed an algorithm which attempts to maximize the detection performance under a control both on the region of achievable values for the Doppler estimation accuracy, and on the similarity with a given radar code. The proposed

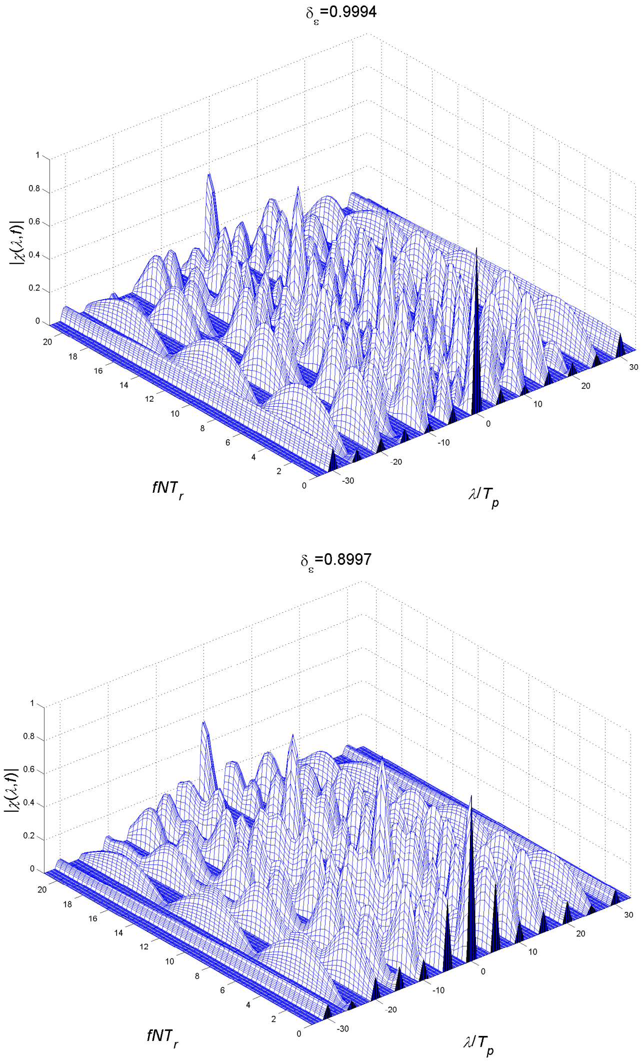

Figure 3.6: Ambiguity function modulus of code which maximizes the SNR for $N = 7$, $\delta_a = 10^{-6}$, $\mathbf{c}_0$ generalized Barker code, and several values of δ_ϵ: (up) $\delta_\epsilon = 0.9994$, (down) $\delta_\epsilon = 0.8997$.

technique, whose implementation requires a polynomial computational complexity, is based on the SDP relaxation of nonconvex quadratic problems and on a suitable rank-one decomposition of a positive semidefinite Hermitian matrix. The analysis of the algorithm has been conducted in terms of

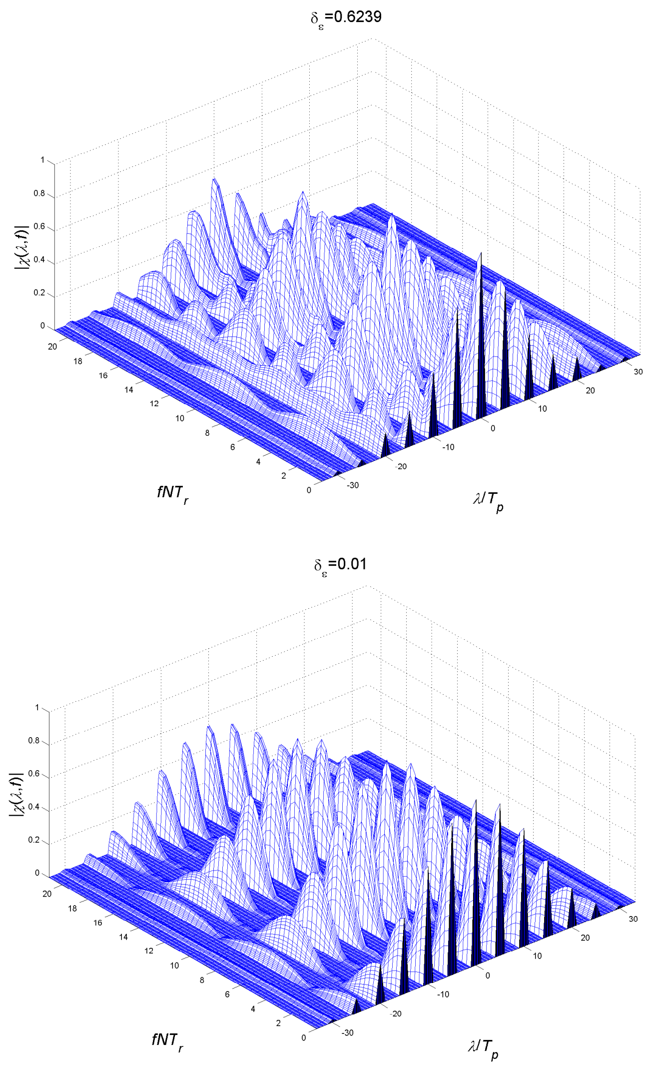

Figure 3.7: Ambiguity function modulus of code which maximizes the SNR for $N = 7$, $\delta_a = 10^{-6}$, $\mathbf{c}_0$ generalized Barker code, and several values of δ_ϵ: (up) $\delta_\epsilon = 0.6239$, (down) $\delta_\epsilon = 0.01$.

the following performance metrics:

- detection performance,
- region of achievable Doppler estimation accuracies,

- ambiguity function of the coded pulse waveform.

Hence, the trade-off among the three considered performance measures has been thoroughly studied and commented.

Possible future research tracks might concern the possibility to make the algorithm adaptive with respect to the disturbance covariance matrix, namely to devise techniques which jointly estimate the code and the covariance. Moreover, it should be investigated the introduction in the code design optimization problem of knowledge-based constraints, ruled by the *apriori* information that the radar has about the surrounding environment.

In the next chapter, we will extend the proposed framework to the general case of spatial-temporal processing. It implies that we will add another accuracy constraint. As a consequence, a perfect equivalence between the nonconvex formulation and the relaxed convex formulation[5] is not possible. However, in the following chapter, we will identify most cases where the equivalence is valid, proposing appliable algorithms.

[5]This case is usually referred as *hidden convexity*.

Chapter 4

Coding for Space-Time Processing

In this chapter, we deal with the problem of constrained code optimization for radar Space-Time Adaptive Processing (STAP) in the presence of colored Gaussian disturbance. At the design stage, we devise a code design algorithm complying with the following optimality criterion: maximization of the detection performance under a control on the regions of achievable values for the temporal and spatial Doppler estimation accuracy, and on the degree of similarity with a prefixed radar code. The resulting quadratic optimization problem is solved resorting to a convex relaxation that belongs to the SDP class. An optimal solution of the initial problem is then constructed through a suitable rank-one decomposition of an optimal solution of the relaxed one. At the analysis stage, we assess the performance of the new algorithm both on simulated data and on the standard challenging Knowledge-Aided Sensor Signal Processing and Expert Reasoning (KASSPER) datacube.

The chapter is organized as follows. In Section 4.1, we present the model for both the transmitted and the received coded signal. In Section 4.2, we formulate the code design optimization problem. In Section 4.3, we introduce the algorithm which exploits SDP relaxation and provides a solution to the aforementioned problem. In Section 4.4, we assess the performance of the proposed encoding method also in comparison with a standard radar code. Finally, in Section 4.5, we draw conclusions and outline possible future research tracks.

4.1 System Model

The STAP signal model adopted in this chapter is that developed by Ward [31, ch. 1], with the addition of a temporal coding on the transmitted coherent burst of pulses. Specifically, data are collected by a narrowband antenna array with M spatial channels which, for simplicity, we assume colinear, omnidirectional, and equally spaced. Each channel receives N echoes corresponding to the returns of a coherent coded pulse train composed of N pulses. It is assumed that the complex envelope of the transmitted signal is

$$u(t) = a_t e^{j\Phi_t} \sum_{i=0}^{N-1} c(i) p(t - iT_r)$$

where T_r is the Pulse Repetition Time (PRT), $[c(0), c(1), \ldots, c(N-1)]^T = \boldsymbol{c} \in \mathbb{C}^N$ is the radar code (assumed without loss of generality with unit norm), $p(t)$ is the pulse waveform of duration T_p and with unit energy, a_t and Φ_t are respectively the amplitude and the random phase of $u(t)$.

Following Ward's model [31], we formulate the problem of detecting a target in the presence of observables in terms of the following binary hypothesis test:

$$\begin{cases} H_0 : & \boldsymbol{r} = \boldsymbol{i} + \boldsymbol{n} \\ \\ H_1 : & \boldsymbol{r} = \alpha\boldsymbol{p} + \boldsymbol{i} + \boldsymbol{n} \end{cases}$$

where $\boldsymbol{r}$ is the $MN \times 1$ *space-time snapshot* at the range of interest, $\boldsymbol{i}$ and $\boldsymbol{n}$ denote respectively the clutter/interference and receiver noise vectors which are assumed statistically independent zero-mean complex circular Gaussian vectors, α is the complex amplitude accounting for both the target as well as the channel propagation effects, and $\boldsymbol{p}$ the target *space-time steering vector*, i.e $\boldsymbol{p} = (\boldsymbol{c} \odot \boldsymbol{p}_t) \otimes \boldsymbol{p}_s$, with $\boldsymbol{p}_t \in \mathbb{C}^N$ and $\boldsymbol{p}_s \in \mathbb{C}^M$ being respectively the temporal and the spatial steering vectors. More precisely [31],

$$\boldsymbol{p}_t = \frac{1}{\sqrt{N}}[1, \exp(j2\pi f_t), \ldots, \exp(j2\pi(N-1)f_t)]^T ,$$

$$\boldsymbol{p}_s = \frac{1}{\sqrt{M}}[1, \exp(j2\pi f_s), \ldots, \exp(j2\pi(M-1)f_s)]^T ,$$

with f_t and f_s the normalized temporal and spatial Doppler frequencies, respectively.

4.2 Problem Formulation

A common measure of a STAP processor performance is the output Signal-to-Interference-plus-Noise Ratio (SINR) [31, pp. 62-69], which, for the optimum filter, is given by

$$\text{SINR} = |\alpha|^2[(\boldsymbol{c} \odot \boldsymbol{p}_t) \otimes \boldsymbol{p}_s]^\dagger \boldsymbol{M}[(\boldsymbol{c} \odot \boldsymbol{p}_t) \otimes \boldsymbol{p}_s] , \tag{4.1}$$

where $\boldsymbol{M} = \boldsymbol{R}_{\boldsymbol{i},\boldsymbol{n}}^{-1} \succ 0$ and $\boldsymbol{R}_{\boldsymbol{i},\boldsymbol{n}} = E[(\boldsymbol{i}+\boldsymbol{n})(\boldsymbol{i}+\boldsymbol{n})^{\dagger}]$ is the $MN \times MN$-dimensional disturbance space-time covariance matrix (due to clutter/interference and thermal noise). Indeed, due to the Gaussian assumption, maximizing the SINR is tantamount to maximizing the detection performance. The following proposition will be useful in simplifying some of the subsequent expressions and derivations.

Proposition II. Let $\boldsymbol{M} \in \mathbb{H}^{MN}$, $\boldsymbol{a} \in \mathbb{C}^{N}$, and $\boldsymbol{b} \in \mathbb{C}^{M}$. Then,

$$[(\boldsymbol{c} \odot \boldsymbol{a}) \otimes \boldsymbol{b}]^{\dagger} \boldsymbol{M} [(\boldsymbol{c} \odot \boldsymbol{a}) \otimes \boldsymbol{b}] = \boldsymbol{c}^{\dagger} \boldsymbol{R} \boldsymbol{c},$$

where $\boldsymbol{R} \in \mathbb{H}^{N}$ is given by

$$\boldsymbol{R} = [(\boldsymbol{I} \otimes \boldsymbol{b})^{\dagger} \boldsymbol{M} (\boldsymbol{I} \otimes \boldsymbol{b})] \odot (\boldsymbol{a}\boldsymbol{a}^{\dagger})^{*}.$$

Furthermore,

1. if $\boldsymbol{M}$ is positive semidefinite, then $\boldsymbol{R}$ is positive semidefinite,
2. if $\boldsymbol{M}$ is positive definite, all the entries of $\boldsymbol{a}$ are nonzero, and $\boldsymbol{b} \neq \boldsymbol{0}$, then $\boldsymbol{R}$ is positive definite, and
3. if $\boldsymbol{M}$ is positive definite, and $\boldsymbol{a}$ has at least a zero entry, then $\boldsymbol{R}$ is positive semidefinite.

Proof. See De Maio et al. [14].

The goal of this chapter is to design the code $\boldsymbol{c}$ that maximizes the output SINR (4.1), under some constraints that allow controlling the region of achievable temporal and spatial Doppler estimation accuracies and force a similarity with a given radar code $\boldsymbol{c}_0$ (assumed with unit norm). This last constraint is necessary in order to control the ambiguity function of the transmitted coded pulse train (as $\boldsymbol{c}_0$ has a good ambiguity function); it can be formalized as $\|\boldsymbol{c} - \boldsymbol{c}_0\|^2 \leq \epsilon$, where the parameter ϵ (with $0 < \epsilon < 2$ for unit norm vectors $\boldsymbol{c}$ and $\boldsymbol{c}_0$) rules the size of the similarity region [13, Section III C].

Concerning the region of achievable temporal and spatial Doppler estimation, the most natural choice would be forcing upper bounds on the CRB's on f_t and f_s for known α and unknown temporal and spatial Doppler frequencies. Unfortunately, this approach leads to intractable nonconvex constraints. However, this drawback can be circumvented constraining the CRB on f_t for known α and f_s, and the CRB on f_s for known α and f_t. As we will see, this formulation still leads to nonconvex constraints which, despite the previous case, are quadratic. Further developments require specifying that:

- the CRB, for known α and f_s, with respect to the estimation of f_t is given by [32, Section 8.2.3.1]

$$\Delta_{CR}(f_t) = \Psi \left\{ \left[\left(\boldsymbol{c} \odot \frac{\partial \boldsymbol{p}_t}{\partial f_t} \right) \otimes \boldsymbol{p}_s \right]^\dagger \boldsymbol{M} \left[\left(\boldsymbol{c} \odot \frac{\partial \boldsymbol{p}_t}{\partial f_t} \right) \otimes \boldsymbol{p}_s \right] \right\}^{-1}, \tag{4.2}$$

  with $\Psi = \dfrac{1}{2|\alpha|^2}$;

- the CRB, for known α and f_t, with respect to the estimation of f_s is given by

$$\Delta_{CR}(f_s) = \Psi \left\{ \left[(\boldsymbol{c} \odot \boldsymbol{p}_t) \otimes \frac{\partial \boldsymbol{p}_s}{\partial f_s} \right]^\dagger \boldsymbol{M} \left[(\boldsymbol{c} \odot \boldsymbol{p}_t) \otimes \frac{\partial \boldsymbol{p}_s}{\partial f_s} \right] \right\}^{-1}. \tag{4.3}$$

As to the regions of achievable temporal and spatial Doppler estimation accuracies (denoted by $\mathcal{A}_t$ and $\mathcal{A}_s$, respectively), they can be controlled forcing upper bounds on the respective CRB's. To this end, forcing upper bounds to (4.2) and (4.3), for a specified Ψ value, results in lower bounds on the sizes of $\mathcal{A}_t$ and $\mathcal{A}_s$. Hence, according to this guideline, we focus on radar codes complying with

$$\Delta_{CR}(f_t) \leq \frac{\Psi}{\delta_t} \qquad \text{and} \qquad \Delta_{CR}(f_s) \leq \frac{\Psi}{\delta_s}\,,$$

or equivalently

$$\left[\left(\boldsymbol{c} \odot \frac{\partial \boldsymbol{p}_t}{\partial f_t}\right) \otimes \boldsymbol{p}_s\right]^{\dagger} \boldsymbol{M} \left[\left(\boldsymbol{c} \odot \frac{\partial \boldsymbol{p}_t}{\partial f_t}\right) \otimes \boldsymbol{p}_s\right] \geq \delta_t\,, \tag{4.4}$$

$$\left[(\boldsymbol{c} \odot \boldsymbol{p}_t) \otimes \frac{\partial \boldsymbol{p}_s}{\partial f_s}\right]^{\dagger} \boldsymbol{M} \left[(\boldsymbol{c} \odot \boldsymbol{p}_t) \otimes \frac{\partial \boldsymbol{p}_s}{\partial f_s}\right] \geq \delta_s\,, \tag{4.5}$$

where δ_t and δ_s are two positive real numbers ruling the upper bounds on CRB's.

Exploiting Proposition II, the SINR in (4.1) and the Left Hand Side (LHS) of (4.4) and (4.5) can be rewritten as

$$\begin{aligned}
[(\boldsymbol{c} \odot \boldsymbol{p}_t) \otimes \boldsymbol{p}_s]^{\dagger} \boldsymbol{M} [(\boldsymbol{c} \odot \boldsymbol{p}_t) \otimes \boldsymbol{p}_s] &= \boldsymbol{c}^{\dagger} \boldsymbol{R} \boldsymbol{c}, \\
\left[\left(\boldsymbol{c} \odot \frac{\partial \boldsymbol{p}_t}{\partial f_t}\right) \otimes \boldsymbol{p}_s\right]^{\dagger} \boldsymbol{M} \left[\left(\boldsymbol{c} \odot \frac{\partial \boldsymbol{p}_t}{\partial f_t}\right) \otimes \boldsymbol{p}_s\right] &= \boldsymbol{c}^{\dagger} \boldsymbol{R}_t \boldsymbol{c}, \\
\left[(\boldsymbol{c} \odot \boldsymbol{p}_t) \otimes \frac{\partial \boldsymbol{p}_s}{\partial f_s}\right]^{\dagger} \boldsymbol{M} \left[(\boldsymbol{c} \odot \boldsymbol{p}_t) \otimes \frac{\partial \boldsymbol{p}_s}{\partial f_s}\right] &= \boldsymbol{c}^{\dagger} \boldsymbol{R}_s \boldsymbol{c},
\end{aligned}$$

where

$$\boldsymbol{R} = [(\boldsymbol{I} \otimes \boldsymbol{p}_s)^\dagger \boldsymbol{M}(\boldsymbol{I} \otimes \boldsymbol{p}_s)] \odot (\boldsymbol{p}_t \boldsymbol{p}_t^\dagger)^* \quad \succ \quad \mathbf{0},$$

$$\boldsymbol{R}_t = [(\boldsymbol{I} \otimes \boldsymbol{p}_s)^\dagger \boldsymbol{M}(\boldsymbol{I} \otimes \boldsymbol{p}_s)] \odot (\frac{\partial \boldsymbol{p}_t}{\partial f_t} \frac{\partial \boldsymbol{p}_t}{\partial f_t}^\dagger)^* \quad \succeq \quad \mathbf{0},$$

$$\boldsymbol{R}_s = [(\boldsymbol{I} \otimes \frac{\partial \boldsymbol{p}_s}{\partial f_s})^\dagger \boldsymbol{M}(\boldsymbol{I} \otimes \frac{\partial \boldsymbol{p}_s}{\partial f_s})] \odot (\boldsymbol{p}_t \boldsymbol{p}_t^\dagger)^* \quad \succ \quad \mathbf{0}.$$

It follows that the problem of devising the STAP code, under (4.4) and (4.5), the similarity and the energy constraints, can be formulated as the following nonconvex quadratic optimization problem (QP_2)

$$\mathrm{QP}_2 \begin{cases} \underset{\boldsymbol{c}}{\mathsf{maximize}} & \boldsymbol{c}^\dagger \boldsymbol{R} \boldsymbol{c} \\ \mathsf{subject\ to} & \boldsymbol{c}^\dagger \boldsymbol{c} = 1 \\ & \boldsymbol{c}^\dagger \boldsymbol{R}_t \boldsymbol{c} \geq \delta_t \\ & \boldsymbol{c}^\dagger \boldsymbol{R}_s \boldsymbol{c} \geq \delta_s \\ & \|\boldsymbol{c} - \boldsymbol{c}_0\|^2 \leq \epsilon \end{cases}$$

which can be equivalently written as

$$\mathrm{QP}_2 \begin{cases} \underset{\boldsymbol{c}}{\mathsf{maximize}} & \boldsymbol{c}^\dagger \boldsymbol{R} \boldsymbol{c} \\ \mathsf{subject\ to} & \boldsymbol{c}^\dagger \boldsymbol{c} = 1 \\ & \boldsymbol{c}^\dagger \boldsymbol{R}_t \boldsymbol{c} \geq \delta_t \\ & \boldsymbol{c}^\dagger \boldsymbol{R}_s \boldsymbol{c} \geq \delta_s \\ & \Re\left(\boldsymbol{c}^\dagger \boldsymbol{c}_0\right) \geq 1 - \epsilon/2 \end{cases} \tag{4.6}$$

Evidently, problem (5.21) requires the specification of f_t and f_s; as a consequence, the solution code depends on these preassigned values. It is thus necessary to provide some guidelines on the importance and the applicability of the proposed framework. To this end, we highlight that:

- the performance level which can be obtained through the optimal solution of (5.21), in correspondence of the design f_t and f_s, represents an upper bound to that achievable by any practically implementable system;

- the encoding procedure might be applied in a waveform diversity context, where more coded waveforms on different carriers are transmitted [33]. These waveforms are chosen frequency orthogonal and each of them is optimized for the detection in a given spatial-temporal frequency bin. At the receiver end, the detector tuned to the specific bin processes its matched waveform [34].

- a single coded waveform designed for the challenging condition of slowly moving target on the clutter ridge [31] can be transmitted.

- a single coded waveform optimized to an average scenario can be selected. Otherwise stated, the code might be chosen as the solution to the problem (5.21) with $\boldsymbol{R}$, $\boldsymbol{R}_t$, and $\boldsymbol{R}_s$ replaced by $E[\boldsymbol{R}]$, $E[\boldsymbol{R}_t]$, and $E[\boldsymbol{R}_s]$, where the expectation operator is over f_t and f_s. If these last quantities are modeled as independent random variables, the expectations can be evaluated after some algebra, i.e.

$$E\left[\boldsymbol{R}(h,k)\right] = \mathrm{tr}\left[\boldsymbol{M} \odot (\boldsymbol{e}_h \boldsymbol{e}_k^T \otimes \boldsymbol{B})\right] \boldsymbol{A}(h,k),$$

$$E\left[\boldsymbol{R}_t(h,k)\right] = 4\pi^2 h\, k\, \mathrm{tr}\left[\boldsymbol{M} \odot (\boldsymbol{e}_h \boldsymbol{e}_k^T \otimes \boldsymbol{B})\right] \boldsymbol{A}(h,k),$$

$$E\left[\boldsymbol{R}_s(h,k)\right] = 4\pi^2 \mathrm{tr}\left\{\boldsymbol{M} \odot \left[\boldsymbol{e}_h \boldsymbol{e}_k^T \otimes (\boldsymbol{B} \odot \boldsymbol{U})\right]\right\} \boldsymbol{A}(h,k),$$

where $\boldsymbol{B} = E[\boldsymbol{p}_s \boldsymbol{p}_s^\dagger]$ and $\boldsymbol{A} = E[\boldsymbol{p}_t \boldsymbol{p}_t^\dagger]$, while $\boldsymbol{U}$ is the $M \times M$ matrix with entries $\boldsymbol{U}(m,n) = mn$. In particular, if f_t and f_s modeled as independent random variables uniformly distributed in $[-\Delta_t, \Delta_t]$ and $[-\Delta_s, \Delta_s]$ respectively, we have $\boldsymbol{B}(h,k) = \frac{1}{M}\mathrm{sinc}\,(2\Delta_s(h-k))$ and $\boldsymbol{A}(h,k) = \frac{1}{N}\mathrm{sinc}\,(2\Delta_t(h-k))$.

- assume that, after an uncoded (or a possibly standard coded) transmission, a detection is declared in a given spatial-temporal Doppler bin. Our coding procedure can be thus employed to shape the waveform for the next transmission in order to confirm the detection in the previously identified bin.

4.3 Problem Solution

In this section, we demonstrate how to obtain an optimal solution of QP_2. Toward this, we consider the following Enlarged Quadratic Problem (EQP_2):

$$\mathrm{EQP}_2 \begin{cases} \underset{\boldsymbol{c}}{\text{maximize}} & \boldsymbol{c}^\dagger \boldsymbol{R} \boldsymbol{c} \\ \text{subject to} & \boldsymbol{c}^\dagger \boldsymbol{c} = 1 \\ & \boldsymbol{c}^\dagger \boldsymbol{R}_t \boldsymbol{c} \geq \delta_t \\ & \boldsymbol{c}^\dagger \boldsymbol{R}_s \boldsymbol{c} \geq \delta_s \\ & \Re^2\left(\boldsymbol{c}^\dagger \boldsymbol{c}_0\right) + \Im^2\left(\boldsymbol{c}^\dagger \boldsymbol{c}_0\right) = \boldsymbol{c}^\dagger \boldsymbol{c}_0 \boldsymbol{c}_0{}^\dagger \boldsymbol{c} \geq \delta_\epsilon \end{cases}$$

where $\delta_\epsilon = (1-\epsilon/2)^2$. As in the previous chapter, we can obtain an optimal solution of QP_2 from an optimal solution of EQP_2. Thus, if $\bar{\boldsymbol{c}}$ is optimal for EQP_2, then $\bar{\boldsymbol{c}} e^{j \arg(\bar{\boldsymbol{c}}^\dagger \boldsymbol{c}_0)}$ is optimal for QP_2. Now, we are going to find an optimal solution of EQP_2. To this end, we exploit the equivalent matrix formulation

$$\mathrm{EQP}_2 \begin{cases} \underset{\boldsymbol{C}}{\text{maximize}} & \mathrm{tr}\left(\boldsymbol{C}\boldsymbol{R}\right) \\ \text{subject to} & \mathrm{tr}\left(\boldsymbol{C}\right) = 1 \\ & \mathrm{tr}\left(\boldsymbol{C}\boldsymbol{R}_t\right) \geq \delta_t \\ & \mathrm{tr}\left(\boldsymbol{C}\boldsymbol{R}_s\right) \geq \delta_s \\ & \mathrm{tr}\left(\boldsymbol{C}\boldsymbol{C}_0\right) \geq \delta_\epsilon \\ & \boldsymbol{C} = \boldsymbol{c}\boldsymbol{c}^\dagger \end{cases} \tag{4.7}$$

where $\boldsymbol{C}_0 = \boldsymbol{c}_0 \boldsymbol{c}_0{}^\dagger$.

Problem (4.7) can be relaxed into a SDP problem neglecting the rank-one constraint [26]. By doing so, we obtain a Relaxed Enlarged Quadratic

Problem (REQP_2)

$$\mathrm{REQP}_2 \begin{cases} \underset{\boldsymbol{C}}{\text{maximize}} & \mathrm{tr}\left(\boldsymbol{C}\boldsymbol{R}\right) \\ \text{subject to} & \mathrm{tr}\left(\boldsymbol{C}\right) = 1 \\ & \mathrm{tr}\left(\boldsymbol{C}\boldsymbol{R}_t\right) \geq \delta_t \\ & \mathrm{tr}\left(\boldsymbol{C}\boldsymbol{R}_s\right) \geq \delta_s \\ & \mathrm{tr}\left(\boldsymbol{C}\boldsymbol{C}_0\right) \geq \delta_\epsilon \\ & \boldsymbol{C} \succeq \boldsymbol{0}\,. \end{cases} \tag{4.8}$$

The dual problem of REQP_2 (REQPD_2) is

$$\mathrm{REQPD}_2 \begin{cases} \underset{y_1,y_2,y_3,y_4}{\text{minimize}} & y_1 - y_2\delta_t - y_3\delta_s - y_4\delta_\epsilon \\ \text{subject to} & y_1\boldsymbol{I} - y_2\boldsymbol{R}_t - y_3\boldsymbol{R}_s - y_4\boldsymbol{C}_0 \succeq \boldsymbol{R} \\ & y_2 \geq 0, y_3 \geq 0, y_4 \geq 0. \end{cases}$$

Throughout the paper, we assume that QP_2 is strictly feasible, namely there is $\boldsymbol{c}_1$ such that $\|\boldsymbol{c}_1\| = 1$, $\boldsymbol{c}_1^\dagger\boldsymbol{R}_t\boldsymbol{c}_1 > \delta_t$, $\boldsymbol{c}_1^\dagger\boldsymbol{R}_s\boldsymbol{c}_1 > \delta_s$, and $\Re\left({\boldsymbol{c}_1}^\dagger\boldsymbol{c}_0\right) > 1 - \epsilon/2$ (to this end, it is sufficient to suppose that the initial code $\boldsymbol{c}_0$ is a strictly feasible solution of QP_2). We claim that both REQP_2 and REQPD_2 are strictly feasible[1]. It follows, by the weak duality theorem, that REQP_2 is bounded above and REQPD_2 is bounded below. Also, it follows, by the strong duality theorem of SDP [27, Theorem 1.7.1], that the optimal values of REQP_2 and REQPD_2 are equal and attainable at some optimal points. Moreover, the complementary slackness conditions are satisfied at the optimal points of the primal and the dual problems. Denote by $v(\cdot)$ the optimal

[1]Further details on the strict feasibility of REQP_2 and REQPD_2 can be found in the work of De Maio et al. [14].

value of the problem $(\cdot)$. It is known from optimization theory that REQPD_2 is also the dual problem of EQP_2. So far, we have established the following relationships:

$$\begin{aligned} v(\text{REQP}_2) &= v(\text{REQPD}_2) \text{ (from strong duality theorem of SDP)} \\ &\geq v(\text{EQP}_2) \text{ (from the weak duality theorem)} \\ &= v(\text{QP}_2). \end{aligned}$$

As a consequence, solving the SDP problem REQP_2 provides an upper bound to EQP_2 (or the original problem QP_2). Furthermore, as long as we can get a rank-one optimal solution of REQP_2 in some way, the upper bound is tight; in other words, the SDP relaxation of EQP_2 is exact, or equivalently, strong duality for the nonconvex problem EQP_2 holds (i.e., $v(\text{REQPD}_2) = v(\text{EQP}_2)$). Therefore, to solve EQP_2 (or QP_2), it suffices for us to find a rank-one optimal solution of the SDP problem, which is our focus in the remainder of the chapter.

Before proceeding, let us compare the optimization problem solved in the previous chapter with that we are faced with in the present one. In chapter 3, we have shown that strong duality hold for problem (3.9): in other words, (3.9) has been proven to be a *hidden convex* program. The most significant difference between (3.9) and (4.7) is that the former includes only three homogeneous quadratic constraints, while the latter has four. As a consequence, strong duality for problem EQP_2 may or may not hold. In what follows, we identify most cases where the strong duality is valid, and propose solution procedures, resorting to the decomposition method used in the previous chapter [28], or a new rank-one decomposition theorem proposed in a more recent paper [35]. We explicitly highlight that the techniques used in this chapter is far trickier and more involved than those exploited in previous one.

The analysis of the relaxed problem REQP$_2$ and its dual REQPD$_2$ is easy as REQP$_2$ is a convex problem. Indeed, denote by $\bar{\boldsymbol{C}}$ an optimal solution of REQP$_2$, and by $(\bar{y}_1, \bar{y}_2, \bar{y}_3, \bar{y}_4)$ an optimal solution of REQPD$_2$. Then, the primal-dual optimal solution pair $(\bar{\boldsymbol{C}}, \bar{y}_1, \bar{y}_2, \bar{y}_3, \bar{y}_4)$ satisfies the Karush-Kuhn-Tucker optimality conditions (which are sufficient and necessary, since SDP is a convex optimization problem and constraint qualification conditions are satisfied) [3]. In particular, the complementary slackness conditions are

$$\operatorname{tr}\left[\left(\bar{y}_1 \boldsymbol{I} - \bar{y}_2 \boldsymbol{R}_t - \bar{y}_3 \boldsymbol{R}_s - \bar{y}_4 \boldsymbol{C}_0 - \boldsymbol{R}\right) \bar{\boldsymbol{C}}\right] = 0 \tag{4.9}$$

$$\left(\operatorname{tr}\left(\bar{\boldsymbol{C}} \boldsymbol{R}_t\right) - \delta_t\right) \bar{y}_2 = 0 \tag{4.10}$$

$$\left(\operatorname{tr}\left(\bar{\boldsymbol{C}} \boldsymbol{R}_s\right) - \delta_s\right) \bar{y}_3 = 0 \tag{4.11}$$

$$\left(\operatorname{tr}\left(\bar{\boldsymbol{C}} \boldsymbol{C}_0\right) - \delta_\epsilon\right) \bar{y}_4 = 0. \tag{4.12}$$

Further developments require introducing the new rank-one decomposition propositions.

Proposition III. Let $\boldsymbol{X} \in \mathbb{H}^N$ be a nonzero positive semidefinite matrix ($N \geq 3$), and suppose that $(\operatorname{tr}(\boldsymbol{Y}\boldsymbol{A}_1), \operatorname{tr}(\boldsymbol{Y}\boldsymbol{A}_2), \operatorname{tr}(\boldsymbol{Y}\boldsymbol{A}_3), \operatorname{tr}(\boldsymbol{Y}\boldsymbol{A}_4)) \neq (0,0,0,0)$ for any nonzero positive semidefinite matrix $\boldsymbol{Y} \in \mathbb{H}^N$. Then,

- if $\operatorname{rank}(\boldsymbol{X}) \geq 3$, one can find, in polynomial time, a rank-one matrix $\boldsymbol{x}\boldsymbol{x}^\dagger$ (synthetically denoted as $\mathcal{D}_2(\boldsymbol{X}, \boldsymbol{A}_1, \boldsymbol{A}_2, \boldsymbol{A}_3, \boldsymbol{A}_4)$) such that $\boldsymbol{x}$ is in range($\boldsymbol{X}$), and

$$\boldsymbol{x}^\dagger \boldsymbol{A}_i \boldsymbol{x} = \mathrm{tr}\left(\boldsymbol{X}\boldsymbol{A}_i\right), \quad i = 1, 2, 3, 4;$$

- if rank($\boldsymbol{X}$) $= 2$, for any $\boldsymbol{z}$ not in the range space of $\boldsymbol{X}$, one can find a rank-one matrix $\boldsymbol{x}\boldsymbol{x}^\dagger$ such that $\boldsymbol{x}$ is in the linear subspace spanned by $\{\boldsymbol{z}\} \cup$ range($\boldsymbol{X}$), and

$$\boldsymbol{x}^\dagger \boldsymbol{A}_i \boldsymbol{x} = \mathrm{tr}\left(\boldsymbol{X}\boldsymbol{A}_i\right), \quad i = 1, 2, 3, 4.$$

Proof. See the recent work of Ai et al. [35, Theorem 2.3].

The computational complexity of each rank-one decomposition theorem requires $O(N^3)$ [28] [35]. In fact, the computation involves both a Cholesky factorization and suitable rotations. Hence, the required amount of operations is dominated by that necessary for the Cholesky decomposition, which is known to be $O(N^3)$.

As already pointed out, once a rank-one positive semidefinite matrix $\boldsymbol{C}$ satisfying (4.9)-(4.12) and feasible to (4.8) has been found, we can claim that $\boldsymbol{C} = \boldsymbol{c}\boldsymbol{c}^\dagger$ is an optimal solution of (4.8), or equivalently, $\boldsymbol{c}$ is an optimal solution of (5.21). Now, we aim at finding a procedure to construct a rank-one optimal solution of REQP$_2$ from a general rank optimal solution $\bar{\boldsymbol{C}}$ of REQP$_2$, which can always be found by an SDP solver. We claim the following two main propositions:

Proposition IV. Let $\bar{\boldsymbol{C}}$ be an optimal solution of REQP$_2$ with rank($\bar{\boldsymbol{C}}$) $\geq$ 3. Then, we can find a rank-one optimal solution of REQP$_2$ in polynomial time.

Proof. See De Maio et al. [14].

Proposition V. Let $\bar{\boldsymbol{C}}$ be an optimal solution of REQP$_2$ with $\text{rank}(\bar{\boldsymbol{C}}) = 2$. Then, if one of the inequalities is satisfied: $\text{tr}\left(\bar{\boldsymbol{C}}\boldsymbol{R}_t\right) > \delta_t$, $\text{tr}\left(\bar{\boldsymbol{C}}\boldsymbol{R}_s\right) > \delta_s$, or $\text{tr}\left(\bar{\boldsymbol{C}}\boldsymbol{C}_0\right) > \delta_\epsilon$, we can find a rank-one optimal solution of REQP$_2$ in polynomial time.

Proof. See De Maio et al. [14].

We remark that in Proposition IV the assumption $\text{rank}(\bar{\boldsymbol{C}}) \geq 3$ implies that the size N of $\bar{\boldsymbol{C}}$ is greater than or equal to 3, i.e., the length of radar code is not smaller than 3, which is practical. Note that in Proposition V, the size N of $\bar{\boldsymbol{C}}$ could be greater than or equal to 2.

In the following, we summarize the procedure that leads to an optimal solution of EQP$_2$, by distinguishing among three possible cases:

Case 1: $\text{rank}\left(\bar{\boldsymbol{C}}\right) = 1$. In this case, a vector $\boldsymbol{c}$ with $\bar{\boldsymbol{C}} = \boldsymbol{c}\boldsymbol{c}^\dagger$ is an optimal solution of EQP$_2$.

Case 2: $\text{rank}\left(\bar{\boldsymbol{C}}\right) \geq 3$. Exploiting Proposition IV, we can obtain a rank-one optimal solution of REQP$_2$.

Case 3: $\text{rank}\left(\bar{\boldsymbol{C}}\right) = 2$. Let $\text{tr}\left(\bar{\boldsymbol{C}}\boldsymbol{R}_t\right) = \delta_2$, $\text{tr}\left(\bar{\boldsymbol{C}}\boldsymbol{R}_s\right) = \delta_3$ and $\text{tr}\left(\bar{\boldsymbol{C}}\boldsymbol{C}_0\right) = \delta_4$. We have to consider two possible situations:

Case 3.1: One of the inequalities $\delta_2 > \delta_t$, $\delta_3 > \delta_s$, or $\delta_4 > \delta_\epsilon$ holds. In this case, we invoke Proposition V to output a rank-one optimal solution of REQP$_2$.

Case 3.2: $\delta_2 = \delta_t$, $\delta_3 = \delta_s$, $\delta_4 = \delta_\epsilon$. In this case, we are not able to judge whether the strong duality is valid for (4.8). Nevertheless, we can still provide a procedure aimed at constructing feasible solutions for (4.8). Precisely, according to the last claim of Proposition III, for any vector $\boldsymbol{z} \notin \text{range}(\bar{\boldsymbol{C}})$, we can obtain a vector $\boldsymbol{c}_z$ such that

$$\begin{aligned}
\text{tr}\left(\boldsymbol{c}_z\boldsymbol{c}_z^\dagger\right) &= \text{tr}\left(\bar{\boldsymbol{C}}\right) = 1 \\
\text{tr}\left(\boldsymbol{c}_z\boldsymbol{c}_z^\dagger\boldsymbol{R}_t\right) &= \text{tr}\left(\bar{\boldsymbol{C}}\boldsymbol{R}_t\right) = \delta_t \\
\text{tr}\left(\boldsymbol{c}_z\boldsymbol{c}_z^\dagger\boldsymbol{R}_s\right) &= \text{tr}\left(\bar{\boldsymbol{C}}\boldsymbol{R}_s\right) = \delta_s \\
\text{tr}\left(\boldsymbol{c}_z\boldsymbol{c}_z^\dagger\boldsymbol{C}_0\right) &= \text{tr}\left(\bar{\boldsymbol{C}}\boldsymbol{C}_0\right) = \delta_\epsilon
\end{aligned}$$

namely feasible for EQP_2. Hence, given H different vectors $\boldsymbol{z} \notin \text{range}(\bar{\boldsymbol{C}})$, which can be randomly generated so that $\text{rank}(\bar{\boldsymbol{C}} + \boldsymbol{z}\boldsymbol{z}^\dagger) = 3$, we can get H feasible solutions of EQP_2 and, then, we can select the one which has the largest objective function value. Besides the randomized way to generate feasible solutions, which is suboptimal, we can also consider a deterministic approach. In particular, the following method provides a feasible solution with a loss of optimality by $\bar{y}_4\left(\text{tr}(\boldsymbol{C}_0\boldsymbol{c}\boldsymbol{c}^\dagger) - \delta_\epsilon\right)$:

1. Perform the rank-one decomposition $[\boldsymbol{c}_1, \boldsymbol{c}_2] = \mathcal{D}_1(\bar{\boldsymbol{C}}, \delta_t\boldsymbol{I} - \boldsymbol{R}_t, \delta_s\boldsymbol{I} - \boldsymbol{R}_s)$;

2. Choose a sub-optimal solution $\boldsymbol{c}$ from $\boldsymbol{c}_1/||\boldsymbol{c}_1||$ or $\boldsymbol{c}_2/||\boldsymbol{c}_2||$, say $\boldsymbol{c} = \boldsymbol{c}_1/||\boldsymbol{c}_1||$, such that $\text{tr}(\boldsymbol{C}_0\boldsymbol{c}\boldsymbol{c}^\dagger) \geq \delta_\epsilon$.

As our simulation shows, the subcase 3.2 happens in less than 0.1% of the experiments (see Figure 4.19, and we report the details of the simulation in Section 4.4.3).

Summarizing, the STAP code, which is optimum for problem QP_2 (except for case 3.2), can be constructed according to Algorithm 2.

Algorithm 2 Space-Time Encoding Procedure (STEP)

`Input:` $\boldsymbol{M}$, $\boldsymbol{p}_s$, $\boldsymbol{p}_t$, $\boldsymbol{c}_0$, δ_s, δ_t, δ_ϵ;

`Output:` $\boldsymbol{c}_{STEP}$;

solve the SDP problem REQP$_2$ finding an optimal solution $\bar{\boldsymbol{C}}$;

evaluate $R = \text{rank}(\bar{\boldsymbol{C}})$;

if $R = 1$ **then**

  evaluate $\bar{\boldsymbol{c}}$ such that $\bar{\boldsymbol{C}} = \bar{\boldsymbol{c}}\bar{\boldsymbol{c}}^\dagger$;

else if $R \geq 3$ **then**

  evaluate $\bar{\boldsymbol{c}} = \mathcal{D}_2(\bar{\boldsymbol{C}}, \boldsymbol{I}, \boldsymbol{R}_s, \boldsymbol{R}_t, \boldsymbol{C}_0)$;

else if $R = 2$ **then**

  $\bar{\boldsymbol{c}} =$ Algorithm 3 $\left(\bar{\boldsymbol{C}}, \boldsymbol{R}_s, \boldsymbol{R}_t, \boldsymbol{C}_0, \delta_s, \delta_t, \delta_\epsilon\right)$;

end

$\boldsymbol{c}_{STEP} = \bar{\boldsymbol{c}}e^{j\phi}$, with $\phi = \arg(\bar{\boldsymbol{c}}^\dagger \boldsymbol{c}_0)$.

The computational complexity, connected with the implementation of the algorithm, is polynomial, since $O\left(N^{3.5}\right)$ is the amount of operations involved in solving the SDP problem, and $O\left(N^3\right)$ is the complexity required by the decompositions $\mathcal{D}_1(\cdot, \cdot, \cdot)$ and $\mathcal{D}_2(\cdot, \cdot, \cdot, \cdot, \cdot)$.

4.4 Performance Analysis

The present section is aimed at analyzing the performance of the proposed encoding scheme. The analysis is conducted in terms of P_d, regions of achievable Doppler estimation accuracies ($\mathcal{A}_t$ and $\mathcal{A}_s$), and ambiguity function of the pulse train modulated through the proposed code $\bar{\boldsymbol{c}}$. To proceed further, we recall that, for a specified value of P_{fa} and for nonfluctuating target [24], P_d can be evaluated as

$$P_d = Q\left(\sqrt{2|\alpha|^2 \bar{\boldsymbol{c}}^\dagger \boldsymbol{R} \bar{\boldsymbol{c}}}, \sqrt{-2 \ln P_{fa}}\right).$$

Algorithm 3 EQP_2 feasible solution for $R = 2$

`Input:` $\bar{\boldsymbol{C}}$, $\boldsymbol{R}_s$, $\boldsymbol{R}_t$, $\boldsymbol{C}_0$, δ_s, δ_t, δ_ϵ

`Output:` $\bar{\boldsymbol{c}}$

evaluate $\delta_2 = \mathrm{tr}\left(\bar{\boldsymbol{C}}\boldsymbol{R}_t\right)$, $\delta_3 = \mathrm{tr}\left(\bar{\boldsymbol{C}}\boldsymbol{R}_s\right)$ and $\delta_4 = \mathrm{tr}\left(\bar{\boldsymbol{C}}\boldsymbol{C}_0\right)$;
`if` $\delta_2 > \delta_t$ `then`
  evaluate $[\boldsymbol{c}_1, \boldsymbol{c}_2] = \mathcal{D}_1(\bar{\boldsymbol{C}}, \delta_3\boldsymbol{I} - \boldsymbol{R}_s, \delta_4\boldsymbol{I} - \boldsymbol{C}_0)$;
  `if` $\boldsymbol{c}_1^\dagger\boldsymbol{R}_t\boldsymbol{c}_1/||\boldsymbol{c}_1||^2 > \delta_t$ `then`
    evaluate $\bar{\boldsymbol{c}} = \boldsymbol{c}_1/||\boldsymbol{c}_1||$;
  `else`
    evaluate $\bar{\boldsymbol{c}} = \boldsymbol{c}_2/||\boldsymbol{c}_2||$;
  `end`
`else if` $\delta_3 > \delta_s$ `then`
  evaluate $[\boldsymbol{c}_1, \boldsymbol{c}_2] = \mathcal{D}_1(\bar{\boldsymbol{C}}, \delta_2\boldsymbol{I} - \boldsymbol{R}_t, \delta_4\boldsymbol{I} - \boldsymbol{C}_0)$;
  `if` $\boldsymbol{c}_1^\dagger\boldsymbol{R}_s\boldsymbol{c}_1/||\boldsymbol{c}_1||^2 > \delta_s$ `then`
    evaluate $\bar{\boldsymbol{c}} = \boldsymbol{c}_1/||\boldsymbol{c}_1||$;
  `else`
    evaluate $\bar{\boldsymbol{c}} = \boldsymbol{c}_2/||\boldsymbol{c}_2||$;
  `end`
`else if` $\delta_4 > \delta_\epsilon$ `then`
  evaluate $[\boldsymbol{c}_1, \boldsymbol{c}_2] = \mathcal{D}_1(\bar{\boldsymbol{C}}, \delta_2\boldsymbol{I} - \boldsymbol{R}_t, \delta_3\boldsymbol{I} - \boldsymbol{R}_s)$;
  `if` $\boldsymbol{c}_1^\dagger\boldsymbol{C}_0\boldsymbol{c}_1/||\boldsymbol{c}_1||^2 > \delta_\epsilon$ `then`
    evaluate $\bar{\boldsymbol{c}} = \boldsymbol{c}_1/||\boldsymbol{c}_1||$;
  `else`
    evaluate $\bar{\boldsymbol{c}} = \boldsymbol{c}_2/||\boldsymbol{c}_2||$;
  `end`
`else if` $\delta_2 = \delta_t$, $\delta_3 = \delta_s$ and $\delta_4 = \delta_\epsilon$ `then`
  determine, using Proposition III, H feasible solutions $\boldsymbol{c}_i$, $i = 1, \ldots, H$;
  select $\bar{\boldsymbol{c}}$ from $\{\boldsymbol{c}_1, \ldots, \boldsymbol{c}_H\}$ such that $\bar{\boldsymbol{c}}^\dagger\boldsymbol{R}\bar{\boldsymbol{c}} \geq \boldsymbol{c}_i^\dagger\boldsymbol{R}\boldsymbol{c}_i$ for all $i = 1, \ldots, H$.
`end`

As benchmark code for the detection probability, we consider the unconstrained unitary code

$$\boldsymbol{c}_{benchmark} = \arg\max_{\boldsymbol{c}} \left\{ \boldsymbol{c}^{\dagger}\boldsymbol{R}\boldsymbol{c} \,|\, \|\boldsymbol{c}\|^2 = 1 \right\},$$

which does not necessarily satisfy the similarity constraints or spatial/temporal Doppler accuracy constraints. Since that $\boldsymbol{c}_{benchmark}^{\dagger}\boldsymbol{R}\boldsymbol{c}_{benchmark} = \lambda_{max}(\boldsymbol{R})$, the benchmark P_d can be expressed as

$$P_d^{benchmark} = Q\left(\sqrt{2|\alpha|^2\lambda_{max}(\boldsymbol{R})}, \sqrt{-2\ln P_{fa}}\right).$$

Analogously, we consider a benchmark CRB for both spatial and temporal Doppler frequencies, i.e.

$$\mathrm{CRB}_l^{benchmark} = \frac{\Psi}{\lambda_{max}(\boldsymbol{R}_l)}, \quad l \in \{s, t\}.$$

Notice that, in general, the three values $P_d^{benchmark}$, $\mathrm{CRB}_s^{benchmark}$, and $\mathrm{CRB}_t^{benchmark}$ are not obtained in correspondence of the same unitary norm code. Besides, the ambiguity function of the coded pulse train can be evaluated as

$$\chi(\tau,\nu) = \sum_{m=0}^{N-1}\sum_{n=0}^{N-1} c_{STEP}(m)c_{STEP}^{*}(n)\chi_p(\tau-(m-n)T_r,\nu),$$

where $[c_{STEP}(0),\ldots,c_{STEP}(N-1)]^T = \boldsymbol{c}_{STEP}$, and $\chi_p(\cdot,\cdot)$ is the ambiguity function of an unmodulated pulse [22].

In our scenario, we consider a STAP system with $M = 11$ channels and

$N = 32$ pulses. Moreover, we fix P_{fa} to 10^{-6}. As to the temporal steering vector $\boldsymbol{p}_t$, we set the normalized temporal Doppler frequency $f_t = 0.25$, while we use the normalized spatial Doppler frequency $f_s = 0.15$ for the spatial steering vector $\boldsymbol{p}_s$. As similarity code $\boldsymbol{c}_0$, we resort to a generalized Barker sequence [22, pp. 109-113]: such codes are polyphase sequences whose autocorrelation function has minimal peak-to-sidelobe ratio excluding the outermost sidelobe. Examples of these sequences have been found for all $N \leq 45$ [29] [30], using numerical optimization techniques. In our simulations, we choose a unitary norm version of the generalized Barker code $\boldsymbol{c}_0$ of length 32 [22, p. 111].

In order to compare the performance of our algorithm with that of the similarity code, we have also evaluated P_d and CRBs obtained using $\boldsymbol{c}_0$, i.e.

$$P_d^0 = Q\left(\sqrt{2|\alpha|^2 \boldsymbol{c}_0^\dagger \boldsymbol{R} \boldsymbol{c}_0}, \sqrt{-2\ln P_{fa}}\right),$$

and

$$\mathrm{CRB}_l^0 = \frac{\Psi}{\boldsymbol{c}_0^\dagger \boldsymbol{R}_l \boldsymbol{c}_0}, \quad l \in \{s, t\}.$$

Concerning the inverse disturbance covariance matrix $\boldsymbol{M}$, we consider the two following scenarios:

- simulated covariance, according to the disturbance model described by Ward [31];
- covariance, from the KASSPER database [36].

Regarding the parameters δ_t and δ_s, in general, what can be assigned is the interval of δ_s and δ_t values which can be exploited. Evidently, they depend on $\boldsymbol{M}$, f_s, and f_t and must be smaller than the maximum eigenvalue of $\boldsymbol{R}_s$ and $\boldsymbol{R}_t$ respectively. From a practical point of view, the selection of the quoted parameters depend on the desired accuracy region (provided it is compatible with strict feasibility). In the numerical examples, we have considered a wide variation range for the parameters so as to better highlight the performance trade-off due to different parameters combinations.

Finally, in the numerical simulations, we have exploited the Matlab© toolbox SeDuMi [4] for solving the SDP relaxation.

4.4.1 Simulated Covariance

The disturbance covariance matrix $\boldsymbol{M}^{-1}$ has been simulated according to Ward's model [31, ch. 2], as the sum of a clutter term plus a thermal noise contribution, i.e. $\boldsymbol{M}^{-1} = \boldsymbol{R}_{clutter} + \sigma^2\boldsymbol{I}$, where $\boldsymbol{R}_{clutter}$ is the clutter covariance and σ^2 is the thermal noise level. More precisely, $\boldsymbol{R}_{clutter}$ can be obtained using the general clutter model described by Ward [31, par. 2.6.1]. It accounts for the effects of velocity misalignment (due to aircraft crab) and intrinsic clutter motion [31]. A synthetic description of the principal radar system parameters, used in the simulations, is reported in Table 4.1 (for a more exhaustive list, please refer to the classic Ward's book [31]).

In Figure 4.1, we plot P_d of the optimum code (according to the proposed criterion) versus $|\alpha|^2$ for nonfluctuating target, $\delta_s = 3.8$, $\delta_\epsilon = 0.001$, and for several values of δ_t. In the same figure, we also represent both the P_d^0 and the $P_d^{benchmark}$. The curves show that, increasing δ_t, we get lower and lower values of P_d for a given $|\alpha|^2$ value. This was expected since the higher δ_t the smaller the feasibility region of the optimization problem to be solved

Table 4.1: Radar System Parameters.

Peak power	200 kW	Transmit Gain	21 dB
Pulse width	0.2 ms	Receiver Gain	10 dB
System Losses	4 dB	Instantaneous Bandwidth	4 MHz
Operating frequency	300 MHz	Noise Figure	3 dB
PRF	300 Hz	Clutter-to-Noise Ratio	30 dB
Duty Factor	6%	Number of clutter foldovers	$\beta = 1$
Platform Velocity	50 m/s	Platform Altitude	9000 m

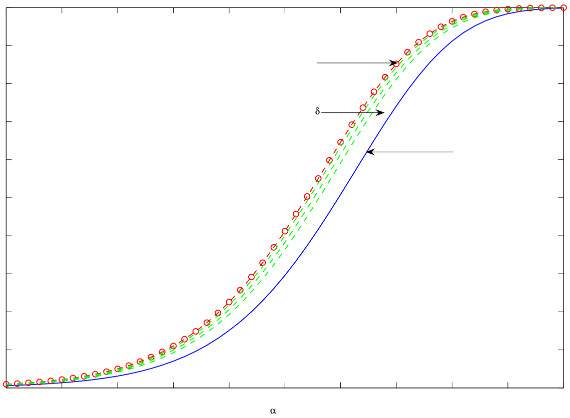

Figure 4.1: P_d versus $|\alpha|^2$ for nonfluctuating target, simulated data, $P_{fa} = 10^{-6}$, $N = 32$, $M = 11$, $f_t = 0.25$, $f_s = 0.15$, $\delta_s = 3.8$, $\delta_\epsilon = 0.001$, and several values of $\delta_t \in \{494.4, 516.0, 543.0\}$. Generalized Barker code (solid curve). P_d of the proposed code for a given δ_t (dashed curves). Benchmark P_d (o-marked dashed curve).

for finding the code. Nevertheless, the proposed encoding algorithm usually ensures a better detection performance than the original generalized Barker code.

In Figure 4.2, $\Delta_{CR}(f_t)$ is plotted versus $|\alpha|^2$ for the same values of δ_t as in Figure 4.1. The benchmark CRB_t and CRB_t^0 are plotted too. The curves highlight that, increasing δ_t, better and better $\Delta_{CR}(f_t)$ values can be

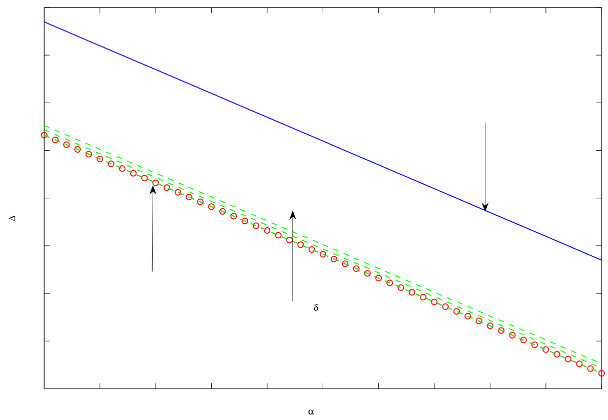

Figure 4.2: $\Delta_{CR}(f_t)$ versus $|\alpha|^2$ for nonfluctuating target, simulated data, $f_t = 0.25$, $f_s = 0.15$, $N = 32$, $M = 11$, $\delta_s = 3.8$, $\delta_\epsilon = 0.001$, and several values of $\delta_t \in \{494.4, 516.0, 543.0\}$. Generalized Barker code (solid curve). $\Delta_{CR}(f_t)$ of the proposed code for a given δ_t (dashed curves). Benchmark $\Delta_{CR}(f_t)$ (o-marked dashed curve).

achieved. This is in accordance with the considered criterion, because the higher δ_t the larger the size of the region $\mathcal{A}_t$.

In Figure 4.3, we plot P_d versus $|\alpha|^2$ for nonfluctuating target, $\delta_t = 0.5$, $\delta_\epsilon = 0.001$, and for several values of δ_s. Also in this case, we can notice a gain of the proposed encoding scheme over the classic generalized Barker code. However, the gain slightly reduces as the parameter δ_s increases, since the feasibility region becomes smaller and smaller.

In Figure 4.4, we plot $\mathrm{CRB}_s^{benchmark}$, CRB_s^0 and $\Delta_{CR}(f_s)$ versus $|\alpha|^2$ for the same values of the parameters considered in the previous figure. We observe that increasing δ_s, we slightly enlarge the region of achievable spatial Doppler accuracy. Moreover, the proposed encoding technique assures a larger $\mathcal{A}_s$ than the generalized Barker code.

Summarizing, the joint analysis of Figures 4.1$\div$4.4 shows that a trade-off

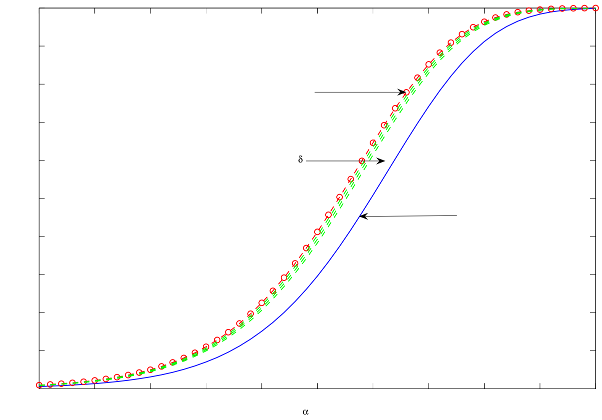

Figure 4.3: P_d versus $|\alpha|^2$ for nonfluctuating target, simulated data, $P_{fa} = 10^{-6}$, $N = 32$, $M = 11$, $f_t = 0.25$, $f_s = 0.15$, $\delta_t = 0.5$, $\delta_\epsilon = 0.001$, and several values of $\delta_s \in \{656.7, 658.9, 669.9\}$. Generalized Barker code (solid curve). P_d of the proposed code for a given δ_s (dashed curves). Benchmark P_d (o-marked dashed curve).

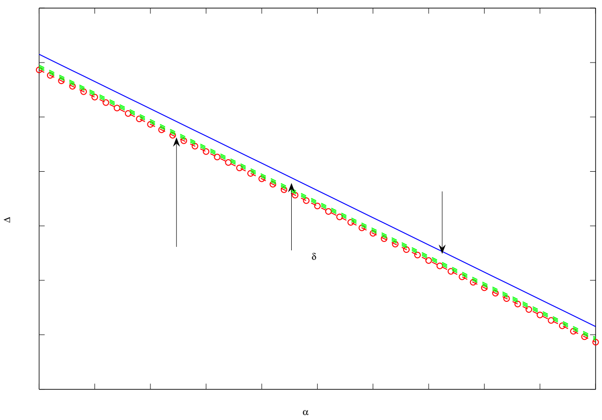

Figure 4.4: $\Delta_{CR}(f_s)$ versus $|\alpha|^2$ for nonfluctuating target, simulated data, $N = 32$, $M = 11$, $f_t = 0.25$, $f_s = 0.15$, $\delta_t = 0.5$, $\delta_\epsilon = 0.001$, and several values of $\delta_s \in \{656.7, 658.9, 669.9\}$. Generalized Barker code (solid curve). $\Delta_{CR}(f_s)$ of the proposed code for a given δ_s (dashed curves). Benchmark $\Delta_{CR}(f_s)$ (o-marked dashed curve).

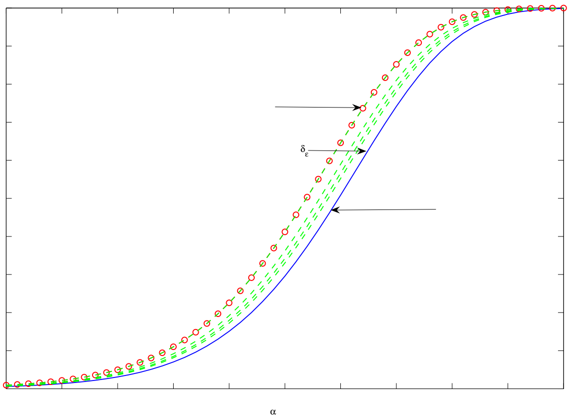

Figure 4.5: P_d versus $|\alpha|^2$ for nonfluctuating target, simulated data, $P_{fa} = 10^{-6}$, $N = 32$, $M = 11$, $f_t = 0.25$, $f_s = 0.15$, $\delta_t = 0.5$, $\delta_s = 3.8$, and several values of $\delta_\epsilon \in \{0, 0.9811, 0.9918, 0.9957\}$. Generalized Barker code (solid curve). P_d of the proposed code for a given δ_ϵ (dashed curves). Benchmark P_d (o-marked dashed curve).

can be realized between the detection performance and the estimation accuracy of both the temporal and the spatial Doppler frequencies. Additionally, there exist codes capable of outperforming the generalized Barker code both in terms of P_d and sizes of $\mathcal{A}_t$ and $\mathcal{A}_s$.

The effects of the similarity constraint are analyzed in Figure 4.5. Therein, we set $\delta_t = 0.5$, $\delta_s = 3.8$, and consider several values of δ_ϵ. The plots show that increasing δ_ϵ worse and worse P_d values are obtained; this behavior can be explained observing that the smaller δ_ϵ the larger the size of the similarity region. However, this detection loss is compensated for an improvement of the coded pulse train ambiguity function, as we can see in Figures 4.7 and 4.8, where the modulus of that function is plotted assuming rectangular pulses, and $T_r = 3T_p$. For comparison purposes, the ambiguity function modulus of $\boldsymbol{c}_0$ is plotted in Figure 4.8. The plots highlight that the closer δ_ϵ

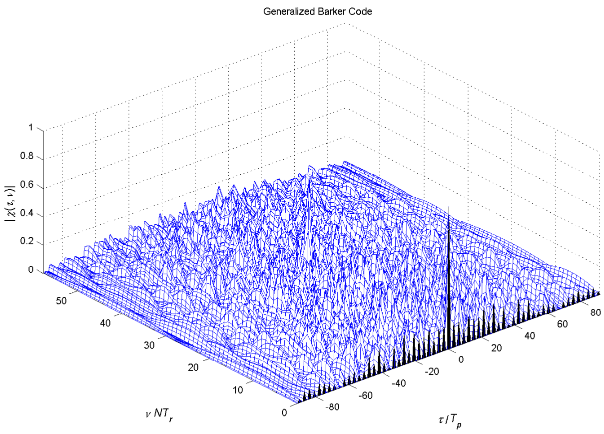

Figure 4.6: Ambiguity function modulus of the generalized Barker code $\boldsymbol{c}_0$ with $T_r = 3T_p$.

to 1 the higher the degree of similarity between the ambiguity functions of the devised and prefixed codes. This is due to the fact that increasing δ_ϵ is tantamount to reducing the size of the similarity region. In other words, we force the devised code to be similar and similar to the prefixed one and, as a consequence, we get closer and closer ambiguity functions.

In the previous figures, we have fixed two parameters, and have changed the other in order to analyze the impact on the performance of a particular constraint. In Figures 4.9 $\div$ 4.11, we analyze the joint effect of the three parameters, so as to show that there are situations where the proposed encoding method can outperform the generalized Barker coding in terms of P_d, $\Delta_{CR}(f_t)$, and $\Delta_{CR}(f_s)$. In particular, in Figure 4.9 we plot P_d, in Figure 4.10 $\Delta_{CR}(f_t)$, and in Figure 4.11 $\Delta_{CR}(f_s)$ versus $|\alpha|^2$, assuming $(\delta_t, \delta_s, \delta_\epsilon) = (325.7, 403.2, 0.8)$. Evidently, for the considered values of the parameters, the proposed code, whose ambiguity function is plotted in

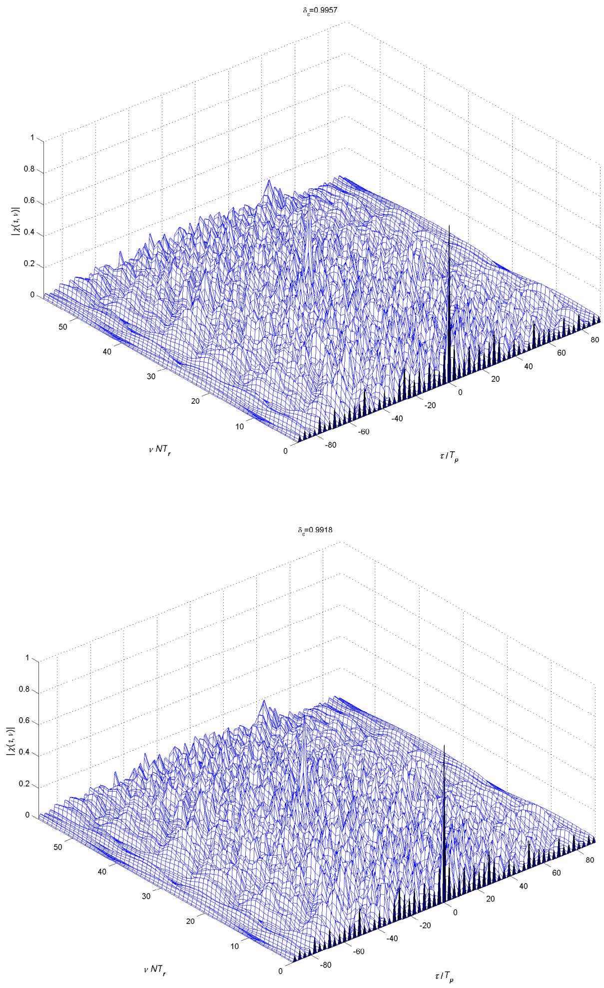

Figure 4.7: Ambiguity function modulus of code which maximizes the SINR for $N = 32$, $T_r = 3T_p$, $\delta_t = 0.5$, $\delta_s = 3.8$, $\mathbf{c}_0$ generalized Barker code, and (up) $\delta_\epsilon = 0.9957$, (down) $\delta_\epsilon = 0.9918$.

Figure 4.12, outperforms the generalized Barker in terms of P_d, CRB_t, and CRB_s.

As to the robustness of the proposed method, we study the behaviour of the algorithm when a mismatch on the temporal or spatial Doppler is present. In particular, we design two codes, one assuming $f_t = 0.25$ and

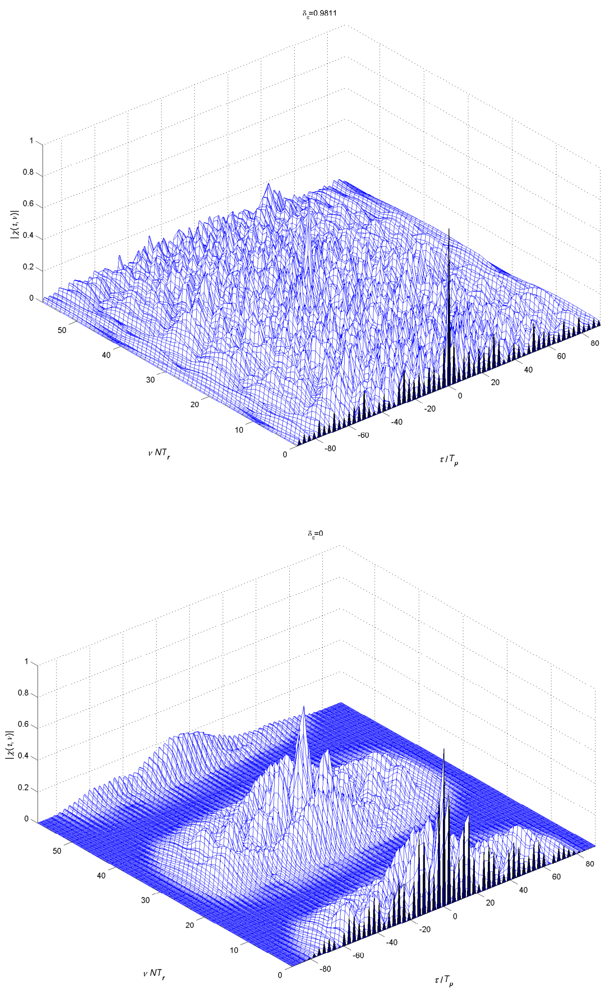

Figure 4.8: Ambiguity function modulus of code which maximizes the SINR for $N = 32$, $T_r = 3T_p$, $\delta_t = 0.5$, $\delta_s = 3.8$, $\mathbf{c}_0$ generalized Barker code, and (up) $\delta_\epsilon = 0.9811$, (down) $\delta_\epsilon = 0$.

$f_s = 0.15$, and another where f_t and f_s are modeled as random parameter uniformly distributed in the interval $[-1/3; 1/3]$, i.e. $f_t \sim \mathcal{U}\,(-1/3; 1/3)$ and $f_t \sim \mathcal{U}\,(-1/3; 1/3)$. We analyze the performance when f_t (left column) or f_s (right column) ranges in the interval $[-1/2; 1/2]$. In Figure 4.13, we plot the P_d versus f_t in the left column (versus f_s in the right one) for $|\alpha|^2 = 14$ dB

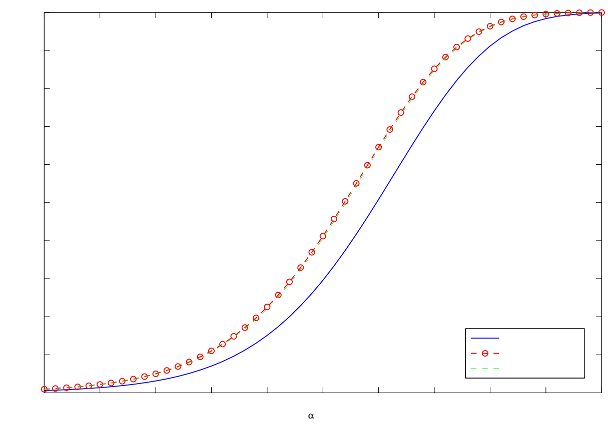

Figure 4.9: P_d versus $|\alpha|^2$ for nonfluctuating target, simulated data, $P_{fa} = 10^{-6}$, $N = 32$, $M = 11$, $f_t = 0.25$, $f_s = 0.15$, and $(\delta_t, \delta_s, \delta_\epsilon) = (325.7, 403.2, 0.8)$. P_d of the proposed code (dashed curves). Benchmark P_d (o-marked dashed curve).

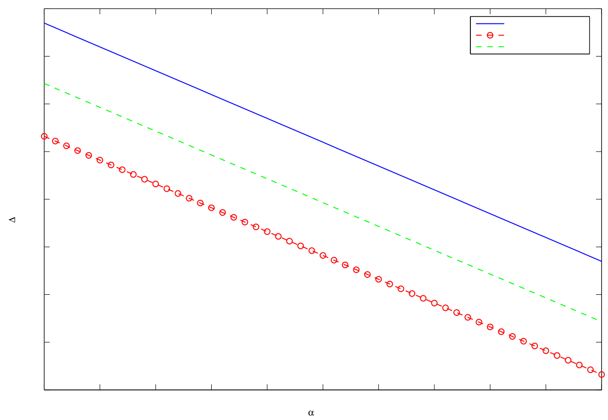

Figure 4.10: $\Delta_{CR}(f_t)$ versus $|\alpha|^2$ for nonfluctuating target, simulated data, $f_t = 0.25$, $f_s = 0.15$, $N = 32$, $M = 11$, and $(\delta_t, \delta_s, \delta_\epsilon) = (325.7, 403.2, 0.8)$. $\Delta_{CR}(f_t)$ of the proposed code (dashed curves). Benchmark $\Delta_{CR}(f_t)$ (o-marked dashed curve).

and $(\delta_t, \delta_s, \delta_\epsilon) = (53.4, 15.6, 0.5)$. We can notice that the proposed method outperforms the generalized Barker code almost everywhere for the case of a

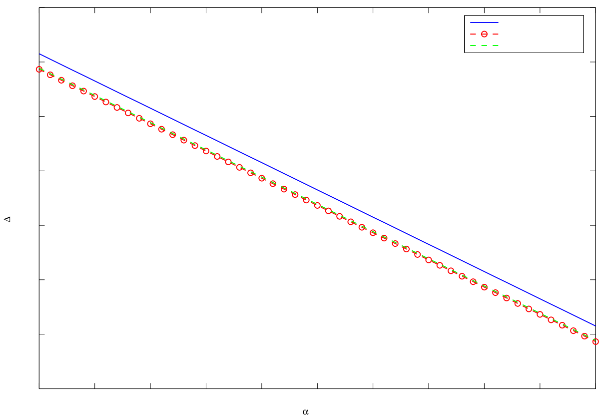

Figure 4.11: $\Delta_{CR}(f_s)$ versus $|\alpha|^2$ for nonfluctuating target, simulated data, $N = 32$, $M = 11$, $f_t = 0.25$, $f_s = 0.15$, and $(\delta_t, \delta_s, \delta_\epsilon) = (325.7, 403.2, 0.8)$. $\Delta_{CR}(f_s)$ of the proposed code (dashed curves). Benchmark $\Delta_{CR}(f_s)$ (o-marked dashed curve).

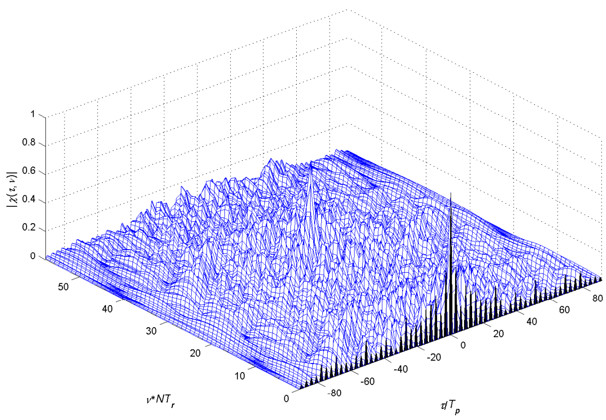

Figure 4.12: Ambiguity function modulus of proposed code for $N = 32$, $T_r = 3T_p$, $\mathbf{c}_0$ generalized Barker code, and $(\delta_t, \delta_s, \delta_\epsilon) = (325.7, 403.2, 0.8)$.

spatial or temporal Doppler mismatch. In other words, simulations indicate that the novel encoding method shares an intrinsic robust behaviour.

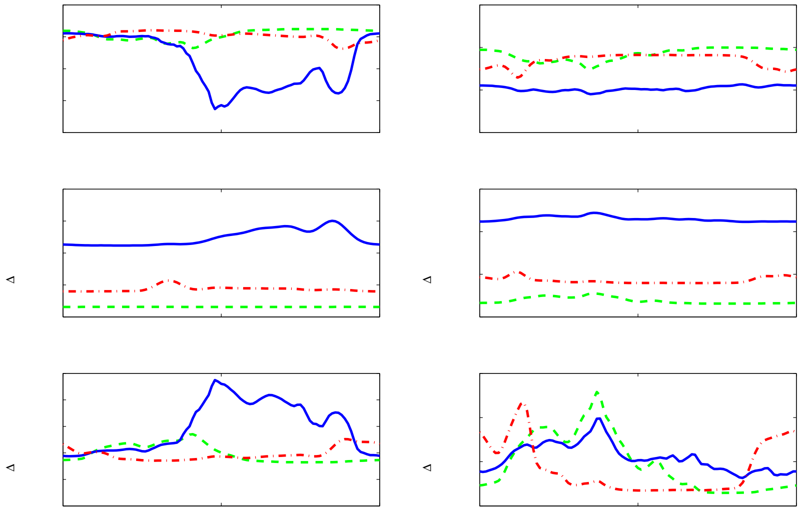

Figure 4.13: Robustness analysis for $|\alpha|^2 = 14$ dB, nonfluctuating target, simulated data, $N = 32$, $M = 11$, $(\delta_t, \delta_s, \delta_\epsilon) = (53.4, 15.6, 0.5)$, $f_t = 0.25$ and $f_s \in [-1/2; 1/2]$ (left column), $f_s = 0.15$ and $f_t \in [-1/2; 1/2]$ (right column). Proposed code for $f_t = 0.25$ and $f_s = 0.15$ (dashed curves), Generalized Barker code (solid curves), Proposed code for $f_t \sim \mathcal{U}(-1/3; 1/3)$ and $f_s \sim \mathcal{U}(-1/3; 1/3)$ (dash-dotted curves). (top left) P_d versus f_t; (top right) P_d versus f_s; (middle left) $\Delta_{CR}(f_t)$ versus f_t; (middle right) $\Delta_{CR}(f_t)$ versus f_s; (bottom left) $\Delta_{CR}(f_s)$ versus f_t; (bottom right) $\Delta_{CR}(f_s)$ versus f_s.

4.4.2 Covariance from the KASSPER Database

In this subsection, we use the ground clutter covariance matrix from the range cell number 10 of the KASSPER [36] datacube. This dataset contains many real-world effects including heterogeneous terrain, sub-space leakage, array errors, and many ground targets. It refers to a California site characterized by large mountains and moderate density of roads. The chosen matrix is loaded with the thermal noise covariance matrix and then the sum is inverted to get $\boldsymbol{M}^{-1}$. As in the previous scenario, we set the Clutter-to-Noise Ratio

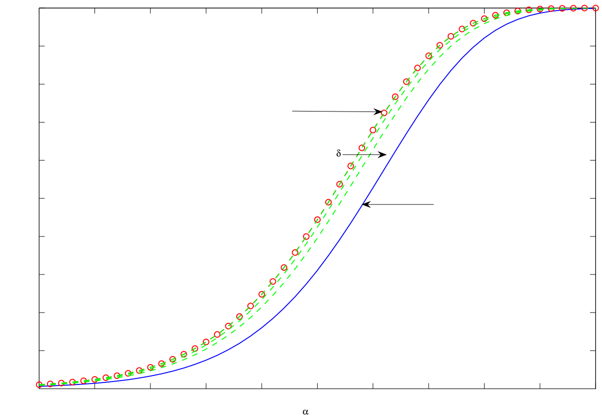

Figure 4.14: P_d versus $|\alpha|^2$ for nonfluctuating target, real data, $P_{fa} = 10^{-6}$, $f_t = 0.25$, $f_s = 0.15$, $\delta_s = 30.6$, $\delta_\epsilon = 0.001$, and several values of $\delta_t \in \{873.3, 1036.0, 1059.5\}$. Generalized Barker code (solid curve). P_d of the proposed code for a given δ_t (dashed curves). Benchmark P_d (o-marked dashed curve).

to 30 dB.

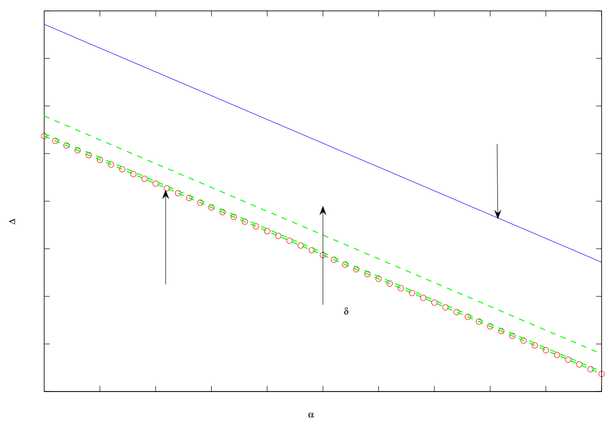

Figure 4.15: $\Delta_{CR}(f_t)$ versus $|\alpha|^2$ for nonfluctuating target, real data, $f_t = 0.25$, $f_s = 0.15$, $\delta_s = 30.6$, $\delta_\epsilon = 0.001$, and several values of $\delta_t \in \{873.3, 1036.0, 1059.5\}$. Generalized Barker code (solid curve). $\Delta_{CR}(f_t)$ of the proposed code for a given δ_t (dashed curves). Benchmark $\Delta_{CR}(f_t)$ (o-marked dashed curve).

In Figures 4.14 and 4.15, we study the effect of the parameter δ_t on P_d and $\Delta_{CR}(f_t)$. In particular, in Figure 4.14, we plot P_d of the optimum code versus $|\alpha|^2$ for nonfluctuating target, $\delta_s = 30.6$, $\delta_\epsilon = 0.001$, and for several values of δ_t. In the same figure, we also represent both P_d^0 and $P_d^{benchmark}$. We can observe a similar behavior as in the simulated case of subsection 4.4.1: increasing δ_t, we get lower and lower values of P_d for a given $|\alpha|^2$ value. Moreover, our proposed encoding scheme can achieve a better detection performance than the classic generalized Barker code. In Figure 4.15, $\Delta_{CR}(f_t)$ is plotted versus $|\alpha|^2$ for the same values of δ_t as in Figure 4.14. The benchmark CRB_t and CRB_t^0 are plotted too. As expected, the curves show that increasing δ_t better and better $\Delta_{CR}(f_t)$ values can be obtained.

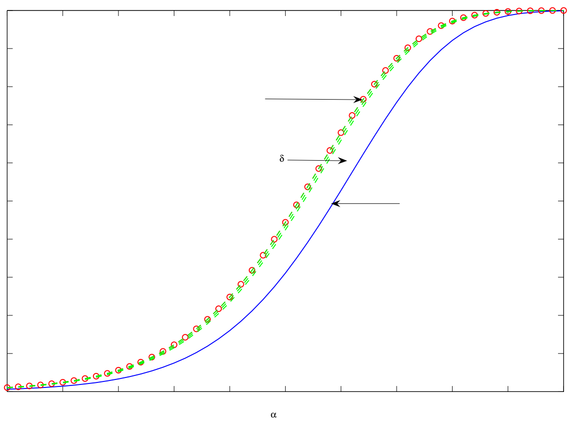

Figure 4.16: P_d versus $|\alpha|^2$ for nonfluctuating target, real data, $f_t = 0.25$, $f_s = 0.15$, $\delta_t = 1.1$, $\delta_\epsilon = 0.001$, and several values of $\delta_s \in \{29.3, 1351.6, 1381.7\}$. Generalized Barker code (solid curve). P_d of the proposed code for a given δ_s (dashed curves). Benchmark P_d (o-marked dashed curve).

In Figure 4.16, we plot P_d versus $|\alpha|^2$ for nonfluctuating target, $\delta_t = 1.1$,

$\delta_\epsilon = 0.001$, and for several values of δ_s. It is evident that an increase of the parameter δ_s leads to a slight deterioration of detection performances. This can be explained observing that the feasibility region becomes smaller and smaller as δ_s increases.

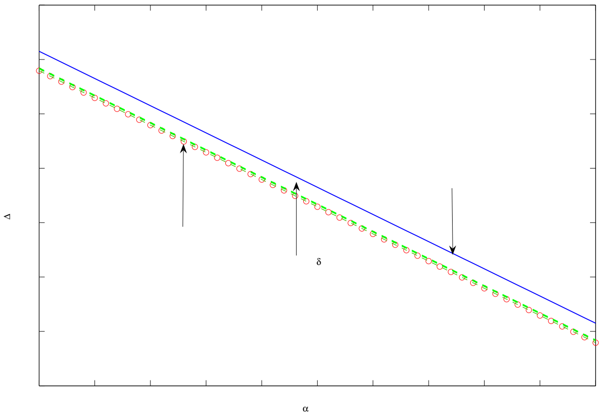

Figure 4.17: $\Delta_{CR}(f_s)$ versus $|\alpha|^2$ for nonfluctuating target, real data, $f_t = 0.25$, $f_s = 0.15$, $\delta_t = 1.1$, $\delta_\epsilon = 0.001$, and several values of $\delta_s \in \{29.3, 1351.6, 1381.7\}$. Generalized Barker code (solid curve). $\Delta_{CR}(f_s)$ of the proposed code for a given δ_s (dashed curves). Benchmark $\Delta_{CR}(f_s)$ (o-marked dashed curve).

In Figure 4.17, we plot $\mathrm{CRB}_s^{benchmark}$, CRB_s^0, and $\Delta_{CR}(f_s)$ versus $|\alpha|^2$ for the same values of the parameters considered in the previous figure. The curves highlight that increasing δ_s lower and lower $\Delta_{CR}(f_s)$ values can be achieved.

Finally, in Figure 4.18, we plot P_d versus $|\alpha|^2$ for nonfluctuating target, $\delta_t = 1.1$, $\delta_s = 30.6$, and for several values of δ_ϵ. We can notice that the closer δ_ϵ to 1, the closer P_d to P_d^0, namely the performances of the proposed code and the generalized Barker code end up coincident.

In conclusion, P_d, $\Delta_{CR}(f_t)$, and $\Delta_{CR}(f_s)$ exhibit a similar behavior both

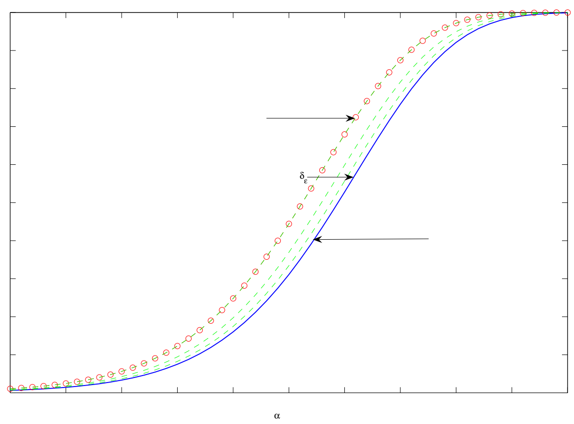

Figure 4.18: P_d versus $|\alpha|^2$ for nonfluctuating target, real data, $P_{fa} = 10^{-6}$, $f_t = 0.25$, $f_s = 0.15$, $\delta_t = 1.1$, $\delta_s = 30.6$, and several values of $\delta_\epsilon \in \{0, 0.9792, 0.9974\}$. Generalized Barker code (solid curve). P_d of the proposed code for a given δ_ϵ (dashed curves). Benchmark P_d (o-marked dashed curve).

with simulated and KASSPER covariance data. Moreover, the proposed analysis shows that it is possible to realize a trade-off among the three parameters δ_t, δ_s, and δ_ϵ to increase the detection performance, or to improve the Doppler estimation accuracy, or to shape the ambiguity function.

4.4.3 Occurrence of Subcase 3.2

In this subsection, we analyze the typical rank of an optimal solution $\bar{\boldsymbol{C}}$ of the SDP problem REQP_2. First of all, we have to deal with the finite precision of Matlab© implementation of the encoding algorithm. To this end, we introduce the $\text{Rank}_\gamma(\boldsymbol{A})$ function, namely the number of eigenvalue of the matrix $\boldsymbol{A}$ greater than the positive threshold γ. For a positive semidefinite matrix $\boldsymbol{A}$, $\text{Rank}_\gamma(\boldsymbol{A})$ represents a good numerical estimation of the rank of

$\boldsymbol{A}$, as $\gamma \to 0$. Moreover, we have to distinguish a *tight* constraint from a *strict* constraint. In this case, we consider the constraint as *practically tight* if the difference of the two sides of the inequality is less than γ. Performing 10000 instances of the problem REQP$_2$ (with clutter covariance matrix from the range cell number 10 of the KASSPER datacube, $M = 11$, $N = 32$, $f_t = 0.25$, $f_s = 0.15$, $\boldsymbol{c}_0$ generalized Barker sequence, δ_t, δ_s, and δ_ϵ randomly chosen[2]), in less than 1% of the cases, we get an optimal solution $\bar{\boldsymbol{C}}$ with $\text{Rank}_\gamma\left(\bar{\boldsymbol{C}}\right) = 2$. For those particular situations, we have also controlled the constraints, and in less than 10% of the cases, we have all the three constraints *practically tight* (namely, case 3.2 described at page 55). Summarizing, in less than 0.1% of the instances, we have a suboptimal solution of the original QP$_2$ problem. This trend holds for all the considered values[3] of the parameter γ. Furthermore, most of the instances presents a $\text{Rank}_\gamma\left(\bar{\boldsymbol{C}}\right) = 1$, even if the number decreases as the precision γ tends to 0 (and consequently the occurrence of the event $\text{Rank}_\gamma\left(\bar{\boldsymbol{C}}\right) \geq 3$ increases). Thus, we can conclude observing that a duality gap between the original problem QP$_2$ and the relaxed problem REQP$_2$ (namely an optimal solution of rank 2 and all the constraints tight) is very rare, and even for high precision (i.e. $\gamma = 10^{-8}$), it happens in less than 0.1% of the cases. The analysis is summarized in Figure 4.19.

[2] δ_t is a uniformly distributed random variable in the interval $[\lambda_{min}(\boldsymbol{R}_t); \lambda_{max}(\boldsymbol{R}_t)]$, δ_s in $[\lambda_{min}(\boldsymbol{R}_s); \lambda_{max}(\boldsymbol{R}_s)]$, and δ_ϵ in $[0; 1]$.

[3] Notice that additional results obtained changing $\boldsymbol{M}$ and $\boldsymbol{c}_0$ randomly in the 10000 experiments also agrees with the aforementioned behavior.

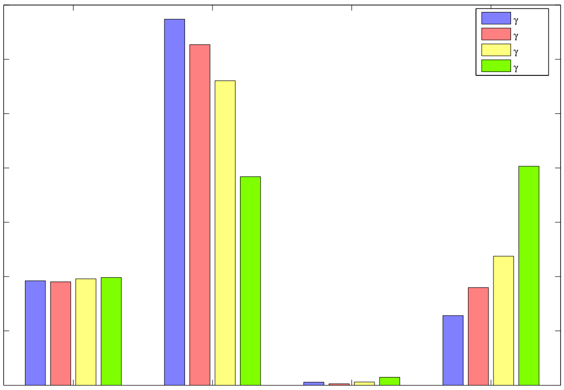

Figure 4.19: $\text{Rank}_\gamma\left(\bar{\boldsymbol{C}}\right)$, over 10000 random experiments, for different values of $\gamma \in \{10^{-2}, 10^{-4}, 10^{-6}, 10^{-8}\}$.

4.5 Conclusions

In this chapter, we have addressed the problem of code design for radar STAP, assuming that the overall disturbance component, which contaminates the useful signal, is a colored complex circular Gaussian vector. We have considered the class of linearly coded pulse trains and have determined the radar code which maximizes the detection performance under a constraint on the region of achievable values for the temporal and spatial Doppler estimation accuracy and forcing a similarity constraint with a given radar code exhibiting some desirable properties.

The optimization problem, we have been faced with, is nonconvex and quadratic. In order to solve it, we have first performed a relaxation into a convex SDP problem. Then, applying appropriately rank-one decomposition theorems [28] [35] to an optimal solution of the relaxed problem, we have determined an optimal code. Remarkably, the proposed code design procedure requires a polynomial computational complexity.

At the analysis stage, we have assessed the performance of the new algorithm both on simulated data and on the KASSPER reference STAP datacube. The analysis has been conducted in terms of detection performance, regions of estimation accuracies that unbiased estimators of the temporal and the spatial Doppler frequencies can theoretically achieve, and ambiguity function. The results have highlighted the trade-off existing among the aforementioned performance metrics. Otherwise stated, detection capabilities can be traded with desirable properties of the coded waveform and/or with enlarged regions of achievable temporal/spatial Doppler estimation accuracies.

Possible future research tracks might concern the possibility to make the algorithm adaptive with respect to the disturbance covariance matrix, namely to devise techniques which jointly estimate the code and the covariance. Moreover, it should be investigated the introduction in the code design optimization problem of constraints related to the probability of correct target classification as well as of knowledge-based constraints, ruled by the *apriori* information that the radar has about the surrounding environment.

In the next chapter, we further extend the proposed encoding framework. In fact, starting from chapter 3, where we have shown a *single transmitter-single receiver* example, in this chapter we have analyzed the STAP case (namely, a *single transmitter-multiple receivers* situation), arriving to chapter 5, where we will face with a radar network scenario (*multiple transmitters-*

multiple receivers). As we will see, in this context we have a Nondeterministic Polynomial (NP) problem. Nevertheless, convex optimization wil be useful, evaluating a quasi-optimal solution in polynomial time, through a relaxation and randomization technique [26].

Chapter 5

Coding for Networked Radar

Networked radar sensors are considered in this chapter. In the last decade, the importance of radar has grown progressively with the increasing dimension of the system: from a single colocated antenna to a large sensor network [37]. The concept of heterogeneous radars working together has been thoroughly studied, opening the door to the the concept of Multiple-Input-Multiple-Output (MIMO) radar [38] [39], Over-The-Horizon (OTH) radar networks [40], and Distributed Aperture Radar (DAR) [41] [42]. These three scenarios are examples of *cooperative radar networks*, in the sense that every single element contributes to the overall detection process. Unfortunately, in many practical situations, it is not possible to design the network *apriori*. As such, the elements are just simply added to the already existing network (*plug and fight*), and each sensor exhibits its own detection scheme. This is the case in *noncooperative radar networks* [43] [44]. In this scenario, it becomes extremely important that each additional sensor interferes as little as possible with the pre-existing elements, and, to this end, some techniques are easily adopted. The usual approaches rely upon the employment of spatial and/or frequency diversity: the former resorts to forming multiple orthogonal beams, while the latter uses separated carrier frequencies to reduce interference [45] [46]. Another possibility is to exploit waveform diversity [47]: in which the basic concept is to suitably modulate the waveform of the new sensor so as to optimize the detection capabilities of a specific sensor, but, at the same time, controlling the interference introduced into the network. Notice that this is different from the approach employed in cooperative sensor network, where one must design waveforms so as to optimize the joint performance of the system [48] [49]. In the noncooperative case, the optimization of radar waveforms has been discussed in two papers [50] [51]. In the former, the design is based upon the maximization of the global Signal-to-Interference-Plus-Noise Ratio (SINR), and classic constraints such as phase-only or finite energy are considered [50]. In the latter, the problem of parameter estimation (e.g. direction of arrival) for a noncooperative radar is analyzed [51]. In this chapter, we propose a different approach: we maximize the Signal-to-Noise Ratio (SNR), but at the same time, we control the interference induced by our sensor on the other elements of the network. Furthermore, we apply a constraint to the transmitted signal, limiting the energy to a specific maximum value. The resulting problem is Nondeterministic Polynomial (NP) hard, namely an optimal solution can not be found in polynomial time. Since a traditional approach is not possible for real-time applications, we propose a new algorithm, referred to as WILD (Waveform Interference Limiting Design), to generate a suboptimal solution with a polynomial time constraint due to computational complexity. The procedure is based on the *relaxation and randomization* theory [26]: first we relax the feasible set of the problem, obtaining a solution; then we use this solution to generate a waveform that is feasible for our original problem. The quality of the solution is guaranteed by the *approximation bound* that ensures that the WILD technique achieves at least a fraction $R \in (0, 1]$ of the optimal value of the relaxed problem [52].

The chapter is organized as follows. In Section 5.1, we present a model for the generic signal received by an element of the network. In Section 5.2, we discuss some relevant guidelines for waveform design and formulate the problem. In Section 5.3, we introduce the optimization procedure. In Section 5.4, we analyze via simulation the performance of the proposed encoding method. Finally, in Section 5.5, we draw conclusions and outline possible future research tracks.

5.1 System Model

We consider a network of L noncooperative monostatic radar systems, where each sensor transmits a coherent burst of pulses

$$s_l(t) = a_l^{tx} u_l(t) \exp[j(2\pi f t + \phi_l)] \,, \qquad l = 0, \ldots, L-1 \,,$$

with a_l^{tx} the transmit signal amplitude,

$$u_l(t) = \sum_{i=0}^{N-1} c_l(i) p(t - iT_r)$$

the signal's complex envelope, $p(t)$ the single pulse shape of the transmitted signal and assumed of duration T_p, and with unit energy, i.e.

$$\int_0^{T_p} |p(t)|^2 dt = 1 \,,$$

T_r ($T_r \geq T_p$) is the pulse repetition period, $\boldsymbol{c}_l = [c_l(0), c_l(1), \ldots, c_l(N-1)]^T \in \mathbb{C}^N$ the radar code associated with the l-th sensor, f is the carrier frequency, and ϕ_l a random phase associated with the l-th transmitted waveform. In other words, we are considering a network of noncooperative homogeneous sensors, which do not cooperate in the detection process, yet exploit the same kind of waveform, namely a linearly coded pulse train with possibly different codes. Assume that the 0-th sensor is the radar of interest: the received signal under the alternative hypothesis (target presence) is the sum of L transmitted signals scattered by the target. Each term of this sum has a characteristic amplitude, delay and Doppler shift (which depend both on the l-th transmitter and the 0-th receiver), so we can express the signal received by the radar sensor of interest as

$$r_0(t) = \sum_{l=0}^{L-1} \alpha_{0,l}^{rx} e^{j2\pi(f+f_{0,l})(t-\tau_{0,l})} u_l(t - \tau_{0,l}) + n_0(t) \,, \tag{5.1}$$

where $n_0(t)$ is an additive disturbance due to clutter and thermal noise, $\alpha_{0,l}^{rx}$, $\tau_{0,l}$, and $f_{0,l}$, $l \in \{0, \ldots, L-1\}$ are respectively the complex echo amplitude (accounting for the transmit amplitude, phase, target reflectivity, and channel propagation effects), the delay, and the target Doppler frequency relative to the l-th transmitter and the 0-th receiver. No synchronization is assumed among the sensors, namely $\tau_{0,l}$, $l = 1, \ldots, L-1$, is considered unknown to the 0-th radar system. To simplify the notation, we use the symbol γ_0 instead of $\gamma_{0,0}$ when the index of the receiver (first index) is equal to the index of the transmitter (second index), where $\gamma_{0,l}$ can be one of the parameters $\alpha_{0,l}^{rx}$, $\tau_{0,l}$, or $f_{0,l}$. We can separate in the Right Hand Side (RHS) of equation (5.1) the term due to the 0-th transmitter:

$$\begin{aligned} r_0(t) = \alpha_0^{rx} e^{j2\pi(f+f_0)(t-\tau_0)} u_0(t-\tau_0) + \\ \sum_{l=1}^{L-1} \alpha_{0,l}^{rx} e^{j2\pi(f+f_{0,l})(t-\tau_{0,l})} u_l(t-\tau_{0,l}) + n_0(t)\,. \end{aligned} \tag{5.2}$$

This signal is down-converted to baseband and filtered through a linear system with impulse response $h(t) = p^*(-t)$. Let the filter output be

$$v_0(t) = \alpha_0^{rx} e^{-j2\pi f \tau_0} \sum_{i=0}^{N-1} c_0(i) e^{j2\pi i f_0 T_r} \chi_p\left(t - iT_r - \tau_0, f_0\right) +$$

$$\sum_{l=1}^{L-1} \alpha_{0,l}^{rx} e^{-j2\pi f \tau_{0,l}} \sum_{i=0}^{N-1} c_l(i) e^{j2\pi i f_{0,l} T_r} \chi_p\left(t - iT_r - \tau_{0,l}, f_{0,l}\right) + w_0(t)$$

where $\chi_p(\lambda, \nu)$ is the (pulse waveform) ambiguity function [22], i.e.

$$\chi_p(\lambda, \nu) = \int_{-\infty}^{+\infty} p(\beta) p^*(\beta - \lambda) e^{j2\pi\nu\beta} d\beta,$$

and $w_0(t)$ is the down-converted and filtered disturbance. The signal $v_0(t)$ is sampled at $t_k = \tau_0 + kT_r$, $k = 0, \ldots, N-1$, providing the observables

$$v_0(t_k) = \alpha_0 c_0(k) e^{j2\pi k f_0 T_r} \chi_p(0, f_0) +$$

$$\sum_{l=1}^{L-1} \alpha_{0,l} \sum_{i=0}^{N-1} c_l(i) e^{j2\pi i f_{0,l} T_r} \chi_p\left(\Delta\tau_{0,l}(k-i), f_{0,l}\right) + w_0(t_k)\,,$$

where $\alpha_{0,l} = \alpha_{0,l}^{rx} e^{-j2\pi f \tau_{0,l}}$, with $l \in \{0, \ldots, L-1\}$ (again, we use the simplified notation $\alpha_0 = \alpha_{0,0}$), and $\Delta\tau_{0,l}(h) = hT_r - \tau_{0,l} + \tau_0$, $l = 1, \ldots, L-1$. Moreover, denoting by

$$\boldsymbol{p}_{0,l} = [1, e^{j2\pi f_{0,l} T_r}, \ldots, e^{j2\pi (N-1) f_{0,l} T_r}]^T$$

the temporal steering vector (with $\boldsymbol{p}_0 = \boldsymbol{p}_{0,0}$),

$$\boldsymbol{v}_0 = [v_0(t_0), v_0(t_1), \ldots, v_0(t_{N-1})]^T,$$

$$\boldsymbol{w}_0 = [w_0(t_0), w_0(t_1), \ldots, w_0(t_{N-1})]^T,$$

and

$$\boldsymbol{i}_{0,l} = \left[\sum_{i=0}^{N-1} c_l(i) e^{j2\pi i f_{0,l} T_r} \chi_p\left(\Delta\tau_{0,l}(-i), f_{0,l}\right), \ldots, \right.$$

$$\left. \sum_{i=0}^{N-1} c_l(i) e^{j2\pi i f_{0,l} T_r} \chi_p\left(\Delta\tau_{0,l}(N-1-i), f_{0,l}\right) \right]^T,$$

we get the following vectorial model for the scattered signal

$$\boldsymbol{v}_0 = \alpha_0 \chi_p(0, f_0) \boldsymbol{c}_0 \odot \boldsymbol{p}_0 + \sum_{l=1}^{L-1} \alpha_{0,l} \boldsymbol{i}_{0,l} + \boldsymbol{w}_0\,. \tag{5.3}$$

In (5.3), we can distinguish the first term due to the 0-th radar ($\alpha_0 \chi_p(0, f_0)\boldsymbol{c}_0 \odot \boldsymbol{p}_0$), the second term due to the interference induced by the other radars ($\sum_{l=1}^{L-1} \alpha_{0,l}\boldsymbol{i}_{0,l}$), and, finally, the disturbance ($\boldsymbol{w}_0$) accounting for clutter and thermal noise.

Moreover, since $\chi_p(t,\nu) = 0$, for $|t| \geq T_p$, the vector $\boldsymbol{i}_{0,l}$ shares a structure which belongs to the finite set $\mathcal{A}_{0,l}$ (of cardinality $2N$) whose elements are

$$\begin{bmatrix} c_l(N-1)e^{j2\pi(N-1)f_{0,l}T_r} \\ 0 \\ \vdots \\ 0 \end{bmatrix} \chi_p\left(\Delta\tau_{0,l}(-N+1), f_{0,l}\right) ,$$

$$\begin{bmatrix} c_l(N-2)e^{j2\pi(N-2)f_{0,l}T_r} \\ c_l(N-1)e^{j2\pi(N-1)f_{0,l}T_r} \\ 0 \\ \vdots \\ 0 \end{bmatrix} \chi_p\left(\Delta\tau_{0,l}(-N+2), f_{0,l}\right) ,$$

$$\vdots$$

$$\begin{bmatrix} c_l(0) \\ c_l(1)e^{j2\pi f_{0,l}T_r} \\ \vdots \\ c_l(N-1)e^{j2\pi(N-1)f_{0,l}T_r} \end{bmatrix} \chi_p\left(\Delta\tau_{0,l}(0), f_{0,l}\right) ,$$

$$\vdots$$

$$\begin{bmatrix} 0 \\ \vdots \\ 0 \\ c_l(0) \\ c_l(1)e^{j2\pi f_{0,l}T_r} \end{bmatrix} \chi_p\left(\Delta\tau_{0,l}(N-2), f_{0,l}\right) ,$$

$$\begin{bmatrix} 0 \\ \vdots \\ 0 \\ c_l(0) \end{bmatrix} \chi_p\left(\Delta\tau_{0,l}(N-1), f_{0,l}\right) ,$$

and the N-dimensional vector $\mathbf{0}$. Defining $\tilde{\boldsymbol{i}}_{0,l}$

$$\tilde{\boldsymbol{i}}_{0,l} = \left[c_l(0), c_l(1)e^{j2\pi f_{0,l}T_r} \ldots, c_l(N-1)e^{j2\pi(N-1)f_{0,l}T_r}\right]^T = (\boldsymbol{c}_l \odot \boldsymbol{p}_{0,l})^T,$$

and

$$\boldsymbol{i}_{0,l}(h) = \boldsymbol{J}_h \tilde{\boldsymbol{i}}_{0,l} \chi_p\left(\Delta\tau_{0,l}(h), f_{0,l}\right) , \tag{5.4}$$

with $\boldsymbol{J}_h$ the $N \times N$ matrix whose entries are

$$\boldsymbol{J}_h(i,j) = \begin{cases} 1 & i - j = h \\ \\ 0 & \text{elsewhere} \end{cases}$$

with $-N+1 \leq h \leq N-1$, the set $\mathcal{A}_{0,l}$ can be compactly written as

$$\mathcal{A}_{0,l} = \left\{\boldsymbol{i}_{0,l}(h)\right\}_{-N+1 \leq h \leq N-1} \bigcup \ \mathbf{0} .$$

5.2 Problem Formulation

In this section, we formulate the problem of designing the code used by the sensor of interest. The design principle is the maximization of the SNR for the sensor of interest (the 0-th), mitigating the mutual interference induced by the sensor of interest on other sensors in the network, and forcing an energy constraint. To this end, it is necessary to introduce explicitly the definition of SNR and the constraints which are required to control the mutual interference and the transmitted energy.

5.2.1 Signal-to-Noise Ratio

Assuming that the disturbance $\boldsymbol{w}_m$, for $m = 0, \ldots, L-1$, is a zero-mean complex circular Gaussian vector with known positive definite covariance matrix

$$E[\boldsymbol{w}_m \boldsymbol{w}_m^\dagger] = \boldsymbol{M} \, ,$$

it is known that the GLRT for the detection of a target component $\boldsymbol{c}_0 \odot \boldsymbol{p}_0$ with unknown complex amplitude in the presence of $\boldsymbol{w}_0$ only (i.e. in the absence of mutual interference among the sensors), is given by

$$|\boldsymbol{v}_0^\dagger \boldsymbol{g}_0|^2 = |\boldsymbol{v}_0^\dagger \boldsymbol{M}^{-1} (\boldsymbol{c}_0 \odot \boldsymbol{p}_0)|^2 \underset{H_0}{\overset{H_1}{\gtrless}} G \, , \tag{5.5}$$

where $\boldsymbol{g}_0 = \boldsymbol{M}^{-1} (\boldsymbol{c}_0 \odot \boldsymbol{p}_0)$ is the 0-th pre-processed steering vector, and G is the detection threshold, set according to a desired value of P_{fa}. This decision rule also coincides with the optimum test (according to the Neyman-Pearson criterion) if the phase of α_0 is uniformly distributed in $[0, 2\pi[$ [24]. From a geometric point of view it is tantamount to projecting the received vector on the pre-processed steering direction and then comparing the energy of the projection with a threshold. An analytical expression of P_d, for a given value of P_{fa}, is available. Precisely, for nonfluctuating targets,

$$P_d = Q\left(\sqrt{2|\alpha_0 \chi_p(0, f_0)|^2 (\boldsymbol{c}_0 \odot \boldsymbol{p}_0)^\dagger \boldsymbol{M}^{-1} (\boldsymbol{c}_0 \odot \boldsymbol{p}_0)}, \Psi\right),$$

where $\Psi = \sqrt{-2 \ln P_{fa}}$. This last expression shows that, given P_{fa}, P_d depends on the radar code, the disturbance covariance matrix, and the temporal steering vector only through the SNR, defined as

$$\mathrm{SNR} = |\alpha_0 \chi_p(0, f_0)|^2 (\boldsymbol{c}_0 \odot \boldsymbol{p}_0)^\dagger \boldsymbol{M}^{-1} (\boldsymbol{c}_0 \odot \boldsymbol{p}_0). \tag{5.6}$$

Moreover, P_d is an increasing function of SNR and, as a consequence, the maximization of P_d can be obtained maximizing

$$(\boldsymbol{c}_0 \odot \boldsymbol{p}_0)^\dagger \boldsymbol{M}^{-1} (\boldsymbol{c}_0 \odot \boldsymbol{p}_0) = \boldsymbol{c}_0^\dagger \boldsymbol{R}_{f_0} \boldsymbol{c}_0 \tag{5.7}$$

over the radar code $\boldsymbol{c}_0$, with

$$\boldsymbol{R}_{f_0} = \boldsymbol{M}^{-1} \odot (\boldsymbol{p}_0 \boldsymbol{p}_0^\dagger)^*. \tag{5.8}$$

Evidently, (5.8) requires the specification of f_0; as a consequence, the solution depends on this pre-assigned value. It is thus necessary to provide some guidelines on the importance and the applicability of the proposed framework. To this end, we highlight that:

- the matched performance (namely when the actual Doppler is exactly f_0) which can be obtained through the optimal solution of (5.7), represents an upper bound to that achievable by any practical system;

- a single coded waveform designed for the challenging condition of slowly moving targets (i.e. $f_0 \simeq 0$) can be devised;

- a single coded waveform optimized over an average scenario may be designed. Otherwise stated, this code might be chosen so as to maximize (5.7) with $\boldsymbol{R}_{f_0}$ replaced by $\boldsymbol{R}_a = \boldsymbol{M}^{-1} \odot \left(E\left[\boldsymbol{p}_0\boldsymbol{p}_0^\dagger\right]\right)^*$, where the expectation operator is over the normalized Doppler frequency. If this last quantity is modeled as a uniformly distributed random variable, i.e. $f_0T_r \sim \mathcal{U}(-\epsilon, \epsilon)$, with $0 < \epsilon < 1/2$, the expectation can be readily evaluated, leading to
$$\boldsymbol{R}_a = \boldsymbol{M}^{-1} \odot \boldsymbol{\Sigma}_\epsilon \,, \tag{5.9}$$
where $\boldsymbol{\Sigma}_\epsilon(m,n) = \operatorname{sinc}\left[2\epsilon(m-n)\right]$.

Summarizing, we can express the objective function as

$$\boldsymbol{c}_0^\dagger \boldsymbol{R} \boldsymbol{c}_0 \,, \tag{5.10}$$

with $\boldsymbol{R}$ equal to $\boldsymbol{R}_a$ or $\boldsymbol{R}_{f_0}$ according to the chosen design context.

5.2.2 Mutual Interference Constraints

To mitigate interference induced by the 0-th sensor, we force our code to produce a small energy level when projected on the l-th pre-processed steering vector, namely on the receiving direction of the l-th sensor. Otherwise stated, we impose the design constraints

$$E\left[|\boldsymbol{i}_{l,0}^{\dagger}\boldsymbol{g}_l|^2\right] \leq \hat{\delta}_l, \quad l = 1, \ldots, L-1\,, \tag{5.11}$$

where $\hat{\delta}_l > 0$ are parameters ruling the acceptable levels of interference: the smaller $\hat{\delta}_l$, the smaller the interference of the radar of interest on the l-th sensor.

As indicated in (5.4), $\boldsymbol{i}_{l,0}$ depends on the particular shift h; hence, in order to circumvent this drawback, we can resort to an average approach, imposing the constraint on the average of all the admissible nonzero $\boldsymbol{i}_{l,0}(h)$ (assumed equiprobable), i.e. (5.11) becomes

$$E\left[\sum_{h=-N+1}^{N-1} |\boldsymbol{i}_{l,0}^{\dagger}(h)\boldsymbol{g}_l|^2\right] \leq \hat{\delta}_l(2N-1), \quad l = 1, \ldots, L-1\,. \tag{5.12}$$

As to the expectation operator, it acts over the parameters $\tau_{l,0}$, τ_l, $f_{l,0}$ and f_l, for $l = 1, \ldots, L-1$, which are practically unknown, and can be reasonably modeled as random variables. Now,

$$E\left[\sum_{h=-N+1}^{N-1} |\boldsymbol{i}_{l,0}^{\dagger}(h)\boldsymbol{g}_l|^2\right] = E\left[\sum_{h=-N+1}^{N-1} |\boldsymbol{i}_{l,0}^{\dagger}(h)\boldsymbol{M}^{-1}(\boldsymbol{c}_l \odot \boldsymbol{p}_l)|^2\right] \leq \hat{\delta}_l(2N-1)\,, \tag{5.13}$$

or equivalently

$$E\left[\sum_{h=-N+1}^{N-1} \boldsymbol{i}_{l,0}^{\dagger}(h)\boldsymbol{M}^{-1}(\boldsymbol{c}_l \odot \boldsymbol{p}_l)(\boldsymbol{c}_l \odot \boldsymbol{p}_l)^{\dagger}\boldsymbol{M}^{-1}\boldsymbol{i}_{l,0}(h)\right] \leq \delta_l,$$

for $l = 1, \ldots, L-1$, with $\delta_l = \hat{\delta}_l(2N-1)$. Hence, denoting by $\boldsymbol{S}_l = \boldsymbol{M}^{-1}\mathrm{diag}(\boldsymbol{c}_l)\boldsymbol{p}_l\boldsymbol{p}_l^{\dagger}\mathrm{diag}(\boldsymbol{c}_l^{*})\boldsymbol{M}^{-1}$, the constraints can be recast as

$$E\left[\sum_{h=-N+1}^{N-1} \boldsymbol{i}_{l,0}^{\dagger}(h)\boldsymbol{S}_l\boldsymbol{i}_{l,0}(h)\right] \leq \delta_l, \qquad l = 1, \ldots, L-1\,. \tag{5.14}$$

According to (5.4),

$$\boldsymbol{i}_{l,0}(h) = \boldsymbol{J}_h(\boldsymbol{c}_0 \odot \boldsymbol{p}_{l,0})\chi_p(\Delta\tau_{l,0}(h), f_{l,0}) = (\boldsymbol{J}_h\boldsymbol{c}_0 \odot \boldsymbol{J}_h\boldsymbol{p}_{l,0})\chi_p(\Delta\tau_{l,0}(h), f_{l,0})\,,$$

so (5.14) becomes

$$E\left[\sum_{h=-N+1}^{N-1} \boldsymbol{c}_0^{\dagger}\boldsymbol{J}_h^{\dagger}\boldsymbol{S}_{l,h}\boldsymbol{J}_h\boldsymbol{c}_0\right] \leq \delta_l, \qquad l = 1, \ldots, L-1\,, \tag{5.15}$$

with $\boldsymbol{S}_{l,h} = |\chi_p(\Delta\tau_{l,0}(h), f_{l,0})|^2\boldsymbol{S}_l \odot \left(\boldsymbol{J}_h\boldsymbol{p}_{l,0}\boldsymbol{p}_{l,0}^{\dagger}\boldsymbol{J}_h^{\dagger}\right)^{*}$. Moreover, denoting by $\boldsymbol{R}_l = \sum_{h=-N+1}^{N-1} \boldsymbol{J}_h^{\dagger}E\left[\boldsymbol{S}_{l,h}\right]\boldsymbol{J}_h$, the mutual interference constraint (5.12) can be expressed as

$$c_0^{\dagger}\boldsymbol{R}_l\boldsymbol{c}_0 \leq \delta_l\,, \qquad l = 1, \ldots, L-1\,. \tag{5.16}$$

Notice that the constraints in (5.16) can be evaluated, assuming a suitable model for the random variables $f_{l,0}$, f_l, $\tau_{l,0}$ and τ_l, with $l = 1, \ldots, L-1$. Assuming f_l, $f_{l,0}$, τ_l and $\tau_{l,0}$ statistically independent, we can factorize $E\left[\boldsymbol{S}_{l,h}\right]$

as

$$E\left[\boldsymbol{S}_{l,h}\right] = \boldsymbol{C}_l \odot \boldsymbol{H}_h\,, \tag{5.17}$$

where the term $\boldsymbol{C}_l$ depends on the code $\boldsymbol{c}_l$, while the term $\boldsymbol{H}_h$ depends on the shift h. In particular,

$$\boldsymbol{C}_l = E\left[\boldsymbol{S}_l\right] = \boldsymbol{M}^{-1}\mathrm{diag}(\boldsymbol{c}_l)E\left[\boldsymbol{p}_l\boldsymbol{p}_l^{\dagger}\right]\mathrm{diag}(\boldsymbol{c}_l^{*})\boldsymbol{M}^{-1}\,, \tag{5.18}$$

and

$$\boldsymbol{H}_h = E\left[|\chi_p(\Delta\tau_{l,0}(h), f_{l,0})|^2\left(\boldsymbol{J}_h\boldsymbol{p}_{l,0}\boldsymbol{p}_{l,0}^{\dagger}\boldsymbol{J}_h^{\dagger}\right)^{*}\right]\,. \tag{5.19}$$

Moreover, assuming the normalized Doppler frequencies f_lT_r uniformly distributed in the interval $[-\Delta, \Delta]$, i.e. $f_lT_r \sim \mathcal{U}(-\Delta, \Delta)$, with $0 < \Delta < 1/2$, we get

$$E\left[\boldsymbol{p}_l\boldsymbol{p}_l^{\dagger}\right] = \boldsymbol{\Sigma}_{\Delta}\,.$$

5.2.3 Energy Constraint

It remains to force a constraint on the transmitted energy by the radar of interest, namely we suppose that the normalized code energy is less than or equal to N, i.e.

$$\|\boldsymbol{c}_0\|^2 \leq N\,. \tag{5.20}$$

5.3 Problem Solution

Now, according to (5.10), (5.16), and (5.20), we can formulate the code design in terms of the following Quadratic optimization Problem (QP_3)

$$\mathrm{QP}_3 \begin{cases} \underset{\boldsymbol{c}_0}{\text{maximize}} & {\boldsymbol{c}_0}^\dagger \boldsymbol{R} \boldsymbol{c}_0 \\ \text{subject to} & {\boldsymbol{c}_0}^\dagger \boldsymbol{R}_l \boldsymbol{c}_0 \leq \delta_l, \qquad l = 1, \ldots, L-1 \\ & {\boldsymbol{c}_0}^\dagger \boldsymbol{c}_0 \leq N\,. \end{cases} \tag{5.21}$$

Letting $\boldsymbol{R}_{\delta_l} = \delta_l^{-1} \boldsymbol{R}_l$, for $l = 1, \ldots, L-1$, problem (5.21) can be recast as

$$\mathrm{QP}_3 \begin{cases} \underset{\boldsymbol{c}_0}{\text{maximize}} & {\boldsymbol{c}_0}^\dagger \boldsymbol{R} \boldsymbol{c}_0 \\ \text{subject to} & {\boldsymbol{c}_0}^\dagger \boldsymbol{R}_{\delta_l} \boldsymbol{c}_0 \leq 1, \qquad l = 0, \ldots, L-1 \end{cases} \tag{5.22}$$

with $\boldsymbol{R}_{\delta_0} = N^{-1} \boldsymbol{I}$. Now, we have a homogeneous quadratic optimization problem defined in complex field $\mathbb{C}^N$. Moreover, $\boldsymbol{R}_{\delta_l}$ are positive semidefinite matrices. The equivalent matrix formulation of QP_3 is

$$\mathrm{QP}_3 \begin{cases} \underset{\boldsymbol{C}_0}{\text{maximize}} & \mathrm{Tr}\,(\boldsymbol{C}_0 \boldsymbol{R}) \\ \text{subject to} & \mathrm{Tr}\,(\boldsymbol{C}_0 \boldsymbol{R}_{\delta_l}) \leq 1, \qquad l = 0, \ldots, L-1 \\ & \boldsymbol{C}_0 = \boldsymbol{c}_0 \boldsymbol{c}_0^\dagger \end{cases} \tag{5.23}$$

Unfortunately, this problem is NP-hard [52]. One approach to approximating the solution to the NP-hard quadratic programs is the relaxation and randomization technique [26]: first relax the feasible solution set of the problem, obtaining a Convex Problem (CP) that can be solved in polynomial time through the *interior point methods*; then use the optimal solution of the relaxed problem to produce a feasible solution for the original problem.

In the following, we present the WILD procedure to obtain a near optimal solution of the original problem (5.23), and give the approximate bound in the proposed problem.

5.3.1 Relaxation and Randomization

A possible relaxation of (5.23) is the following SDP problem

$$\text{CP}\begin{cases} \underset{\boldsymbol{C}_0}{\mathsf{maximize}} & \mathrm{Tr}\left(\boldsymbol{C}_0\boldsymbol{R}\right) \\ \mathsf{subject\ to} & \mathrm{Tr}\left(\boldsymbol{C}_0\boldsymbol{R}_{\delta_l}\right) \leq 1, \qquad l = 0, \ldots, L-1 \\ & \boldsymbol{C}_0 \succeq \boldsymbol{0} \end{cases} \tag{5.24}$$

where we have removed the rank-one constraint. An SDP is a convex problem which can be solved using interior point methods [3], so CP can be easily solved in polynomial time, obtaining the optimal solution $\overline{\boldsymbol{C}}$.

Factorize the optimal solution $\overline{\boldsymbol{C}}$ such that $\overline{\boldsymbol{C}} = \boldsymbol{U}\boldsymbol{U}^\dagger$, with $\boldsymbol{U}$ a complex $N \times r$ matrix[1], where $r = \mathrm{rank}\left(\overline{\boldsymbol{C}}\right)$. Evaluate the orthogonal $r \times N$ complex matrix $\boldsymbol{Q}$ such that $\boldsymbol{Q}^\dagger\boldsymbol{U}^\dagger\boldsymbol{R}\boldsymbol{U}\boldsymbol{Q}$ is a diagonal matrix.

The next step is to generate a random vector that is feasible (with probability one) for the problem QP_3. Let us define $\boldsymbol{x}$ as a real normal vector, i.e. $\boldsymbol{x} \sim \mathcal{N}\left(\boldsymbol{0}, \boldsymbol{I}\right)$, and

$$\boldsymbol{\xi} = \mathrm{sign}\left(\boldsymbol{x}\right) = \left[\mathrm{sign}\left(x(0)\right), \ldots, \mathrm{sign}\left(x(N-1)\right)\right]^T,$$

[1]Notice that in the particular case of $r = 1$, $\boldsymbol{U}$ is an optimal solution of QP_3.

where

$$\mathrm{sign}\,(x(i)) = \begin{cases} 1 & x(i) \geq 0 \\ -1 & x(i) < 0\,. \end{cases}$$

Now, we can define a feasible solution of QP_3, say $\boldsymbol{c}_\xi$, in the following way

$$\boldsymbol{c}_\xi = \frac{\boldsymbol{UQ\xi}}{\sqrt{\max\limits_{0\leq l\leq L-1} \boldsymbol{\xi}^T \widehat{\boldsymbol{R}_{\delta_l}} \boldsymbol{\xi}}}\,, \tag{5.25}$$

where $\widehat{\boldsymbol{R}_{\delta_l}} = \boldsymbol{Q}^\dagger \boldsymbol{U}^\dagger \boldsymbol{R}_{\delta_l} \boldsymbol{UQ}$.

5.3.2 Approximation Bound

A "measure of goodness" of the randomization algorithm is provided by the approximate bound which characterizes the quality of the produced solutions. In the literature, a randomized approximation method for a maximization problem has a bound (or performance guarantee, or worst case ratio) $R \in (0, 1]$, if for all instances of the problem, it always delivers a feasible solution whose expected value is at least R times the maximum value of the relaxed problem [26].

With reference to the WILD algorithm, we have

$$R \times v(\mathrm{CP}) \leq v_{WILD}(\mathrm{QP}_3) \leq v(\mathrm{CP})\,,$$

where R is the approximate bound, $v(\mathrm{CP})$ is the optimal value of CP, and $v_{WILD}(\mathrm{QP}_3)$ is the objective value of QP_3 achieved by the WILD algorithm.

It has been proven [52] that the approximate bound for this technique is

$$R = \frac{1}{2\ln(2L\mu)},$$

where $\mu = \min\{L, N\}$.

For example, if $N = L = 2$, $R = 0.24$; if $N = L = 3$, $R = 0.17$; if $N = L = 4$, $R = 0.14$. However, we remark that the approximate bound is a worst-case result [26], and, in practice, the actual performance v_{WILD} is substantially better than the lower bound $R \times v(\text{CP})$ (see Section 5.4.1): such behavior is quite common for randomized techniques [54] [7].

Summarizing, the WILD can be formulated as reported in Algorithm 4.

Algorithm 4 Waveform Interference Limiting Design (WILD)

`Input:` $\boldsymbol{R}$, $\boldsymbol{R}_{\delta_l}$ for $l = 0, \ldots, L-1$;
`Output:` $\boldsymbol{c}_{WILD}$;
1: solve CP finding an optimal solution $\overline{\boldsymbol{C}}$;
2: evaluate $\boldsymbol{U}$ such that $\overline{\boldsymbol{C}} = \boldsymbol{U}\boldsymbol{U}^\dagger$;
3: evaluate $\boldsymbol{Q}$ such that $\boldsymbol{Q}^\dagger\boldsymbol{U}^\dagger\boldsymbol{R}\boldsymbol{U}\boldsymbol{Q}$ is diagonal;
4: generate $\boldsymbol{\xi}$ with $\boldsymbol{\xi}(i) \in \{-1, 1\}$ independent, with $\Pr(\xi(i) = 1) = 0.5$, for $i = 0, \ldots, N-1$;
5: calculate

$$\boldsymbol{c}_{WILD} = \frac{\boldsymbol{U}\boldsymbol{Q}\boldsymbol{\xi}}{\sqrt{\max\limits_{0 \le l \le L-1} \boldsymbol{\xi}^T \widehat{\boldsymbol{R}_{\delta_l}} \boldsymbol{\xi}}}$$

where $\widehat{\boldsymbol{R}_{\delta_l}} = \boldsymbol{Q}^\dagger\boldsymbol{U}^\dagger\boldsymbol{R}_{\delta_l}\boldsymbol{U}\boldsymbol{Q}$.

5.4 Performance Analysis

The present section discusses the performance of the proposed encoding scheme. The analysis is conducted in terms of normalized average[2] SNR, SNR_{norm} (Subsection 5.4.1) and average normalized interference level induced by the m-th sensor on the l-th one I_m^l (Subsection 5.4.2), respectively defined as

$$\mathrm{SNR}_{norm} = \frac{E_{\boldsymbol{\xi}}\left[\boldsymbol{c}_0^{\dagger}\boldsymbol{R}\boldsymbol{c}_0\right]}{N\lambda_{max}\left(\boldsymbol{R}\right)},$$

and

$$I_m^l = \frac{E_{\boldsymbol{\xi}}\left[\boldsymbol{c}_m^{\dagger}\boldsymbol{R}_l\boldsymbol{c}_m\right]}{N\lambda_{max}\left(\boldsymbol{R}_l\right)}.$$

Notice that $N\lambda_{max}\left(\boldsymbol{R}\right)$ can be viewed as the optimal value of the Unconstrained Problem (UP),

$$\mathrm{UP}\begin{cases} \underset{\boldsymbol{c}_0}{\mathsf{maximize}} & \boldsymbol{c}_0^{\dagger}\boldsymbol{R}\boldsymbol{c}_0 \\ \mathsf{subject\ to} & \boldsymbol{c}_0{}^{\dagger}\boldsymbol{c}_0 \le N \end{cases} \tag{5.26}$$

where the constraints on the interference have been removed. Obviously, the optimal value $v(\mathrm{UP})$ is greater than the optimal value of the problem QP_3, i.e. $v(\mathrm{UP}) \ge v(\mathrm{QP}_3)$, and, as a consequence, $\mathrm{SNR}_{norm} \le 1$. Subsection 5.4.3 illustrates the computational complexity of the proposed algorithm.

We assume that the disturbance covariance matrix is exponentially shaped with one-lag correlation coefficient $\rho = 0.8$, i.e.

$$\boldsymbol{M}(m,n) = \rho^{|m-n|}, \qquad (m,n) \in \{0,\dots,N-1\}^2.$$

[2]The average is performed over $\boldsymbol{\xi}$'s as to make the result independent of the specific randomization.

Moreover, we choose the pulse $p(t)$ with rectangular shape, and duty cycle $T_p/T_r = 1/3$. Finally, we model the normalized delay $\Delta\tau_{m,l}(h)/T_r$ and the normalized Doppler shift $f_{m,l}T_r$ as independent random variables, uniformly distributed in the interval $[-1, 1]$ and $[-1/3, 1/3]$ respectively, i.e. $\Delta\tau_{m,l}(h)/T_r \sim \mathcal{U}(-1, 1)$ and $f_{m,l}T_r \sim \mathcal{U}(-1/3, 1/3)$. The convex optimization Matlab© toolbox SeDuMi [4] is exploited to solve the SDP relaxation.

5.4.1 Maximization of the SNR

In this subsection, we analyze the effect of three different parameters on the SNR_{norm} : normalized Doppler shift on the reference sensor, length of the code, number of interfering sensors. We consider the case of a WILD code $\boldsymbol{c}_0$ of length N, and temporal steering vector $\boldsymbol{p}_0$ with a known normalized Doppler shift $f_d = f_0 T_r$, i.e.

$$\boldsymbol{p}_0 = \left[1, e^{j2\pi f_d}, \ldots, e^{j2\pi f_d(N-1)}\right]^T .$$

All the acceptable interfering levels δ_l with $l = 1, \ldots, L-1$, are set equal to δ, defined as

$$\delta = \delta_{norm} \left(\Lambda_{max} - \Lambda_{min}\right) + \Lambda_{min} ,$$

where

$$\Lambda_{max} = \min_{l=1,\ldots,L-1} \left\{N\lambda_{max}\left(\boldsymbol{R}_l\right)\right\} ,$$
$$\Lambda_{min} = \max_{l=1,\ldots,L-1} \left\{N\lambda_{min}\left(\boldsymbol{R}_l\right)\right\} ,$$

and $\delta_{norm} \in (0, 1)$.

Finally, the operating environment has $L - 1 = 3$ interfering sensors. All the interfering radars use a phase code with the same length and the same energy[3] as our WILD code. In particular, the first radar uses a Barker code, the second one a generalized Barker code, and the third a Zadoff code [22].

In Figure 5.1, we plot SNR_{norm} versus δ_{norm} for $N = 5$, $L = 4$, and four different values of f_d. For comparison purpose, we also plot the SNR_{norm} of a Barker code of length 5. As expected, the higher δ_{norm} the higher SNR_{norm}: this can be easily explained observing that increasing δ_{norm} is tantamount to enlarging the feasibility region, so higher and higher optimal values can be found. It is also noticeable that the WILD code outperforms the classical Barker code for $\delta_{norm} \geq 0.03$. Finally, the performance of the proposed encoding technique depends on the Doppler shift for small values of δ_{norm}, but for $\delta_{norm} \geq 0.6$ at any Doppler frequency the SNR_{norm} of the WILD algorithm is very close to the maximum (i.e. $\mathrm{SNR}_{norm} = 0$ dB).

In Figure 5.2, we illustrate the effect of the length N on the code. In particular, we consider the normalized Doppler frequency $f_d = 0.30$, $L = 4$ sensors in the network, while the length N of the code $\boldsymbol{c}_0$ can be 4, 7, 11, or 13. For comparison purpose, we plot the SNR_{norm} of a Barker code of length 13. In particular, we plot SNR_{norm} versus δ_{norm} for the considered values of N; evidently, increasing N leads to higher values of SNR_{norm}. This can be explained observing that the parameter N governs the energy constraint: the higher N, the higher the maximum energy. Moreover, increasing N enlarges the number of degrees of freedom. Finally, we can observe that the WILD code of length 13 outperforms the Barker code of the same length for almost

[3] We recall that the maximum code energy of our WILD code is equal to N, as required by (5.20).

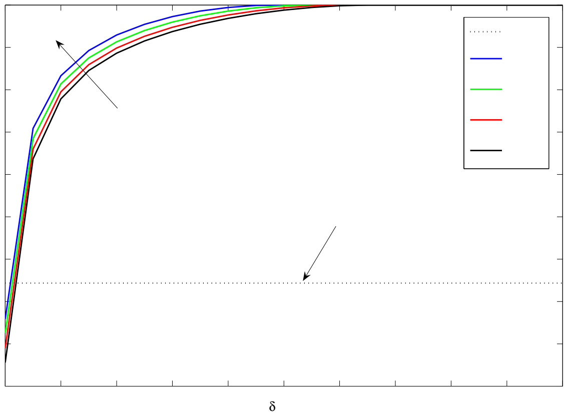

Figure 5.1: SNR_{norm} versus δ_{norm} for $N = 5$, $L = 4$, and some normalized Doppler shifts f_d, i.e. $f_d \in \{0.15; 0.20; 0.25; 0.30\}$ (solid curves). Barker code of length 5 (dotted line).

all values of δ_{norm}.

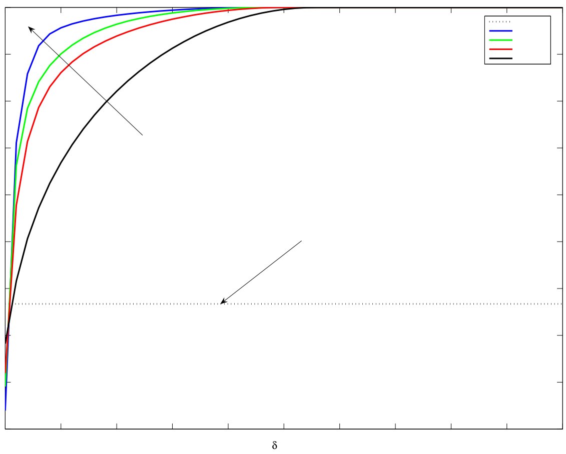

Figure 5.2: SNR_{norm} versus δ_{norm} for $L = 4$, normalized Doppler shift $f_d = 0.30$, and some values of N, i.e. $N \in \{4; 7; 11; 13\}$ (solid curves). Barker code of length 13 (dotted line).

In Figure 5.3, we analyze the effect of the size L of the network. We plot SNR_{norm} versus δ_{norm} with normalized Doppler frequency $f_d = 0.30$, length $N = 13$, and different values of L: when $L = 2$ there is just one interfering code (Barker), $L = 3$ two interfering codes (Barker and generalized Barker), $L = 4$ three interfering codes (Barker, generalized Barker, and Zadoff). In this figure, we also plot the SNR_{norm} of a Barker code of length 13. The curves show that increasing the dimension of the network, leads to degraded performance. In fact, increasing L reduces feasibility, so lower and lower optimal values may be achieved. It can also be observed that for high values of δ_{norm}, the algorithm reaches the maximum value of SNR_{norm} (i.e. $v(\text{UP}) = v_{WILD}(\text{QP}_3)$), and even for small values of δ_{norm} (i.e. $\delta_{norm} = 0.1$) the WILD code exhibits a gain of at least 1 dB over the classic Barker code. Summarizing, there is a trade-off between the SNR_{norm} of the sensor of interest and the interference in the remaining sensors: δ_{norm} is the secondary parameter that rules this relationship.

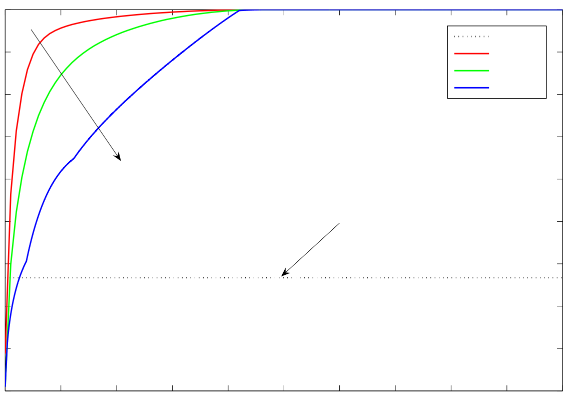

Figure 5.3: SNR_{norm} versus δ_{norm} for $N = 13$, normalized Doppler shift $f_d = 0.30$, and some values of L, i.e. $L \in \{2; 3; 4\}$ (solid curves). Barker code of length 13 (dotted line).

Now, we study the robustness of the proposed algorithm, considering a mismatch between the *nominal* steering vector $\boldsymbol{p}_0$ with $f_d = 0$ (assumed to design the code) and the *actual* steering vector

$$\boldsymbol{p}_F = \left[1, e^{j2\pi F}, \ldots, e^{j2\pi F(N-1)}\right]^T ,$$

with F representing the actual normalized Doppler frequency. We also analyze the WILD version of the code with $\boldsymbol{R} = \boldsymbol{R}_a$, as indicated in (5.9), assuming $\epsilon = 0.3$. To evaluate the performance of the algorithm, we consider the actual average normalized SNR, defined as

$$\mathrm{SNR}_F = \frac{E_{\boldsymbol{\xi}}\left[\boldsymbol{c}_0^\dagger \boldsymbol{R}_F \boldsymbol{c}_0\right]}{N\lambda_{max}\left(\boldsymbol{R}_F\right)} ,$$

where $\boldsymbol{R}_F = \boldsymbol{M}^{-1} \odot \left(\boldsymbol{p}_F \boldsymbol{p}_F^\dagger\right)^*$.

In Figure 5.4, we plot SNR_F versus F for two different values of δ_{norm}, and for $L = 4$ (Barker, generalized Barker, and Zadoff). For comparison purpose, we plot the Barker code of length 5. The classic version of the proposed code outperforms the Barker code only when the effective normalized Doppler frequency F is close to the nominal value f_d. On the contrary, the average version of WILD achieves an higher value of SNR_F than the Barker code in the interval $[-0.3; +0.3]$. As expected, this robustness has a price: a loss of 3 dB in the case of perfect knowledge of the steering vector (i.e. $F = f_d$).

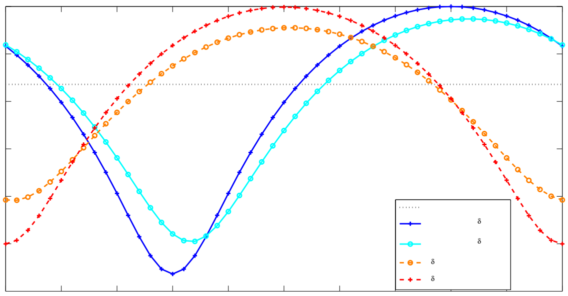

Figure 5.4: SNR_F versus F for $N = 5$, $L = 4$. Barker code of length 5 (dotted curve). Average ($\boldsymbol{R}_a$) WILD code (dashed curves). Classic ($\boldsymbol{R}_{f_0}$) WILD code for $f_d = 0.30$ (solid curves). WILD codes for $\delta_{norm} = 0.2$ (o-marked curves). WILD codes for $\delta_{norm} = 0.8$ (+-marked curves).

5.4.2 Control of the induced interference

In this subsection, we analyze the behavior of the induced interference I_m^l for different network scenarios. In the first case, we study the same operating environment as in Subsection 5.4.1, i.e. three pre-existing radar sensors, which use a Barker code ($\boldsymbol{c}_1$), a generalized Barker code ($\boldsymbol{c}_2$), and a Zadoff code ($\boldsymbol{c}_3$) respectively.

In Figure 5.5, we plot the interference induced on the Barker code $\boldsymbol{c}_1$ (i.e. I_m^1, with $m \in \{0, 2, 3\}$) versus δ_{norm}, for normalized Doppler frequency $f_d = 0.30$, and length $N = 5$. In particular, we plot the interference induced by our code (I_0^1), and, for comparison purpose, we plot the interference induced by the generalized Barker code and by the Zadoff code (I_2^1 and I_3^1 respectively). We notice that the interference level increases as δ_{norm} increases, because the parameter δ_{norm} rules the acceptable amount interference. For $\delta_{norm} = 0.7$ the interference induced by the WILD code becomes higher than I_2^1 and I_3^1. In Figure 5.6, we consider the interferences induced on the generalized Barker code $\boldsymbol{c}_2$ and on the Zadoff code $\boldsymbol{c}_3$ respectively. Analogous considerations can be done in these two cases.

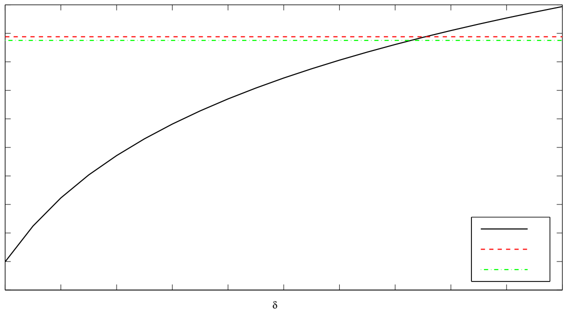

Figure 5.5: I_m^1 versus δ_{norm} for $N = 5$, $L = 4$, and normalized Doppler shift $f_d = 0.30$: I_0^1 (solid curves); I_2^1 (dashed lines); I_3^1 (dotted-dashed lines).

In the second scenario, described in Figure 5.7, we consider an operating environment with only one pre-existing code. This allows us to analyze the effect of a particular code on the algorithm. We selected five possible codes, all of them with energy $N = 7$: four phase codes (Barker, generalized Barker, Zadoff and P4 codes) [22], and an amplitude-phase modulated code (Huffman code) [55]. In Figure 5.7, we plot I_0^1 versus δ_{norm} for normalized Doppler frequency $f_d = 0.15$, network dimension $L = 2$, and different interfering codes $\boldsymbol{c}_1$. We observe that our code induce almost the same value of interference over all the proposed codes: for $\delta_{norm} > 0.8$, there is less than 1 dB between I_0^1 of the P4 code and of the Huffman code.

Finally, in the third scenario, we consider a network with $L - 1 = 3$ pre-existing radar sensors, all of them with a code of length and energy $N = 4$. Moreover, the first code ($\boldsymbol{c}_1$) is a Barker code, while the other two codes ($\boldsymbol{c}_2$ and $\boldsymbol{c}_3$) belong to a certain class: phase codes, Gold codes, orthogonal PN

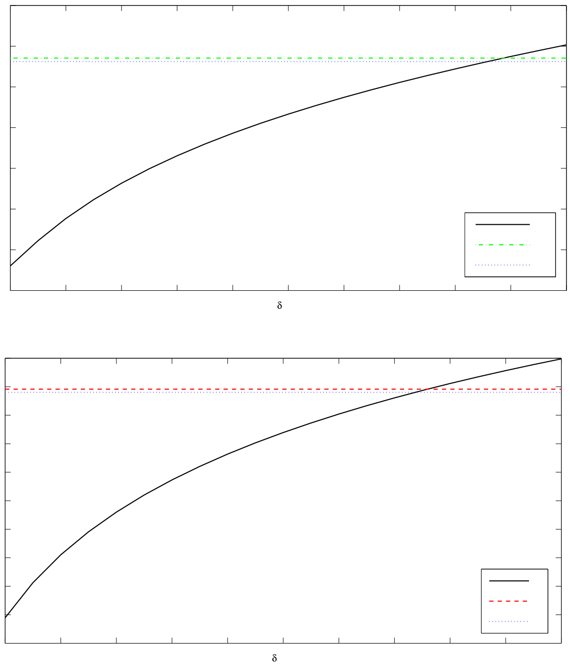

Figure 5.6: I_m^l versus δ_{norm} for $N = 5$, $L = 4$, and normalized Doppler shift $f_d = 0.30$: I_m^2 (up) and I_m^3 (down). I_0^l (solid curves); I_1^l (dotted lines); I_2^l (dashed lines); I_3^l (dotted-dashed lines).

codes, or WILD codes. When the sensors use phase codes, we set $\boldsymbol{c}_2$ and $\boldsymbol{c}_3$ as generalized Barker and Zadoff codes, respectively. In the case of Gold codes [56], the two codes are generated according to the procedure described by Levanon and Mozeson [22], while the PN sequences [57] are generated so that they are orthogonal. Finally, in the last case, we have an initial Barker code $\boldsymbol{c}_1$, a WILD code $\boldsymbol{c}_2$ devised assuming $L = 2$ and $\delta_{norm} = \delta^0$, and a WILD code $\boldsymbol{c}_3$, with $L = 3$ and $\delta_{norm} = \delta^0$ (see Figure 5.8 for a pictorial description of the different scenarios).

In Figure 5.9, we plot the normalized overall induced interference on the

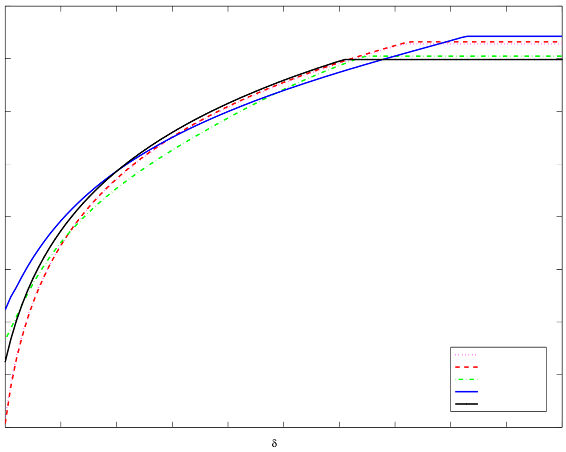

Figure 5.7: $I_0^1(\boldsymbol{c}_1)$ versus δ_{norm} for $N = 7$, $L = 2$, normalized Doppler shift $f_d = 0.15$, and different codes $\boldsymbol{c}_1$: Huffman code (point-marked curve), Zadoff code (dotted-dashed curve), Barker code (dotted curve), generalized Barker code (dashed curve), P4 code (solid curve).

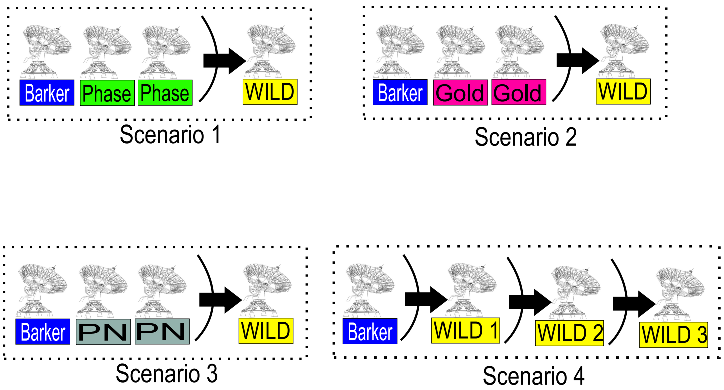

Figure 5.8: Some scenarios where WILD can be applied.

radar sensor which uses the Barker code $\boldsymbol{c}_1$, i.e. I_{TOT}^1, defined as

$$I_{TOT}^1 = \frac{I_0^1 + I_2^1 + I_3^1}{L-1},$$

versus δ_{norm}, for normalized Doppler frequencies $f_d = 0.30$, and different classes of codes. The last class WILD is also parameterized on three different values of δ^0. First of all, we notice that classes of codes with good cross-correlation properties, such as Gold codes and orthogonal PN sequences, achieve lower values of induced interference than phase codes. Moreover, WILD codes can achieve the same performance as PN orthogonal sequences for $\delta^0 = 0.5$, while the overall induced interference can increase in correspondence of higher values of δ^0, or decrease for smaller δ^0 values. This behavior confirms that there is a trade-off between the SNR and the induced interference. It is also noticeable that for a certain range of δ_{norm}, our proposed algorithm can achieve both higher values of SNR and lower values of induced interference than other codes.

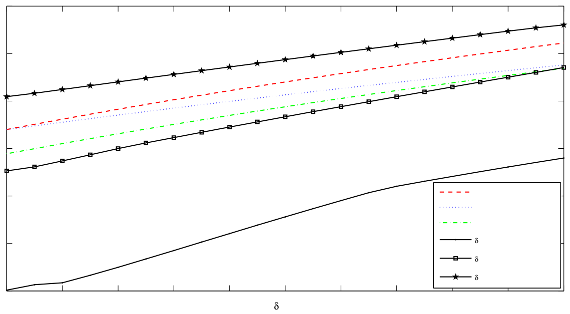

Figure 5.9: I^1_{TOT} versus δ_{norm} for $N = 4$, $L = 4$, normalized Doppler shift $f_d = 0.30$, and different classes of codes $\boldsymbol{c}_2$ and $\boldsymbol{c}_3$: phase codes (dashed curve), Gold code (dotted curve), orthogonal PN codes (dotted-dashed curve), WILD codes with $\delta^0 = 0.2$ (solid curve), WILD codes with $\delta^0 = 0.5$ (square-marked curve), WILD codes with $\delta^0 = 0.8$ (star-marked curve).

Table 5.1: Average N_{it} and average T_{CPU} required to solve problem (5.24).

δ_{norm}	N	L	Average N_{it}	Average T_{CPU}
0.2	4	4	8	0.46
0.5	4	4	9	0.51
0.8	4	4	10	0.56
0.2	13	4	13	0.71
0.5	13	4	14	0.80
0.8	13	4	15	0.83

5.4.3 Computational complexity

Among the five steps of the WILD algorithm, the most bundersome in terms of computational complexity, is the first step. In fact, the resolution of CP has a computational complexity $O\left(N^{3.5}\right)$ [27]. We recall that the complexity is based on a worst-case analysis, and usually the interior point methods are much faster [3]. In Table I, we report the number of iterations N_{it} and the CPU time T_{CPU} in seconds required to solve CP using the toolbox SeDuMi [4]. We have indicated also the corresponding value of δ_{norm} used in the simulation, the dimension N of the problem, and the number L of constraints. The reported averaged values have been evaluated over 100 trials. Finally, the computer used to obtain these results is equipped with a 3 GHz Intel XEON processor.

5.5 Conclusions

In this chapter, we have considered the problem of code design for a single radar that operates in a noncooperative network. We try to maximize the SNR of the radar, controlling, at the same time, the interference induced by our sensor on the others sensors of the network, and forcing a constraint on the transmitted energy by our radar. The resulting problem is NP-hard. Using the well established relaxation and randomization theory [52], we have presented a new coding procedure (referred to as WILD), which in polynomial time generates a suboptimal solution of the original problem. Numerical simulations confirm that the WILD technique can increase the detection performance of the network. Possible future research tracks might concern the extension of the WILD: for istance, it might be interesting to add a constraint on the resulting ambiguity function of the code [6], or on the achievable region of Doppler estimation accuracy. Moreover, it will be of interest to study this procedure applied to a real scenario.

Chapter 6

Conclusions

An extensive discussion about radar waveform design has been presented. In chapter 1 we introduce the concept of optimization theory applied to signal processing. Some examples in the radar field are proposed. Thus, in chapter 2 we explain some basic concepts about code design and ambiguity function. In fact, code design is the main tool to achieve ambiguity function shaping. The following chapters present original works about waveform design. In chapter 3, we start with the problem of pulse code design for a single radar. We determine the optimum radar code, in the sense that it maximizes the detection performance under a control on the region of achievable Doppler estimation accuracies, and under a similarity constraint with a prefixed radar code. In chapter 4, the encoding procedure is extended to a STAP scenario. We look for the best code under particular accuracies and similarity conditions. Using a relaxation and decomposition technique, we evaluate the desired code in polynomial time. Finally, in chapter 5, we apply the coding design to a networked radar. In particular, we try to maximize the

SNR, controlling, at the same time, the interference induced by the radar on the others sensors of the network, and forcing a constraint on the transmitted energy by our radar. We find a quasi-optimal solution with polynomial complexity.

Summarizing, in this thesis we have demonstrated how convex optimization theory can be successfully applied to radar waveform design (and, in general, to radar processing). Remarkably, all the proposed algorithms possess polynomial complexity, so they could be adopted in real scenarios.

Acknowledgement

First of all, I'm sincerely in debt with my tutor, Antonio De Maio, or simply "Antonio". I have spent three exciting years with him, and I'm totally satisfied of my PhD pursuit. Sometimes, people says that if you look to a student, you can recognize his tutor: if true, I consider it an honour. Fortunately, Antonio has not the only professor or student I meet. The Department is full of enthusiastic people, which work simply with passion, sharing new ideas with others. There isn't enough space to name all of them, from A(ubry) to Z(inno), but I can assure you that I remember all of them, even if they have spent roughly an hour in the laboratory (like Pietro P.). In fact, the lab has been indeed my *home* for three years. Fortunately, I've had the best *labmate* (neologism) ever:Angelo Petrella. Thinking of him, Xenophon said '"Οποπα γάκος σκῦππὲττασ'. Not to mention, the *householder* Franco De Luca, which repetitely has stood us. Finally, I have to thanks my coordinators, alias Giovanni Poggi and Niccolò Rinaldi, which have conducted me zelaously towards the PhD, despite my idiosyncrasy for certifications and italian burocracy. In addition to Antonio, it's their credit if I've started and successfully ended the fellowship.

Moving away from the *italian side* of my PhD, I have deeply to thanks emeritus Prof. Shuzhong Zhang to have accepted me as a visiting *neapolitan* student in his Department at Hong Kong University. Thanks to Prof. Zhang, a fantastic teacher and a wonderful person, it was a unique experience. In his group there are always brilliant students. In particular, I'd like to mention one, which a consider not only a collegue, but a real friend: Yongwei Huang. Every time I land in Hong Kong, he is the first person I meet.
And finally, I've to thanks all my coauthors. For me it is a **real pleasure** to work with them. I've started my fellowship reading their works, and I've ended it writing papers with them: for me it's unbelievable (probably, an x-ray effect). I always loved working in group. As Jefferson said *"if two men exchange one dollar they each walk away with 1 dollar. If they exchange an idea they both walk away with 2 ideas"*. Thanks again to (in rigorously alphabetic order) Alfonso, Antonio, Daniel, Danilo, Francesco, in addition to Giuseppe, Goffredo, Yongwei, Luciano, Michael, the new-father Salvatore, Shuzhong, and Tom. Just a mention for Luciano, which always follow me everywhere I go (and *viceversa*).
Two pages are too short to thanks all the people which have supported me in these years[1]. But I have to thanks my family: my parents for encouraging and helping me, my sister for warning me, and my brother as *memento* of the *real* goal of a telecommunication engineer. Finally, I owe this thesis to a special person. There is a bit of her in each chapter.

[1]The complete list, not reported here for the lack of space, can be found in my degree thesis.

Bibliography

[1] Z.-Q. Luo, "Applications of Convex Optimization in Signal Processing and Digital Communication", *Mathematical Programming*, Vol. 97, No. 1-2, pp. 177-207, July 2003.

[2] D. P. Palomar and Y. C. Eldar (edited), *Convex Optimization in Signal Processing and Communications*, Cambridge University Press, 2009.

[3] S. Boyd and L. Vandenberghe, *Convex Optimization*, Cambridge University Press, 2003.

[4] J. F. Sturm, "Using SeDuMi 1.02, a MATLAB Toolbox for Optimization over Symmetric Cones", *Optimization Methods and Software*, Vol. 11-12, pp. 625-653, August 1999.

[5] K. C. Toh, M. J. Todd, and R. H. Tütüncü, "SDPT3 - a Matlab software package for semidefinite programming", *Optimization Methods and Software*, Vol.11-12, pp. 545-581, August 1999.

[6] J. Li, J. R. Guerci, and L. Xu, "Signal Waveform's Optimal-under-Restriction Design for Active Sensing", *IEEE Signal Processing Letters*, Vol. 13, No. 9, pp. 565-568, September 2006.

[7] A. De Maio, S. De Nicola, Y. Huang, Z.-Q. Luo, and S. Zhang, "Design of Phase Codes for Radar Performance Optimization with a Similarity Constraint", *IEEE Transanctions on Signal Processing*, Vol. 57, No. 2, pp. 610-621, February 2009.

[8] A. De Maio, S. De Nicola, Y. Huang, S. Zhang, and A. Farina, "Adaptive Detection and Estimation in the Presence of Useful Signal and Interference Mismatches", *IEEE Transanctions on Signal Processing*, Vol. 57, No. 2, pp. 610-621, February 2009.

[9] A. De Maio, S. De Nicola, A. Farina, and S. Iommelli, "Adaptive Detection of a Signal with Angle Uncertainty", *IET Radar, Sonar and Navigation*, in press.

[10] A. De Maio, S. De Nicola, and A. Farina, "GLRT versus MFLRT for Adaptive CFAR Radar Detection with Conic Uncertainty", *IEEE Signal Processing Letters*, Vol. 16, No. 8, pp. 707-710, August 2009.

[11] R. Abrahamsson, S. M. Kay, and P. Stoica, "Estimation of the parameters of a bilinear model with applications to submarine detection and system identification", *Digital Signal Processing*, Vol. 17, No. 4, pp. 756-773, July 2007.

[12] A. De Maio, S. De Nicola, L. Landi, and A. Farina, "Knowledge-aided covariance matrix estimation: a MAXDET approach", *IET Radar, Sonar and Navigation*, Vol. 3, No. 4, pp. 341-356, August 2009.

[13] A. De Maio, S. De Nicola, Y. Huang, S. Zhang, and A. Farina, "Code Design to Optimize Radar Detection Performance Under Accuracy and

Similarity Constraints", *IEEE Transactions on Signal Processing*, Vol. 56, No. 11, pp. 5618 - 5629, November 2008.

[14] A. De Maio, S. De Nicola, Y. Huang, D. P. Palomar, S. Zhang, and A. Farina, "Code Design for Radar STAP via Optimization Theory", *IEEE Transactions on Signal Processing*, in press.

[15] A. De Maio, S. De Nicola, A. Farina, and M. C. Wicks, "Waveform Design for Noncooperative Radar Networks", submitted to *IET Radar, Sonar and Navigation.*

[16] L. Falk, "From "Information Theory in Radar" - A Tribute to P. M. Woodward", *Swedish Defence Research Agency*, Edinburgh, November 2004.

[17] J. Ville, "Theory and applications of the notion of complex signal", translated by I. Seline in *RAND Technical Report T-92*, RAND Corporation, August 1958.

[18] E. Wigner, "On the quantum correction for thermodynamic equilibrium", *Physical Review*, Vol. 40, No. 5, pp. 749-759, June 1932.

[19] A. W. Rihaczek, *Principles of High Resolution Radar*, McGraw-Hill, New York, 1969.

[20] M. I. Skolnik, *Radar Handbook*, McGraw-Hill, New York, 2008.

[21] E. Mozeson and N. Levanon, "MATLAB code for plotting ambiguity functions", *IEEE Transactions on Aerospace and Electronic Systems*, Vol. 38, No. 3, pp. 1064-1068, July 2002.

[22] N. Levanon and E. Mozeson, *Radar Signals*, John Wiley & Sons, 2004.

[23] C. E. Cook and M. Bernfeld, *Radar Signals: An Introduction to Theory and Application*, Academic Press, New York, 1967.

[24] J. S. Goldstein, I. S. Reed, and P. A. Zulch, "Multistage Partially Adaptive STAP CFAR Detection Algorithm", *IEEE Transactions on Aerospace and Electronic Systems*, Vol. 35, No. 2,

[25] A. Farina and S. Pardini, " A Track-While-Scan Algorithm Using Radial Velocity in a Clutter Environment", *IEEE Transactions on Aerospace and Electronic Systems*, Vol. 14, No. 5, pp. 769-779, September 1978.

[26] A. d'Aspermont and S. Boyd, "Relaxations and Randomized Methods for Nonconvex QCQPs", *EE392o Class Notes, Stanford University*, Autumn 2003.

[27] A. Ben-Tal and A. Nemirovski, *Lectures on Modern Convex Optimization: Analysis, Algorithms, and Engineering Applications*, MPS-SIAM Series on Optimization, 2001.

[28] Y. Huang and S. Zhang, "Complex Matrix Decomposition and Quadratic Programming", *Mathematics of Operations Research*, Vol. 32, No. 3, pp. 758-768, August 2007.

[29] L. Bomer and M. Antweiler, "Polyphase Barker Sequences", *Electronics Letters*, Vol. 25, No. 23, pp. 1577-1579, November 1989.

[30] M. Friese, "Polyphase Barker Sequences up to Length 36", *IEEE Transactions on Information Theory*, Vol. 42, No. 4, pp. 1248-1250, July 1996.

[31] J. Ward, "Space-Time Adaptive Processing for Airborne Radar", *Technical Report No. 1015*, Lincoln Laboratories, December 1994.

[32] H. L. Van Trees, *Optimum Array Processing. Part IV of Detection, Estimation and Modulation Theory*, John Wiley & Sons, 2002.

[33] P. Antonik, M. C. Wicks, H. D. Griffiths, and C. J. Baker, "Frequency Diverse Array Radars", *Proceedings of the IEEE International Radar Conference 2006*, pp. 215-217, Verona, NY, 24-27 April 2006.

[34] P. Antonik, M. C. Wicks, H. D. Griffiths, and C. J. Baker, "Multi-Mission Multi-Mode Waveform Diversity", *Proceedings of the IEEE International Radar Conference 2006*, pp. 580-582, Verona, NY, 24-27 April 2006.

[35] W. Ai, Y. Huang, and S. Zhang, "New Results on Hermitian Matrix Rank-One Decomposition", accepted by *Mathematical Programming*, in press.

[36] J. S. Bergin and P. M. Techau, "High-fidelity site-specific radar simulation: KASSPER '02 workshop datacube", *ISL Technical Report, ISL-SCRD-TR-02-105*, Vienna, VA, May 2002.

[37] C. J. Baker and A. L. Hume, "Netted Radar Sensing", *IEEE Aerospace and Electronic System Magazine*, Vol. 18, No. 2, pp. 3-6, February 2003.

[38] E. Fishler, A. Haimovich, R. Blum, L. Cimini, D. Chizhik, and R. Valenzuela, "Spatial Diversity in Radars: Models and Detection Performance", *IEEE Transactions on Signal Processing*, Vol. 54, No. 3, pp. 823-838, March 2006.

[39] J. Li and P. Stoica, *MIMO Radar Signal Processing*, John Wiley & Sons, 2008.

[40] A. De Maio, G. A. Fabrizio, A. Farina, W. L. Melvin, and L. Timmoneri, "Challenging Issues in Multichannel Radar Array Processing", *Proceedings of the IEEE International Radar Conference 2007*, Edinburgh (UK), pp. 856-862, April 2007.

[41] L. Landi and R. Adve, "Time-orthogonal-waveform-space-time Adaptive Processing for Distributed Aperture Radars", *Proceedings of the International Waveform Diversity and Design Conference 2007*, Orlando (US), pp. 13-17, June 2007.

[42] R. S. Adve, R. A. Schneible, G. Genello, and P. Antonik, "Waveform Space-Time Adaptive Processing for Distributed Aperture Radars", *Proceedings of the IEEE International Radar Conference 2005*,Arlington (US), pp.93-97, May 2005.

[43] K. H. Berthke, B. Röde, M. Schneider, and A. Schroth, "A Novel Noncooperative Near-Range Radar Network for Traffic Guidance and Control on Airport Surfaces", *IEEE Transactions on Control Systems Technology*, Vol. 1, No. 3, pp. 168-178, September 1993.

[44] H. Huang and D. Lang, "The Comparison of Attitude and Antenna Pointing Design Strategies of Noncooperative Spaceborne Bistatic Radar", *Proceedings of the IEEE International Radar Conference 2005*, Arlington (US), pp. 568-571, May 2005.

[45] H. D. Ly and Q. Liang, “Spatial-Temporal-Frequency Diversity in Radar Sensor Networks”, *Proceedings of the IEEE Military Communications Conference 2006*, Washington (US), pp. 1-7, October 2006.

[46] N. Levanon, “Multifrequency Complementary Phase-Coded Radar signal”, *IEE Radar, Sonar and Navigation*, Vol. 147, No. 6, pp. 276-284, December 2000.

[47] A. Farina, “Waveform Diversity: Past, Present, and Future”, *Proceedings of the International Waveform Diversity and Design Conference 2007*, Orlando (US), pp. 1-3, June 2007.

[48] J. Li, L. Xu, P. Stoica, K.W. Forsythe, and D.W. Bliss, “Range Compression and Waveform Optimization for MIMO Radar: A Cramér−Rao Bound Based Study”, *IEEE Transactions on Signal Processing*, Vol. 56, No. 1, pp. 218-232, January 2008.

[49] A. De Maio and M. Lops, “Design Principles of MIMO Radar Detectors”, *IEEE Transactions on Aerospace and Electronic System*, Vol. 43, no. 3, pp. 886-898, July 2007.

[50] N. Subotic, K. Cooper, and P. Zulch, “Conditional and Constrained Joint Optimization of Radar Waveforms”, *Proceedings of the International Waveform Diversity and Design Conference 2007*, Orlando (US), pp. 387-394, June 2007.

[51] M. Greco, F. Gini, P. Stinco, A. Farina, and L. Verrazzani, “Adaptive Waveform Diversity for Cross-Channel Interference Mitigation”, *Pro-*

ceedings of the IEEE International Radar Conference 2008, Roma (IT), pp. 1-6, May 2008.

[52] A. Nemirovski, C. Roos, and T. Terlaki, "On Maximization Of Quadratic Form Over Intersection Of Ellipsoids With Common Center", *Mathematical Programming*, Vol. 86, pp.463-473, September 1999.

[53] R. A. Horn and C. R. Johnson, *Matrix Analysis*, Cambridge University Press, 1985.

[54] W.-K. Ma, T. N. Davidson, K. M. Wong, Z.-Q. Luo, and P.-C. Ching, "Quasi-Maximum-Likelihood Multiuser Detection Using Semi-Definite Relaxation With Application to Synchronous CDMA", *IEEE Transactions on Signal Processing*, Vol. 50, No. 4, pp. 912-922, April 2002.

[55] D. Huffman, "The Generation of Impulse-Equivalent Pulse Trains", *IRE Transactions on Information Theory*, Vol. 8, No. 5, pp. 10-16, September 1962.

[56] R. Gold, "Optimal Binary Sequences for Spread Spectrum Multiplexing", *IEEE Transactions on Information Theory*, Vol. 13, No. 4, pp. 154-156, October 1967.

[57] D. V. Sarwate and M. B. Pursley, "Cross-correlation Properties of Pseudorandom and Related Sequences", *IEEE Proceedings*, Vol. 68, No. 5, pp. 593-619, May 1980.

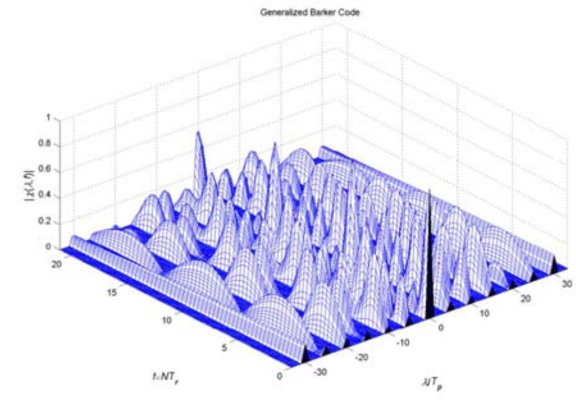

Waveform Design via Convex Optimization

In this thesis, we propose some original examples of radar waveform design via convex optimization theory. After an initial section introducing some basic concepts about waveform design (chapter 2), we analyze in detail code design for a stand-alone radar in case of temporal (chapter 3) or spatial-temporal processing (chapter 4), and for a networked radar with constraints on the induced interference (chapter 5). Finally, some concluding remarks are presented (chapter 6).